UNIVERSITÀ DEGLI STUDI DI PALERMO

Corso di Dottorato di Ricerca in
"Energia e Tecnologie dell'Informazione - curriculum Fisica Tecnica e Ingegneria Nucleare"
Dipartimento di Energia, ingegneria dell'Informazione e modelli Matematici
Settore Scientifico Disciplinare ING-IND/19

NUMERICAL ASSESSMENT OF THE THERMAL-HYDRAULIC PERFORMANCES OF THE ITER BLANKET COOLING SYSTEM

IL DOTTORE
EUGENIO VALLONE

IL COORDINATORE
CH.MO PROF. MAURIZIO CELLURA

IL TUTOR
CH.MO PROF. PIETRO ALESSANDRO DI MAIO

CICLO XXXI
ANNO CONSEGUIMENTO TITOLO 2018

Table of Contents

List of Figures

List of Tables

Abbreviations

Abbreviation	Definition
BC	Boundary Condition
BM	Blanket Module
CC	Coaxial Connector
CEA	Commissariat à l'Energie Atomique
CFD	Computational Fluid-Dynamic
CHF	Critical Heat Flux
DEIM	Department of Energy, Information Engineering and Mathematical Models
EHF	Enhanced Heat Flux
FP	Flexible Pipe
FW	First Wall
HPC	High Performance Computing
IAPWS	International Association for the Properties of Water and Steam
IBED	Integrated Blanket, Edge Localized Mode, Divertor
ICC	Inlet Coaxial Connector
IFS	Inner Flow Separator
IO	ITER Organization
NBI	Neutral Beam Injector
NHF	Normal Heat Flux
OCC	Outlet Coaxial Connector
OFS	Outer Flow Separator
PFU	Plasma-Facing Unit

PHTS	Primary Heat Transfer System
R&D	Research and Development
RANS	Reynolds Averaged Navier-Stokes
SB	Shield Block
TCWS	TOKAMAK Cooling Water System
UPC	Upper Pipe Chase
URM	Upper Ring Manifold
VV	Vacuum Vessel

Disclaimer

The views and opinions expressed herein do not necessarily reflect those of the ITER Organization.

Introduction

At the Geneva Superpower Summit in November 1985, the former Soviet Union General Secretary Gorbachev proposed to the USA President Reagan the idea of an international cooperation to develop fusion energy for peaceful purposes. European Union (Euratom), Japan, the Soviet Union and the USA signed an agreement one year after to carry on the design of the largest international fusion facility, ITER. People's Republic of China, Republic of Korea and India would have joined the project later. In 2005, the ITER Members unanimously agreed to build the facility in southern France and founded the ITER Organization.

ITER will be the first experimental device to produce net energy from nuclear fusion reactions and maintain fusion for long times and, moreover, it will be the underlying stage for the commercial production of fusion-based electricity, making it feasible to test technologies, materials and physics regimes at a power plant scale. Most of the ITER technologies are indeed pioneering experimental applications and, for this reason, they will undergo a long testing phase to let scientists be acquainted with the phenomena related to a large-scale fusion reactor and lay the foundation for a future electricity mass production from fusion power plant.

The most critical component in this sense is the blanket system. It is designed to be the first physical boundary to the plasma and shield the vacuum vessel, the superconducting magnets and the external ITER components from thermal and nuclear radiation and, consequently, it will undergo significant heat loads under nominal conditions. Therefore, the blanket cooling system design results of the utmost importance in order to prevent any risk of Critical Heat Flux (CHF) insurgence, optimizing coolant distribution and complying with the design limits.

Within the framework of the Research and Development (R&D) activities promoted by the ITER Organization (IO), the Department of Energy, Information Engineering and Mathematical Models of the University of Palermo (DEIM) has carried out a theoretical research campaign intended to investigate the thermal-hydraulic behaviour of the ITER blanket cooling system under nominal steady-state conditions.

This research campaign has been the focus of the Ph.D. work during the period that goes from the end of 2015 to the second half of 2018 and it is going to be extensively described in this thesis.

Chapter 1

THE ITER BLANKET SYSTEM

1.1 Introduction

The blanket system represents one of the pivotal components of the ITER reactor, because it provides a physical boundary for the plasma transients and contributes to the thermal and nuclear shielding of the vacuum vessel, the superconducting magnets and the external ITER components.

It is composed of 440 Blanket Modules (BMs), connected to the Vacuum Vessel (VV) through a mechanical attachment system of flexible supports and keys and distributed in 18 toroidal sectors, covering a plasma-facing surface of ~600 m^2. Within each toroidal sector, modules are distributed in three poloidal segments, namely the inboard segment, including 6 modules, the upper segment, containing 4 modules, and the outboard segment, composed of 14 modules. From the structural standpoint, a typical blanket module is ~1 m high in poloidal direction, ~1.5 m long in toroidal direction and ~0.5 m thick in radial direction and it is composed of a First Wall (FW) panel and a Shield Block (SB), actively cooled by pressurized water [1].

A total amount of 736 MW heat power is predicted to be deposited in the blanket under nominal steady-state conditions. In order to extract this deposited power, a set of inlet/outlet manifolds connected to the Integrated Blanket, Edge Localized Mode, Divertor (IBED) Primary Heat Transfer System (PHTS) of the ITER TOKAMAK Cooling Water System (TCWS) are devoted to feed the proper coolant mass flow rate to each blanket module.

Because of its position and functions, the blanket system is foreseen to undergo a significant heat load under nominal conditions. Therefore, the blanket cooling system design results to be particularly demanding since it has to ensure that an adequate cooling is provided to each module and any risk of CHF insurgence is prevented, optimizing mass flow rate distribution and complying with pressure drop limits.

1.2 The Blanket Cooling System

The blanket cooling system consists of 18 separate sectors connected in parallel to the Upper Ring Manifold (URM) of the ITER TCWS IBED PHTS and devoted to cool separately the 24 modules of each standard blanket sector and the 26 modules of each Neutral Beam Injector (NBI) blanket sector. The sectors pertaining to the inboard region are composed of a single column of blanket modules, while the outboard region is divided into two subsectors typically called central and side outboard regions. Moreover, each blanket sector cooling system is typically articulated in 20 module cooling systems, for a total of 363 independent cooling circuits, devoted to provide coolant to all the 440 blanket modules. The main part of the blanket cooling system is therefore intended to individually cool a single blanket module, the remaining part being devoted to feed water coolant in parallel to two or even three blanket modules, usually referred as twinned or triplet modules, respectively [2].

Figure 1.1 and Figure 1.2 show the blanket modules distribution within the plasma chamber. In order to ease the comprehension of the blanket scheme, blanket modules have been divided in inboard and outboard modules, including those typically placed into the upper region that are, namely, BM#07, BM#08, BM#09 and BM#10. Twinned and triplet blanket modules cooling circuit have been coloured in pink.

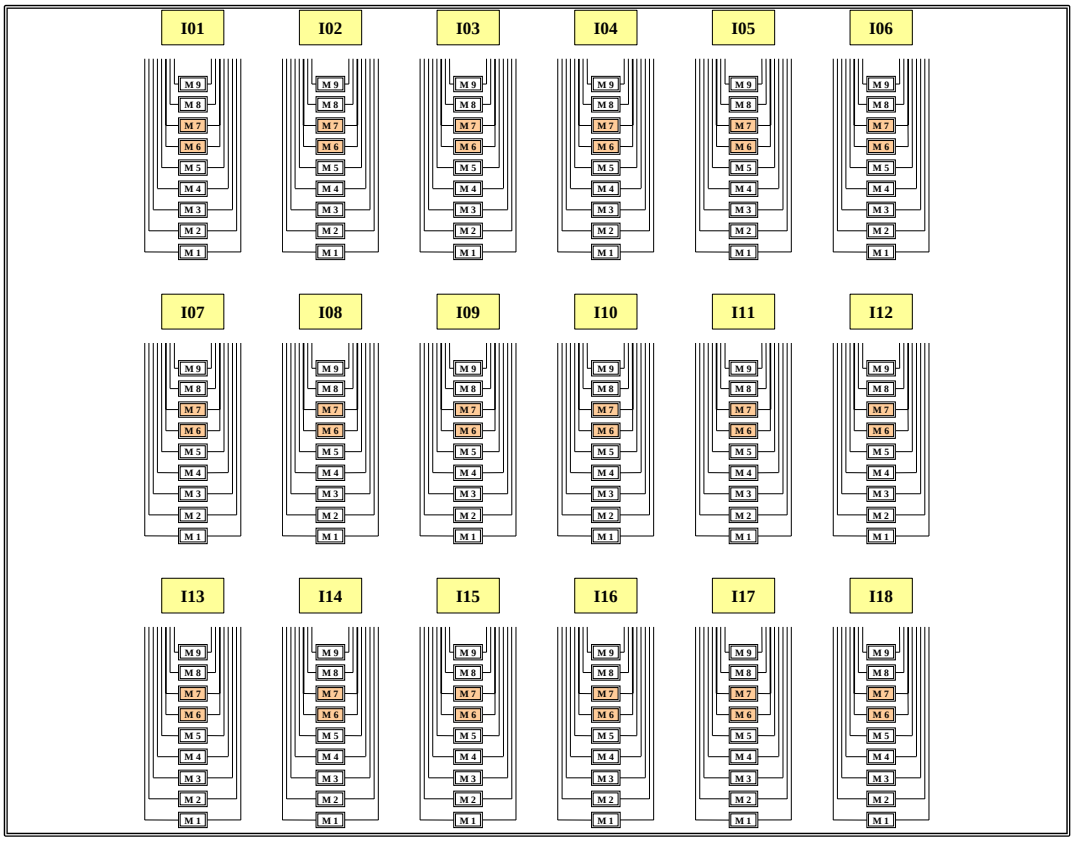

Figure 1.1. Inboard blanket sector cooling system layout.

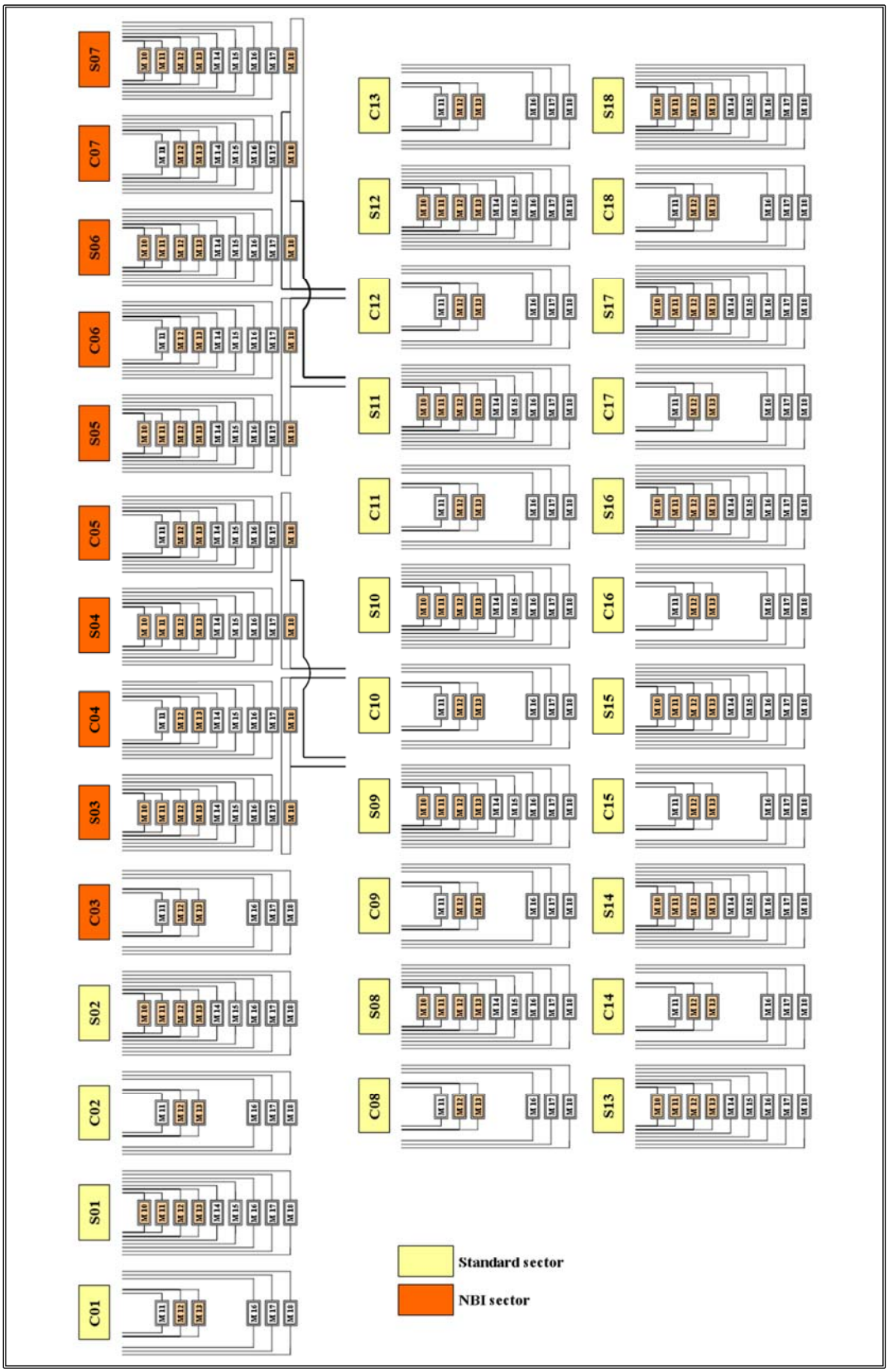

Figure 1.2. Outboard blanket sector cooling system layout.

A generic blanket module cooling system of a typical ITER blanket sector cooling system is composed of the following main components:

- manifolds;
- coaxial connector and flexible pipes;
- blanket module cooling circuit.

The main structural, functional and operational features of these components are hereinafter described.

1.2.1 Manifolds

Blanket manifolds are devoted to route coolant from the TCWS IBED PHTS URM located in the Upper Pipe Chase (UPC) to the module cooling circuits of each blanket sector (Figure 1.3), feeding each of them with a proper mass flow rate, able to allow heat power extraction complying with the prescribed coolant thermal rise and pressure drop limits.

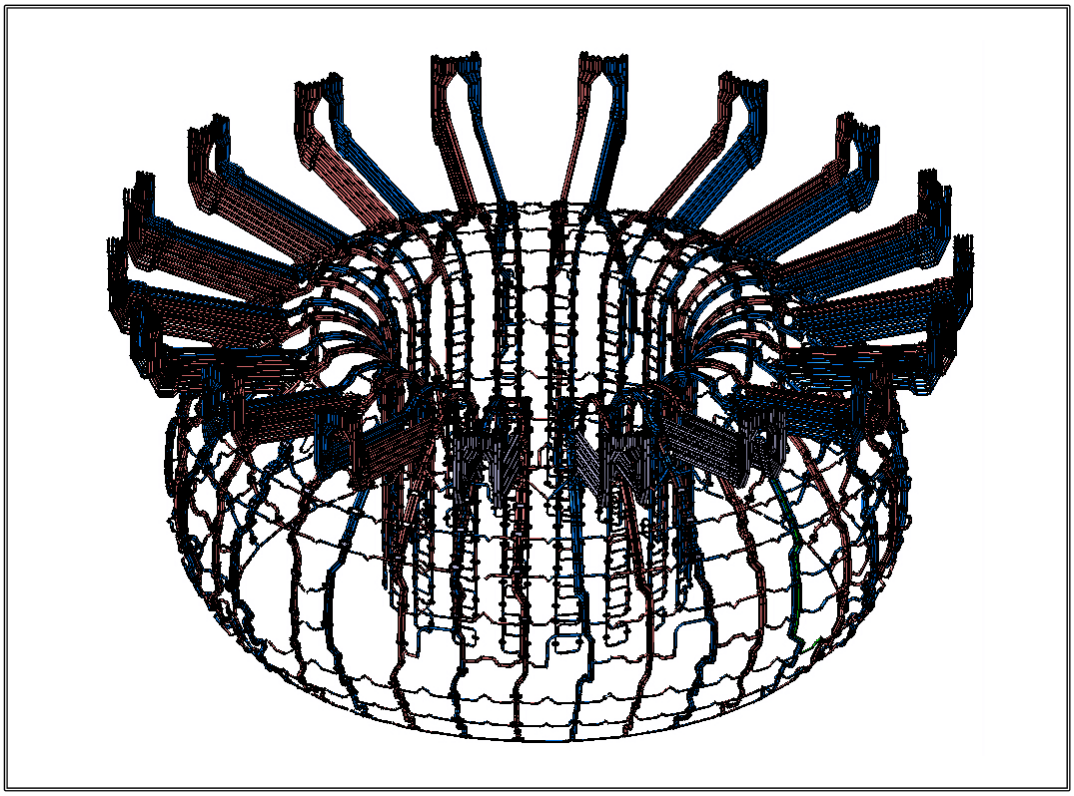

Figure 1.3. ITER blanket cooling system manifolds.

According to their function, blanket manifolds are subdivided into 18 independent sets, each one interfaced with a specific blanket sector cooling system. Each set includes typically 20 inlet/outlet manifolds, subdivided in correspondence to the upper port chimney bulkhead into an in-vessel (Figure 1.4) and an out-vessel (Figure 1.5) segment.

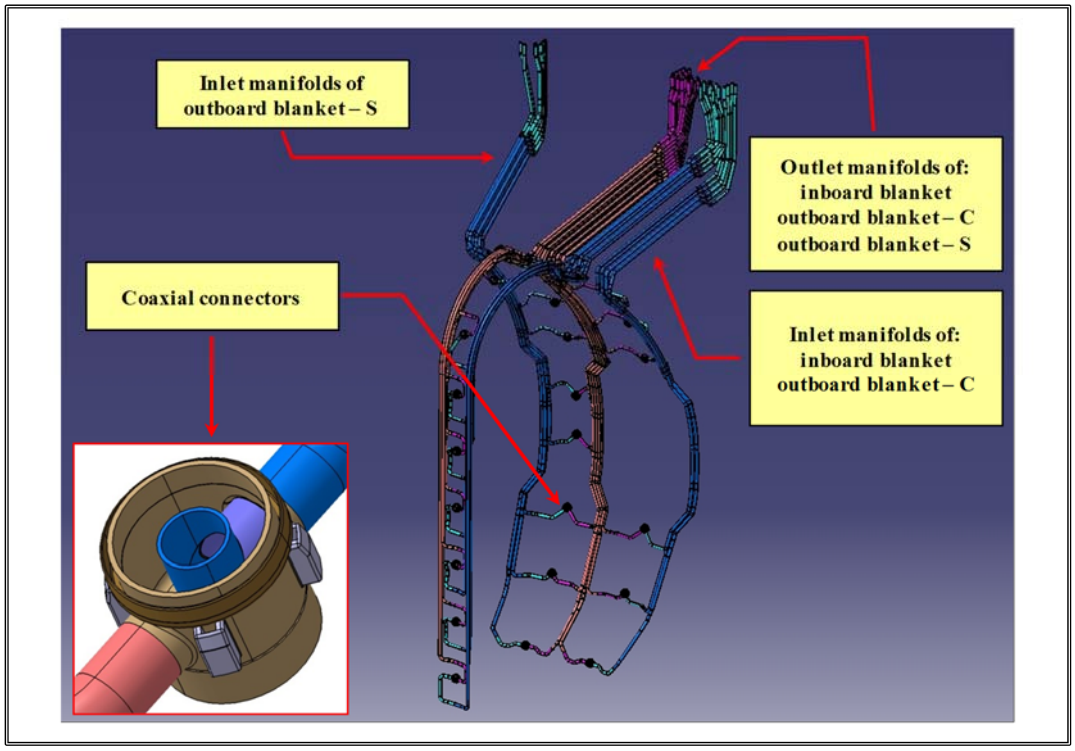

Figure 1.4. Blanket standard sector cooling system in-vessel manifolds.

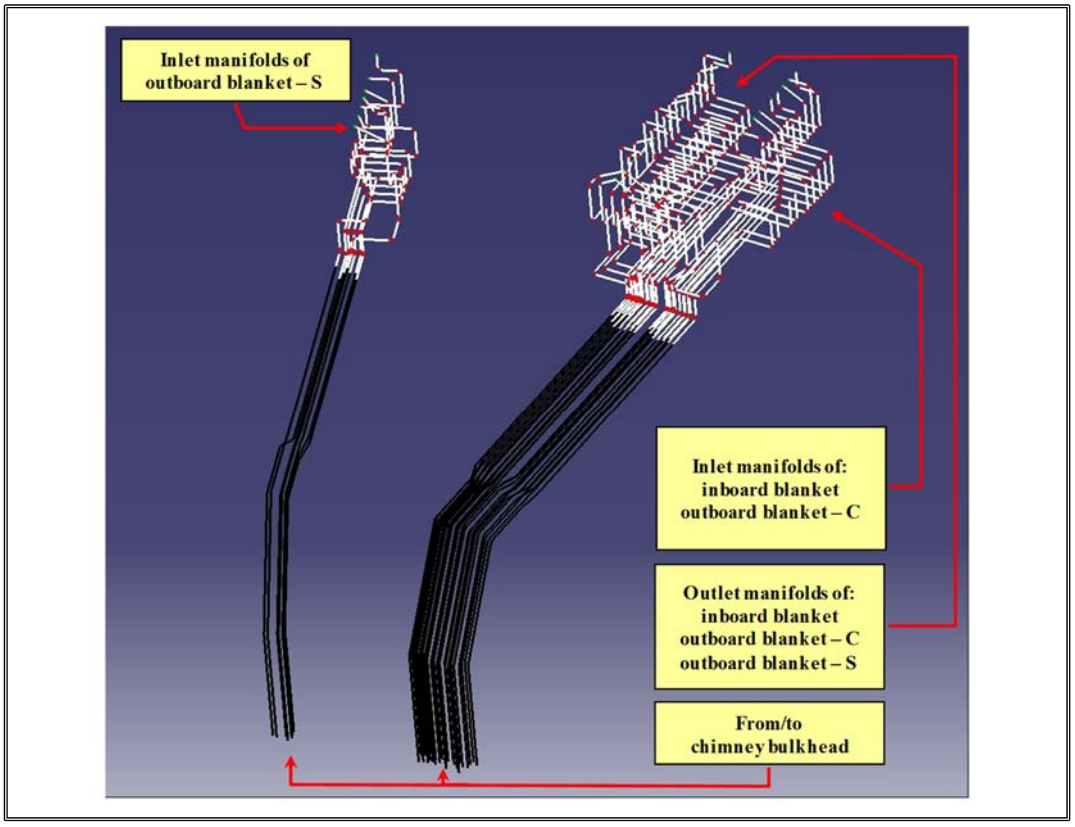

Figure 1.5. Blanket standard sector cooling system out-vessel manifolds.

A typical manifold set is composed of in-vessel manifolds, VV manifold feed-trough, in-cryostat piping and UPC plumbing.

The in-vessel manifolds are composed of poloidal bundles of pipes, subdivided in an inboard and outboard segment, including 8 and 12 pairs of inlet/outlet pipes, respectively. They follow the D-shape of the VV and their layout is strongly determined by internal components of the machine, like blanket modules with their attachment systems, in-vessel coils and diagnostics.

The VV manifold feed through is located in the upper port chimney bulkhead (Figure 1.6) where 40 penetrations equipped with pipe stubs welded on both sides find their place to allow the transition between in-vessel and out-vessel manifold segments.

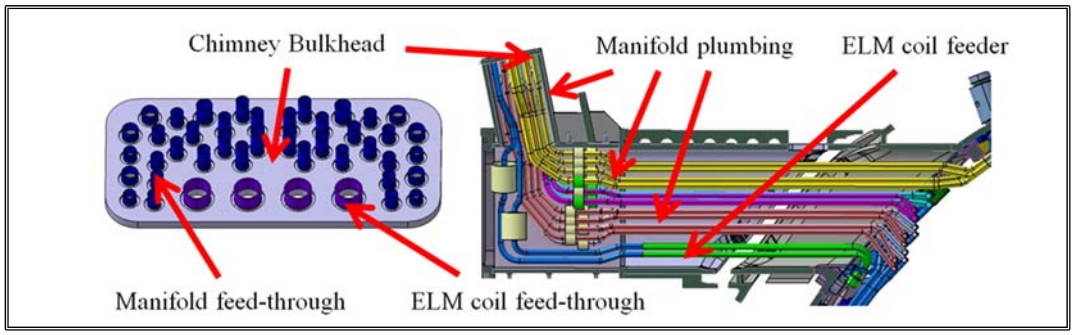

Figure 1.6. VV manifold feed-trough.

Within the cryostat, inlet and outlet bundles of pipes are routed from the VV manifold feed through into the Upper Pipe Chase, being channelled in a common guard compartment to increase the thermal isolation and to avoid water leakage inside the cryostat (Figure 1.7) and crossing the cryostat and bio-shield feed-through.

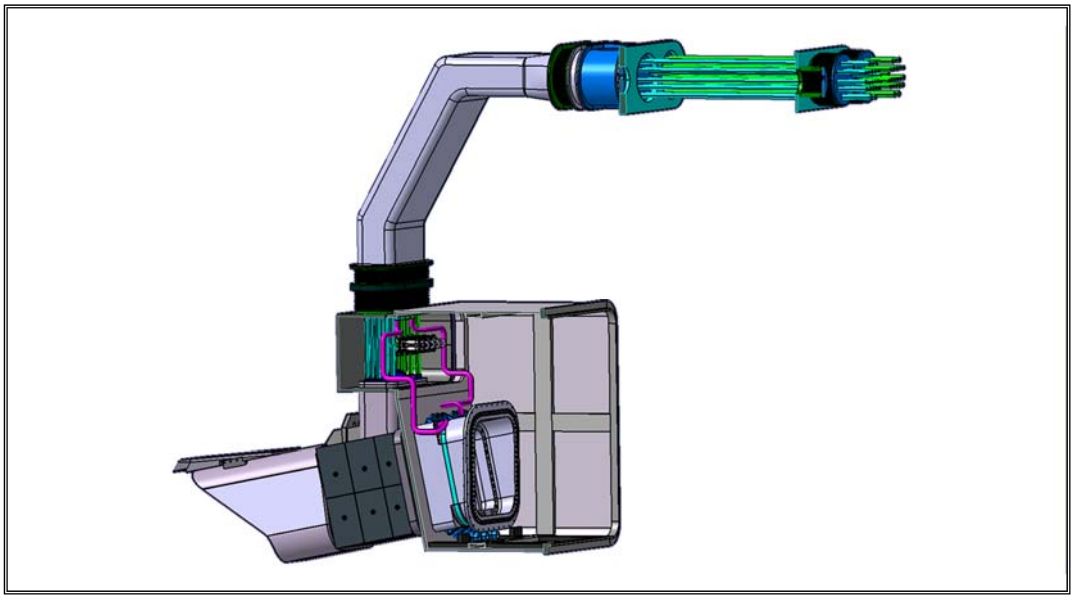

Figure 1.7. In-cryostat piping.

Upper pipe chase plumbing connects the in-cryostat piping to a couple of inlet/outlet sub-headers vertically connected to the URM (Figure 1.8). They are arranged in a complex way to cope with thermal differential expansion and to allow unrestricted man access to the plumbing equipment, being endowed with a set of flow regulators (valves and orifices) to allow mass flow rate balancing among blanket module cooling systems.

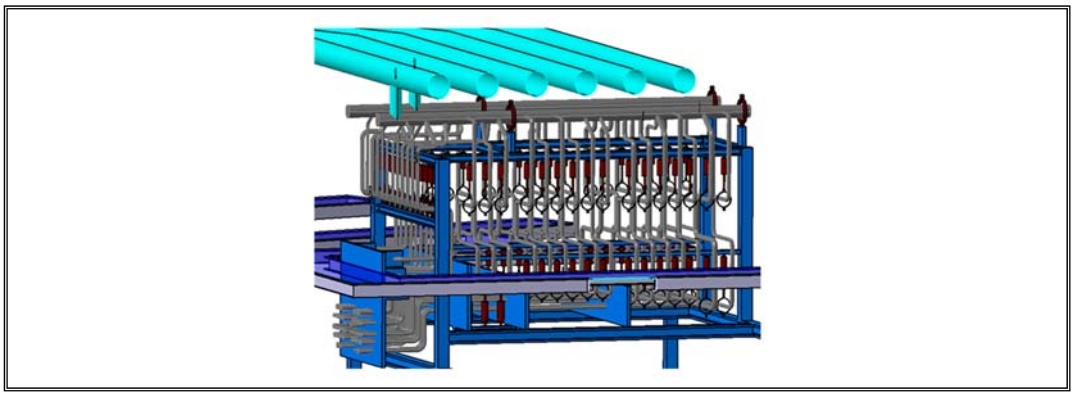

Figure 1.8. UPC plumbing.

1.2.2 Coaxial Connector and Flexible Pipes

Coaxial Connector (CC) and Flexible Pipes (FPs) represents the two kinds of hydraulic connectors commonly adopted at the interfaces between the main segments of a typical blanket module. The CC represents the interface between the inlet/outlet manifolds and the blanket module cooling circuit [2]. It is composed of an internal elbow, which receives coolant from the inlet manifold and routes it to the FW cooling circuit, and an external cylindrical jacket housing the elbow, that receives coolant from the SB cooling circuit and routes it to the outlet manifold (Figure 1.9). The FPs guarantee the connection between the inlet CC and the FW cooling circuit and between this latter and the SB cooling circuit. Finally, a couple inlet/outlet branch pipes find their place inside slots located in the SB rear part to allow the hydraulic connection between the CC and inlet/outlet manifolds.

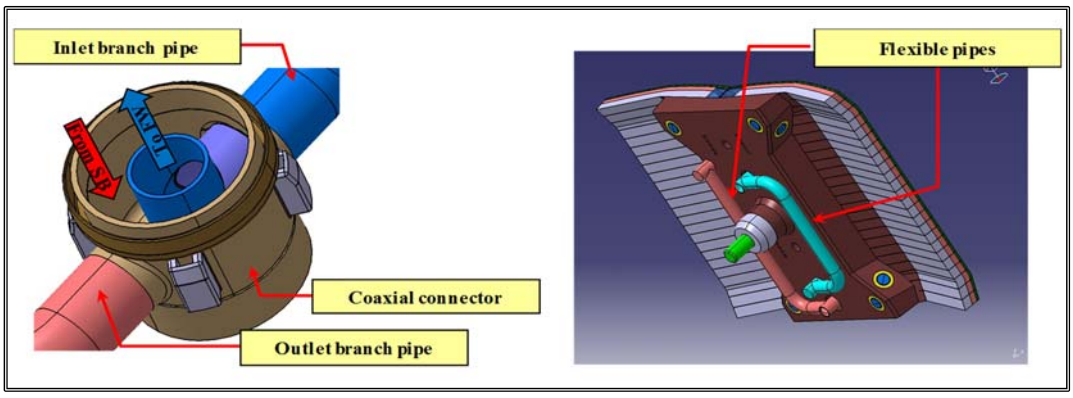

Figure 1.9. Coaxial connector and flexible pipes.

1.2.3 Blanket Module Cooling Circuit

From the structural standpoint, a typical blanket module (Figure 1.10) is mainly composed of a plasma-facing FW panel (Figure 1.11) and a SB (Figure 1.12).

The FW is a multi-metallic water-cooled structure designed to withstand the heat and particle fluxes arising from plasma during normal and transient operations as well as during disruption events. It is typically composed of a stainless steel central poloidal beam and a system of toroidally oriented Plasma-Facing Units (PFUs), typically articulated into two symmetric wings and structurally supported by the poloidal beam. Each PFU is composed of a stainless steel/copper finger (Figure 1.13), covered with beryllium tiles and endowed with two circular tubes or a hypervapotron channel.

The SB is a stainless steel water-cooled structure designed to support the FW and contribute to the thermal and nuclear shielding of the vacuum vessel, the superconducting magnets and the external ITER components. It is equipped with a complex network of cooling channels and plates, where coolant flows absorbing the nuclear deposited heat power.

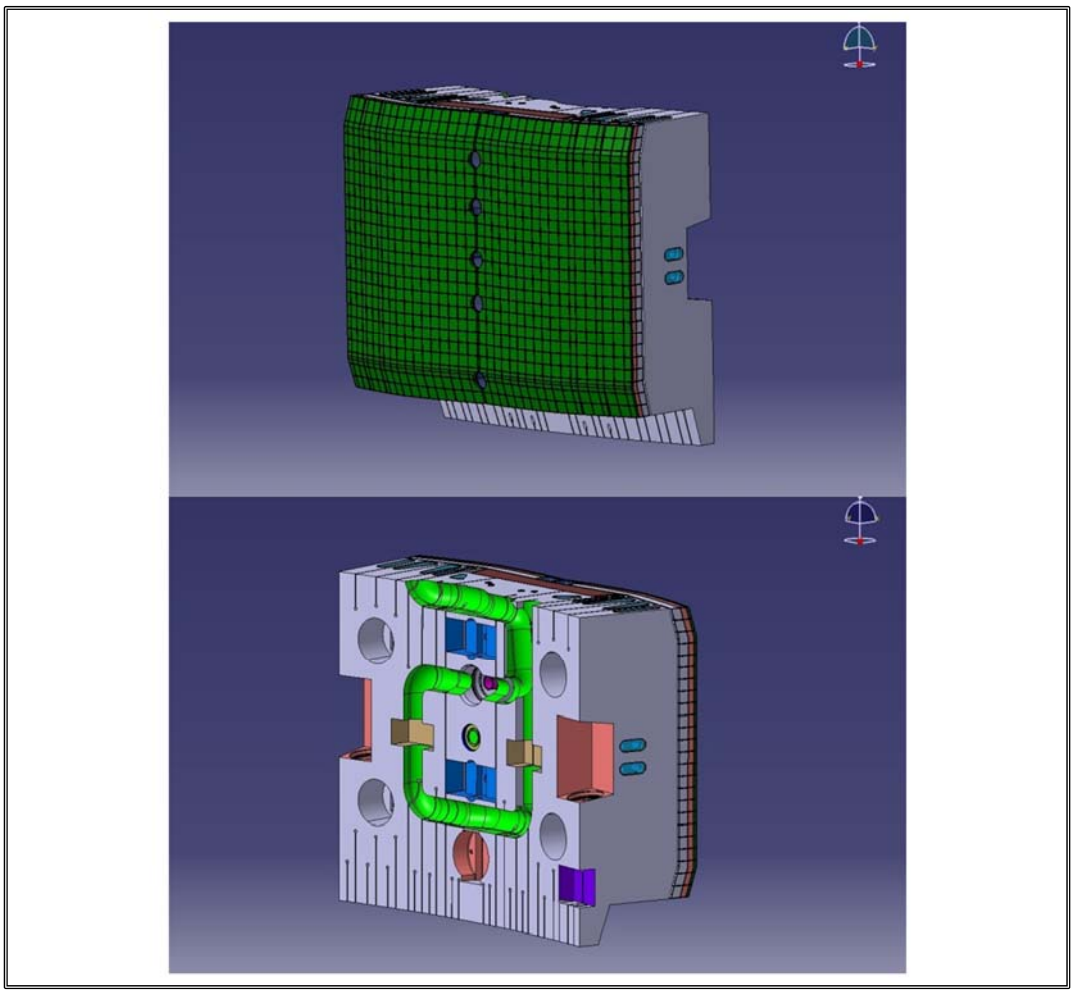

Figure 1.10. Isometric views of a typical ITER blanket module.

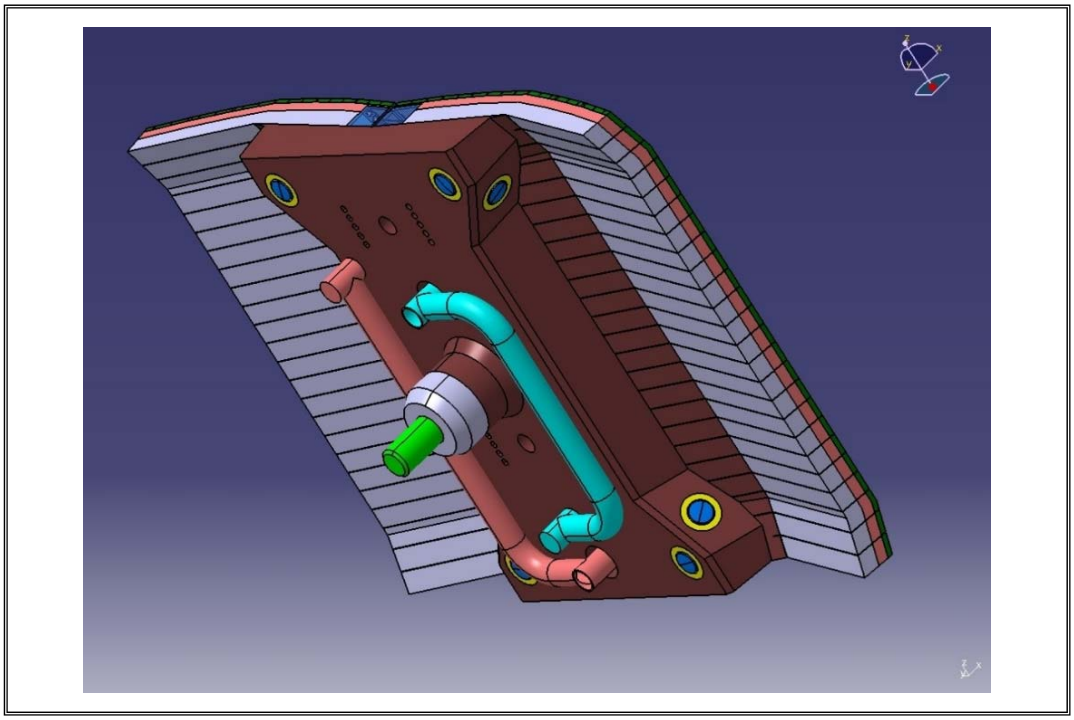

Figure 1.11. Isometric view of a typical FW.

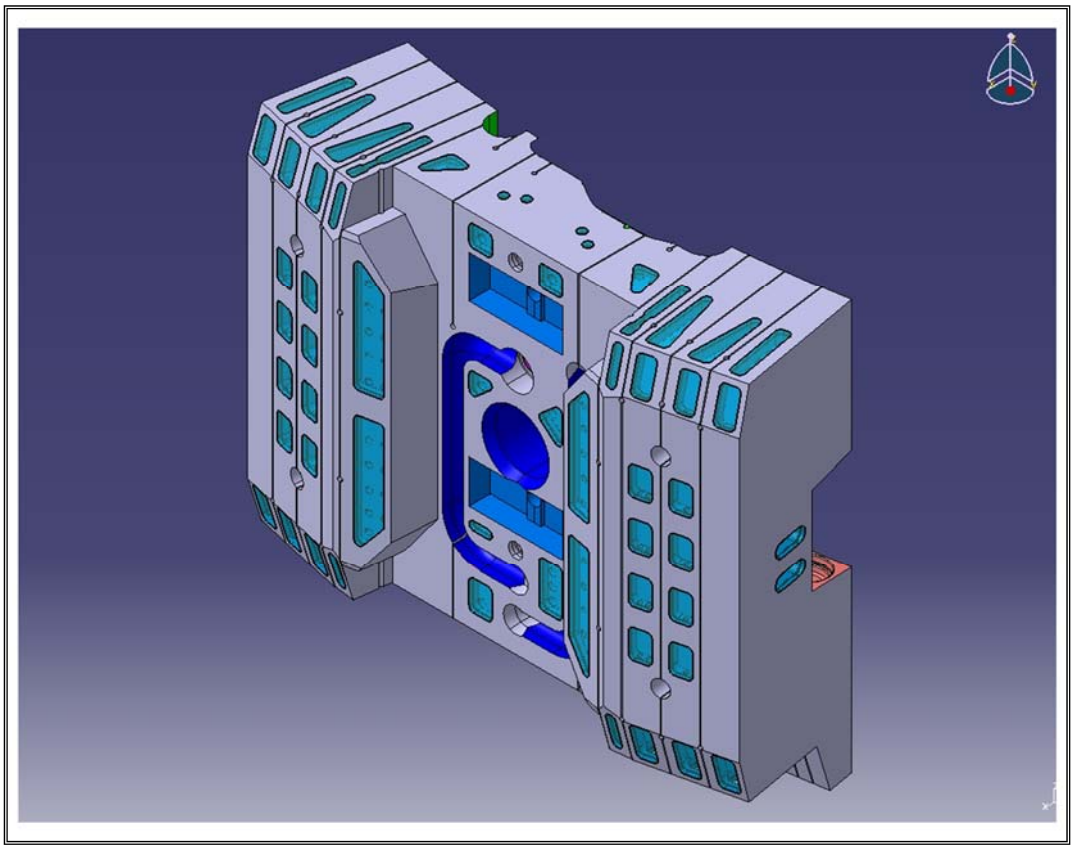

Figure 1.12. Isometric view of a typical SB.

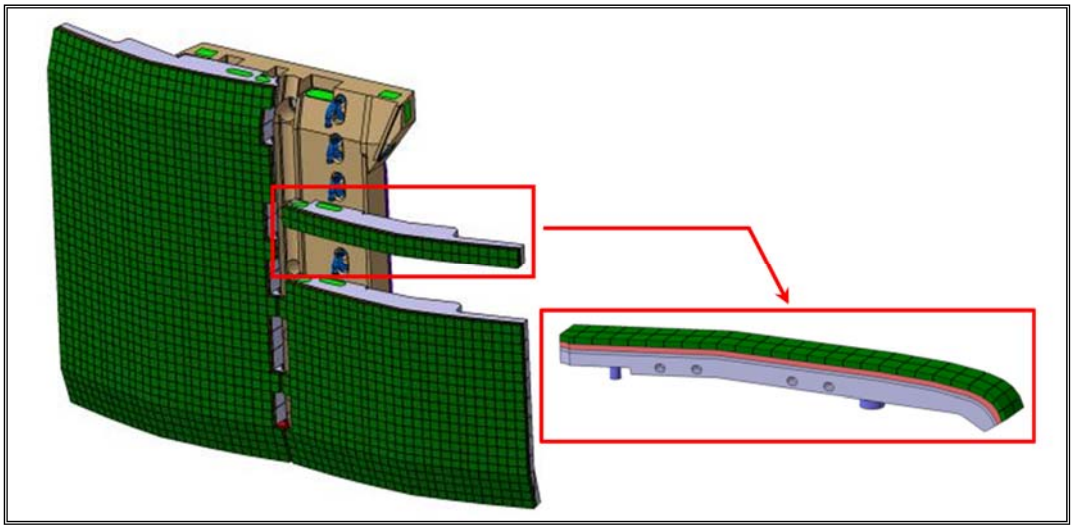

Figure 1.13. Blanket module FW with the detail of a PFU.

Blanket modules may be classified as either Normal Heat Flux (NHF) or Enhanced Heat Flux (EHF) modules depending on the magnitude of the heat flux their FW is expected to be subjected to (Figure 1.14). Specifically, NHF modules are intended to withstand a heat flux ranging between 1 and 2 MW/m^2 while EHF modules are conceived to accommodate the highest heat fluxes, amounting to 3.5÷4.7 MW/m^2 [1].

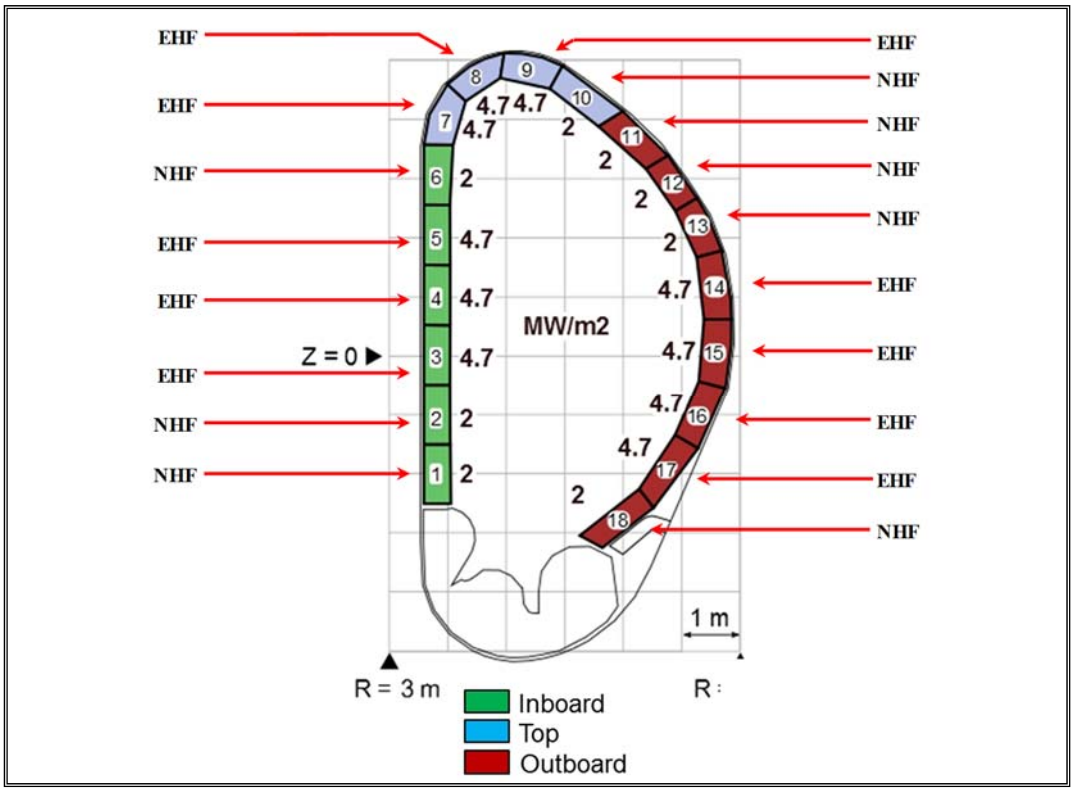

Figure 1.14. Typical poloidal distribution of NHF and EHF blanket modules.

Each blanket module is endowed with a circuit intended to ensure its adequate cooling to prevent any risk of CHF occurrence while complying with pressure drop limits.

The typical blanket module cooling circuit is composed of the FW and the SB independent cooling circuits, that are hydraulically connected in series by means of purposely-designed flexible pipes located at FW-SB interface. Coolant coming from the inlet manifold flows first into the FW cooling circuit by means of the inlet coaxial connector via an FP and then, through another FP, it is passed to the SB cooling circuit, before being routed to the outlet manifold by the outlet coaxial connector.

The layout of the FW cooling circuit is strictly affected by the magnitude of the heat flux it is expected to undergo under nominal conditions and it is, hence, completely different in case of NHF and EHF blanket modules.

Concerning the FW of a typical NHF blanket module (Figure 1.15), coolant flows from the coaxial connector into a central poloidal header that is located within the FW central poloidal beam (Figure 1.16). It results to be hydraulically connected to two sets of PFU cooling circuits, connected in series in groups of 2 up to 4, each set being devoted to separately cool one of the two FW toroidal wings. In particular, from the inlet header the coolant is routed to the first of the PFU cooling circuits connected in series by means of a specific distribution cavity and it flows toroidally along the two circular channels located inside its heat sink, just behind the beryllium armour. It is then directed to the circular channel of the finger steel supporting structure, where it flows toroidally backward towards the central poloidal beam. Once it reaches the distribution cavity, coolant is routed to a further PFU cooling circuit and, finally, to the final PFU cooling circuit, before flowing into the outlet header, from which it is distributed to the SB cooling circuit by means of a FP.

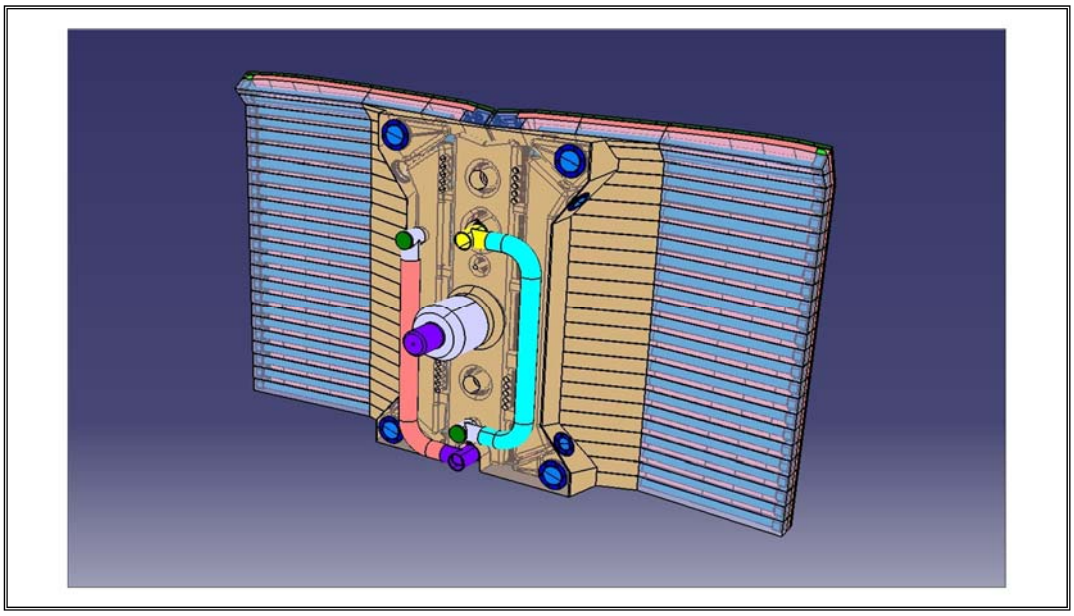

Figure 1.15. NHF blanket module FW cooling circuit.

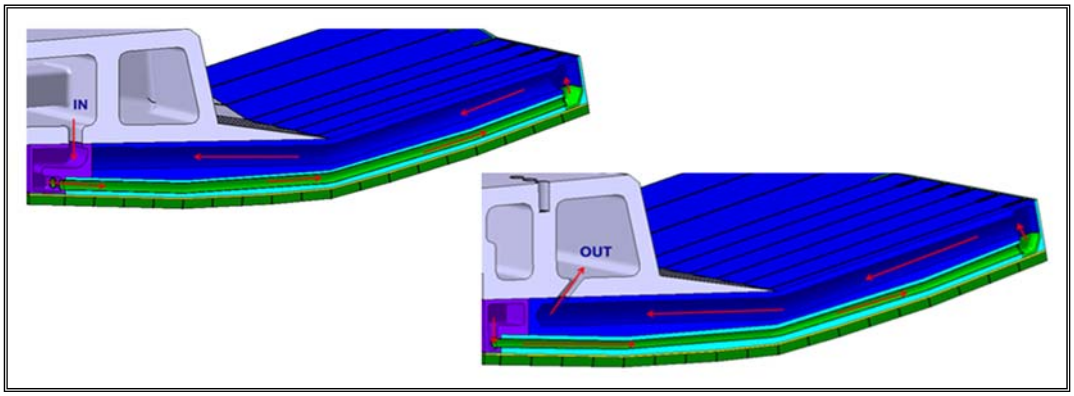

Figure 1.16. Detail of the NHF blanket module FW cooling circuit.

As to a typical EHF blanket module, the FW cooling circuit layout shows specific features intended to withstand the significant heat flux expected on the plasma facing surface (Figure 1.17). In particular, EHF blanket module PFU cooling circuits (Figure 1.18) are endowed with an hypervapotron structure behind the beryllium armour to raise their CHF limit. An additional poloidal finger cooling circuit is included and it is generally connected in series with one of the two FW wings sub-circuits and in parallel with the remaining one. Moreover, the typical central beam cooling circuit of an EHF blanket module consists of an arrangement of gun-drilled channels and plates instead of cavities as for NHF blanket modules cooling circuit.

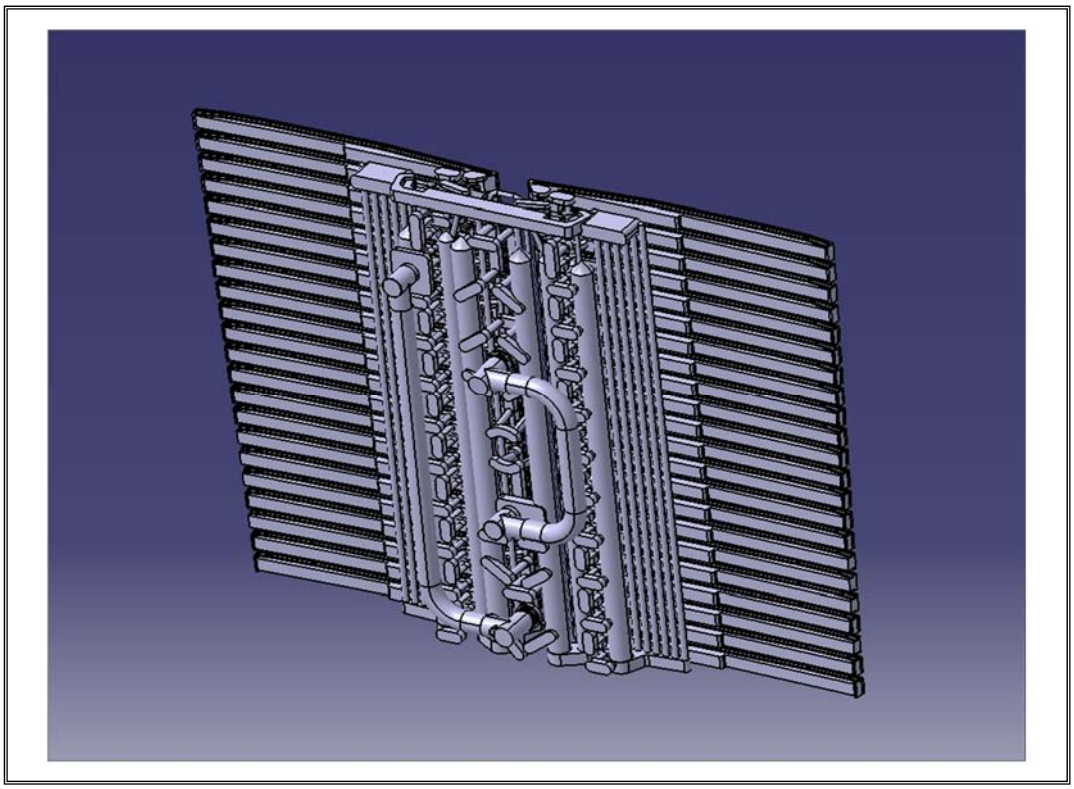

Figure 1.17. EHF blanket module FW cooling circuit.

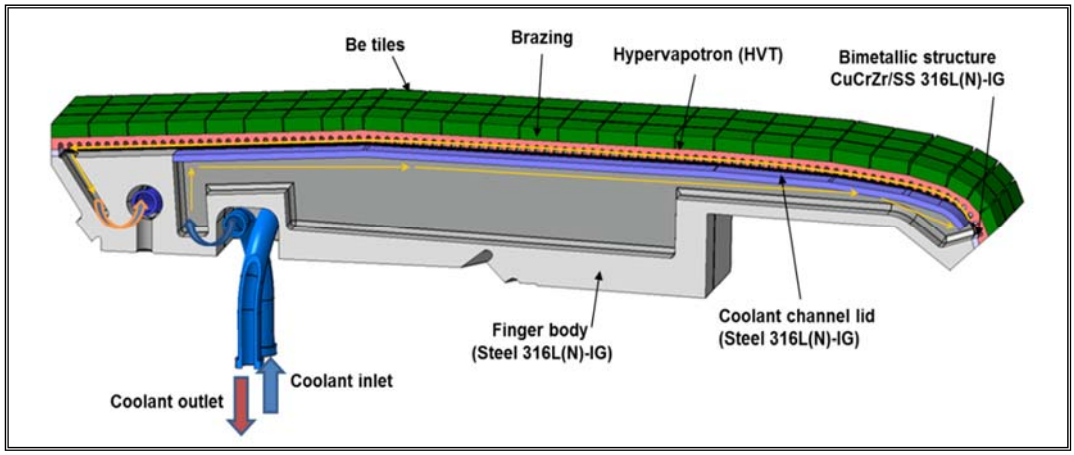

Figure 1.18. Detail of the EHF blanket module FW cooling circuit.

The layout of the SB cooling circuit is mainly driven by the spatial distribution of the nuclear heat power deposited inside its steel structure. It typically consists of a complex network of gun-drilled channels connected in parallel to a system of poloidal-toroidal headers (Figure 1.19 and Figure 1.20). In particular, coolant coming from the FW cooling circuit is routed to a T-shaped inlet header that distributes it to two separate sub-circuits, connected in parallel and devoted to cool the two SB halves. Each sub-circuit is typically composed of an inlet and an outlet header. The first feeds the coolant to a system of channels connected in parallel by plates, while the second receives the coolant from these channels and routes it to the outlet coaxial connector, from which it is distributed to the outlet manifold.

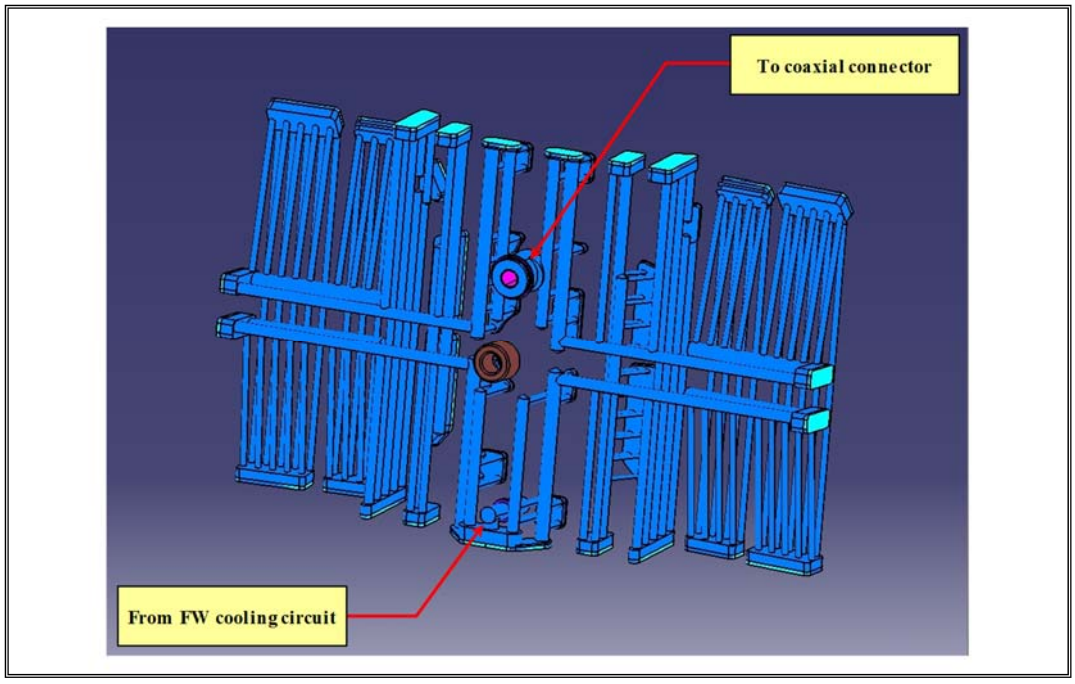

Figure 1.19. Blanket module SB cooling circuit.

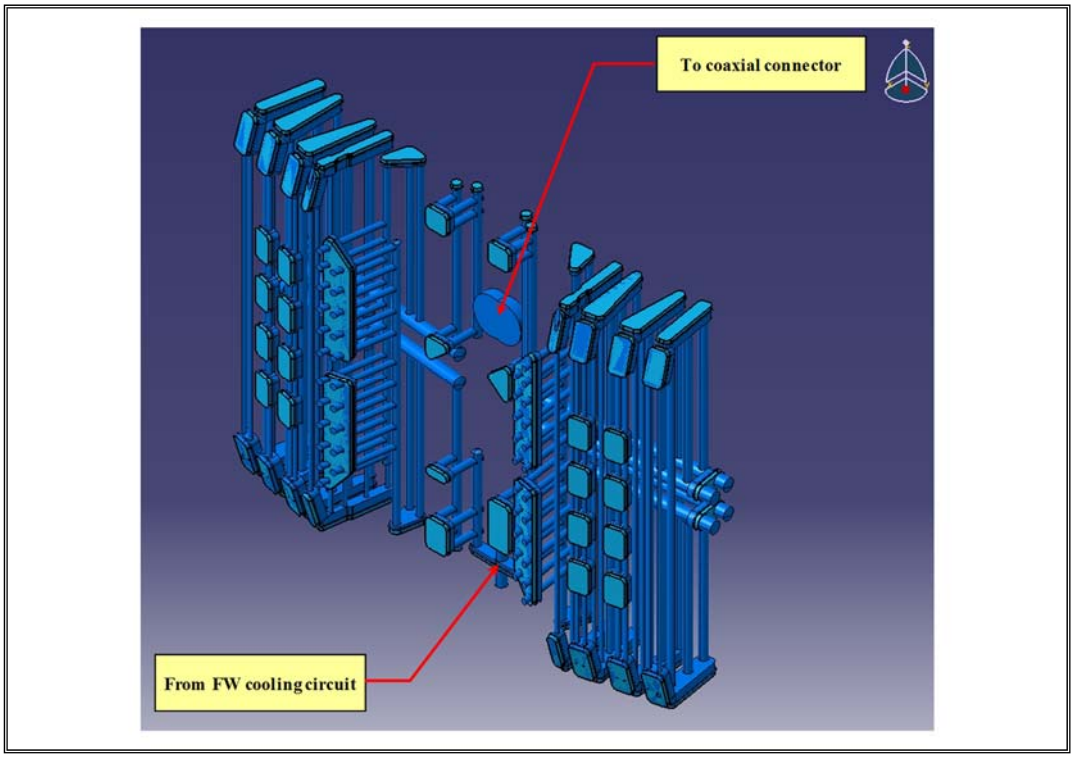

Figure 1.20. Blanket module SB cooling circuit.

1.2.4 Blanket Cooling System Hydraulic Variants

From the configurational point of view, the blanket system involves 185 SB and 80 FW geometric variants that, once properly coupled, constitute the 440 blanket modules. Since many variants differ in minor geometric details, their cooling circuits may result to be the same or they differ so slightly that may be considered the same from the thermal-hydraulic standpoint. For this reason, the actual number of hydraulic variants reduces to:

- 96 SB hydraulic variants;
- 40 FW hydraulic variants;
- 32 inlet manifold hydraulic variants;
- 32 outlet manifold hydraulic variants;

for an overall number of 200 different hydraulic variants, that, once properly combined, allow to obtain each one of the 363 different blanket module cooling systems counted by the ITER blanket cooling system. It may be concluded that, at least from the thermal-hydraulic standpoint, each blanket module cooling system has a modular structure, being articulated in the series of specific hydraulic variants of the inlet blanket manifold, the FW cooling circuit, the SB cooling circuit and the outlet blanket manifold, reported, according to the blanket module position, in [3]. The complete representation of the blanket module cooling circuits breakdown in terms of hydraulic variants is reported in Figure 1.21 and Figure 1.22.

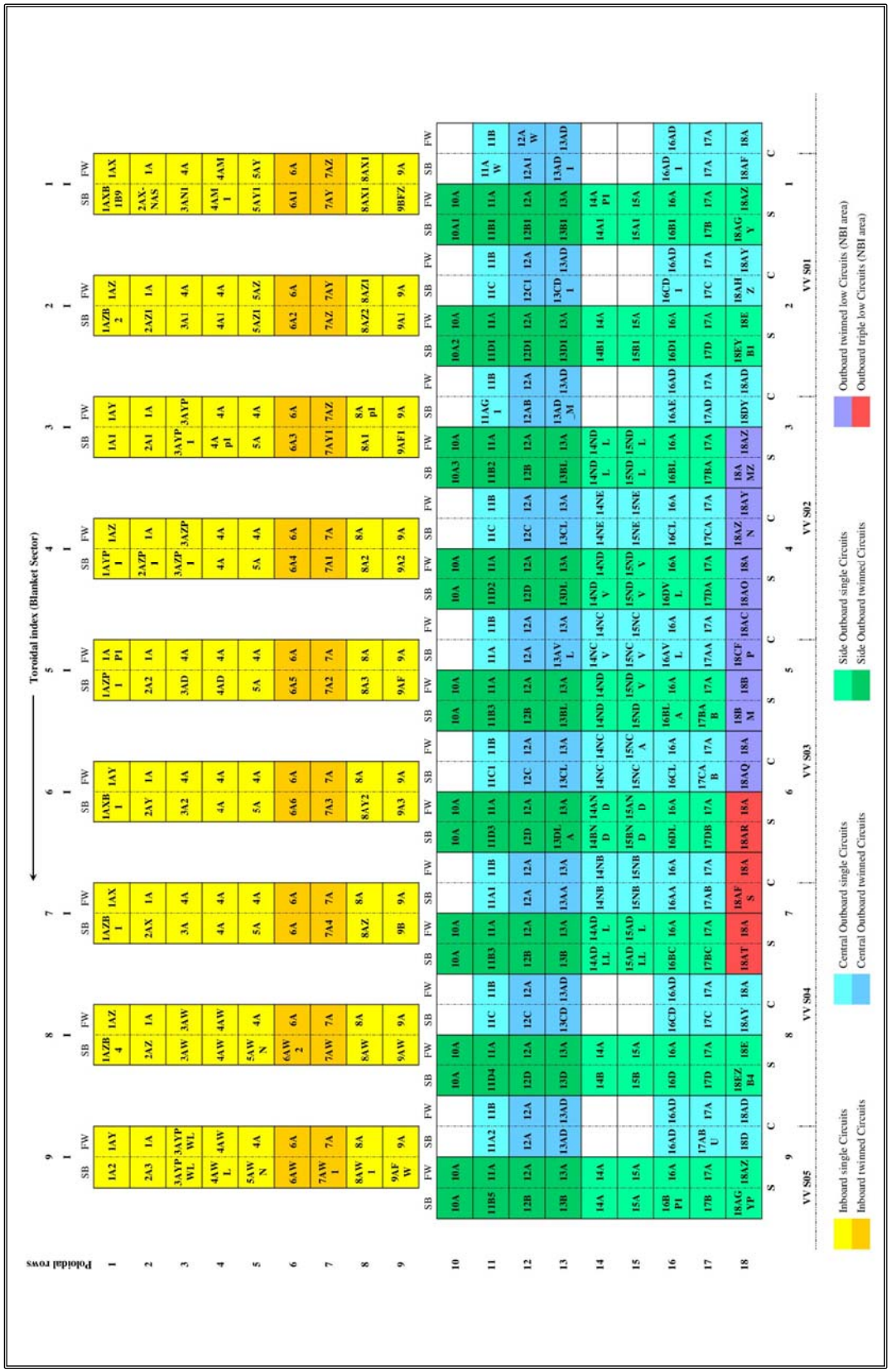

Figure 1.21. Blanket module cooling circuits: blanket sectors 1-9.

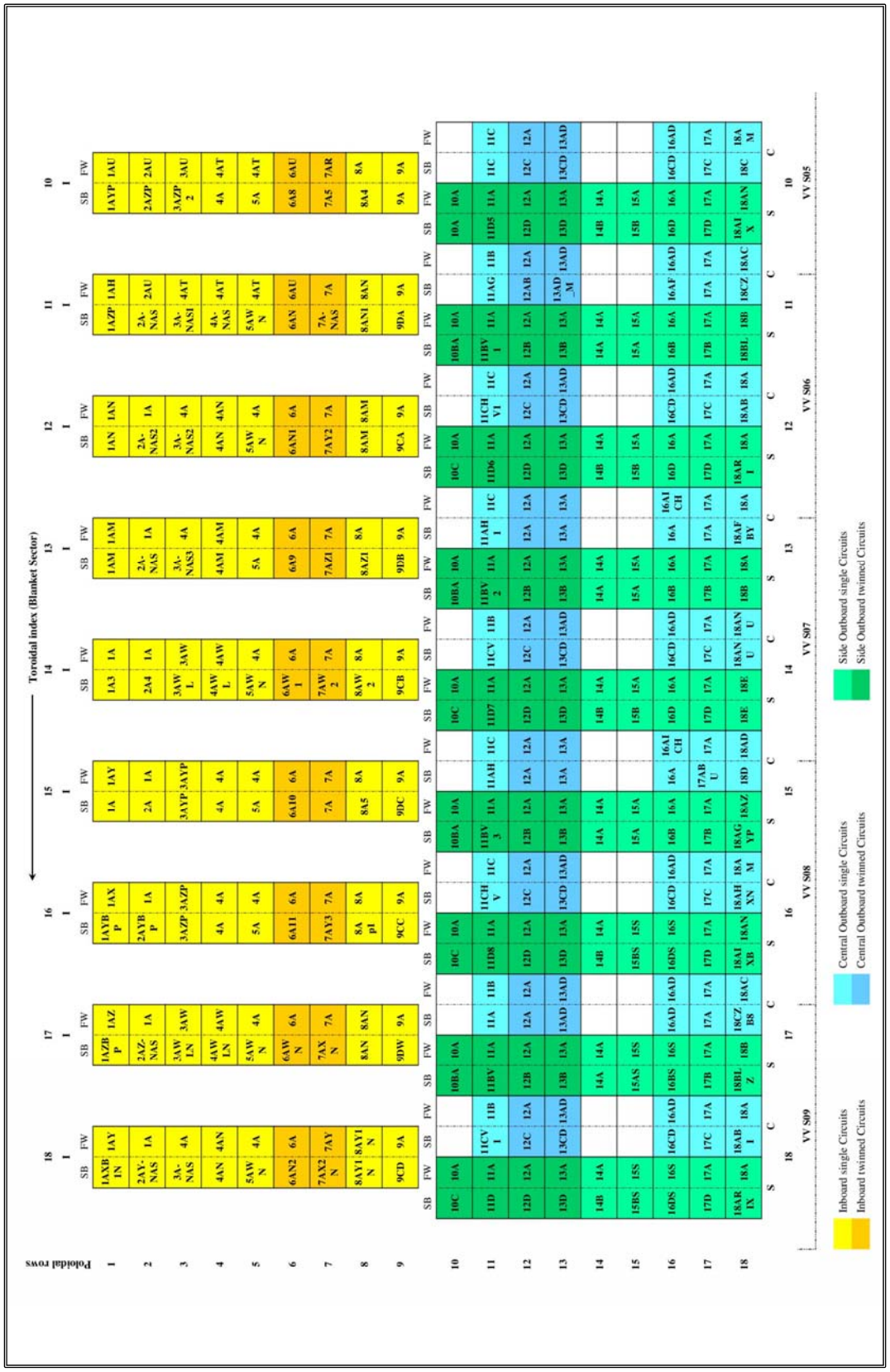

Figure 1.22. Blanket module cooling circuits: blanket sectors 10-18.

1.2.5 Nominal Operating Conditions

The blanket cooling system is cooled by sub-cooled pressurized water, whose inlet temperature and pressure at the URM interface are 70 °C and 4.0 MPa, respectively [1]. The overall nominal coolant mass flow rate amounts to 3140 kg/s. In particular, single blanket module cooling systems are fed with a mass flow rate ranging between 4.7 and 9.6 kg/s, while twinned and triplet blanket module cooling systems are fed by higher mass flow rates up to the maximum value of 18.45 kg/s. A summary of the main thermal-hydraulic operational parameters of the blanket cooling system is reported in Table 1.1, while the mass flow rate (G) distribution calculated by IO for each blanket module cooling circuit is reported in [4].

Table 1.1. Blanket cooling system main operational parameters.

Coolant mass flow rate [kg/s]	3140
Coolant inlet temperature [°C]	70
Coolant outlet temperature [°C]	126
Coolant inlet pressure [MPa]	4.0
Max. in-vessel pressure drop [MPa]	1.35
Max. circuit pressure drop[MPa]	1.60

As a consequence of the extreme heat loads they undergo even under nominal operating conditions, a proper coolant mass flow rate has to be fed to each blanket module cooling circuit in order to effectively remove its nuclear deposited heat power. Insufficient and/or unbalanced mass flow rates may lead to local overheating, which could then result in a water leak in the vessel.

Therefore, according to the safety design margins, it is mandatory to keep unbalancing and/or deviations from the design mass flow rate of each cooling system to a value lower than 10%. This mass flow rate balance among the blanket module cooling systems may be attained uniquely by precisely tuning their pressure drops under nominal operating conditions and minimizing their potential deviations under operational/accidental transient conditions.

To this purpose, flow regulators are foreseen within the UPC plumbing, intended to contribute to its total pressure drop with an adjustable portion of its embedded hydraulic resistance. The feasibility of this solution depends mainly on the difference between the highest and lowest pressure drop values among the blanket module cooling systems. It follows that the precise and reliable assessment of all the blanket module cooling system pressure drops under nominal steady-state conditions represents the prodromal condition for the flow regulators final design and it has to be pursued with the highest priority.

Chapter 2

TECHNICAL BACKGROUND FOR THE ITER BLANKET ANALYSIS CAMPAIGN

2.1 Introduction

Within the framework of the R&D activities promoted by the ITER Organization to investigate the thermal-hydraulic performances of the blanket cooling system in view of its final design, a theoretical research campaign has been carried out at the DEIM on the "Hydraulic Analysis of Blanket Cooling System".

The activity has aimed to investigate numerically the thermal-hydraulic performances of the ITER blanket cooling system under nominal steady-state conditions, evaluating the total pressure drop occurring in each module cooling system, together with its spatial distribution along the main circuital components. Moreover, attention has been paid also to the assessment of coolant flow velocity spatial distribution in the most critical regions of the investigated flow domains. The research activity has been intended to fruitfully contribute to:

- the assessment of the blanket cooling system effectiveness in terms of mass flow rate distribution as well as of total pressure drop acceptability;
- the improvement and potential optimization of the blanket cooling system thermal-hydraulic performances by the assessment of the impact of proposed layout modifications on the investigated cooling circuits steady-state thermal-hydraulic behaviour;
- the identification of the potential need for flow regulators within the blanket module cooling systems in order to balance their coolant mass flow rate distribution.

Due to the modular structure of the blanket module cooling system, the research activity has been carried out following an operative procedure based on the idea of reducing the assessment of its total pressure drop to the proper recombination of those separately calculated for the hydraulic variants of its main components (FW, SB and manifold).

The activity has started in 2015 and, according to CAD models availability, it was originally conceived to last for 48 months, being articulated in five subsequent phases. In particular, each phase concerns the investigation and optimisation of the nominal steady-state thermal-hydraulic performances of the following quasi-definitive (or frozen) cooling circuits:

- 24 SB hydraulic variants;
- 10 FW hydraulic variants;
- 16 inlet/outlet manifold hydraulic variants;

for an overall of 50 frozen hydraulic variants per phase and other still-in-work components. The Ph.D. work has been developed within the context of the first two phases of the activity.

2.2 Methodology

Due to the extreme complexity of the flow domain of the blanket module cooling systems to be investigated, the research activity has been carried out following a theoretical-computational approach based on the finite volume method and adopting a suitable release of the ANSYS CFX Computational Fluid-Dynamic (CFD) code, integrated, whenever needed, by the RELAP5 Mod3.3 thermal-hydraulic system code.

2.2.1 CFD Code

ANSYS CFX is a well-known and qualified CFD code intended to simulate in a fully 3D approach the thermofluid-dynamic behaviour of fluid flows. In particular, it numerically solves the thermofluid-dynamic equations governing the fluid flow over the region of interest with the prescribed boundary conditions by adopting an element-based finite volume method, which is suitable to predict realistically the thermofluid-dynamic behaviour of single-phase, single-component flows both in laminar and turbulent regimes. Its guide [5] provides the complete list of the equations employed by the code. A short summary of equations relevant to the Ph.D. activity is reported in this paragraph. The typical partial differential conservation equations, which describe the behaviour of a Newtonian fluid and are solved by ANSYS CFX, may be written as:

$$\frac{\partial \rho}{\partial t} + \frac{\partial \left(\rho u_j \right)}{\partial x_j} = 0 \qquad \text{continuity equation} \qquad (1)$$

$$\frac{\partial \left(\rho u_i \right)}{\partial t} + \frac{\partial \left(\rho u_i u_j \right)}{\partial x_j} = -\frac{\partial p}{\partial x_i} + \frac{\partial \tau_{ij}}{\partial x_j} + f_i''' \qquad \text{momentum equations} \qquad (2)$$

$$\frac{\partial \left(\rho \, c_p T \right)}{\partial t} - \frac{\partial \left(\rho u_i \, c_p T \right)}{\partial x_i} = \frac{\partial}{\partial x_i} \lambda \frac{\partial T}{\partial x_i} + q''' \qquad \text{energy equation} \qquad (3)$$

with ρ referring to the fluid density, t to the time, u_i to the i-component of vector of velocity, p to the static thermodynamic pressure, T to the static thermodynamic temperature, μ to the dynamic viscosity, c_p to the specific heat capacity, f_i''' to the momentum source, λ to the thermal conductivity (which, in the most general case, is more properly expressed as a tensor λ_{ij}) and q''' to the energy source. If the following "Boussinesq hypothesis" is applied, the viscous stress tensor (τ_{ij}) may be expressed as:

$$\tau_{ij} = \mu\left[\left(\frac{\partial u_i}{\partial x_j} + \frac{\partial u_j}{\partial x_i}\right) - \frac{2}{3}\delta_{ij}\frac{\partial u_k}{\partial x_k}\right] \tag{4}$$

Consequently, integrating equation (2) with equation (4), the momentum equations become the Navier-Stokes equations:

$$\frac{\partial(\rho u_i)}{\partial t} + \frac{\partial(\rho u_i u_j)}{\partial x_j} = -\frac{\partial p}{\partial x_i} + \frac{\partial}{\partial x_j}\left[\mu\left(\frac{\partial u_i}{\partial x_j} + \frac{\partial u_j}{\partial x_i}\right) - \frac{2}{3}\mu\delta_{ij}\frac{\partial u_k}{\partial x_k}\right] + f_i''' \tag{5}$$

Since $\delta_{ij} = 1$ when i = j and is equal to 0 in the other cases, defining a modified pressure (p^*) as:

$$p^* = p + \frac{2}{3}\mu\frac{\partial u_k}{\partial x_k} \tag{6}$$

Equation (5) can be written as:

$$\frac{\partial(\rho u_i)}{\partial t} + \frac{\partial(\rho u_i u_j)}{\partial x_j} = -\frac{\partial p^*}{\partial x_i} + \frac{\partial}{\partial x_j}\mu\left(\frac{\partial u_i}{\partial x_j} + \frac{\partial u_j}{\partial x_i}\right) + f_i''' \tag{7}$$

The conservation equations describe respectively the processes of mass, momentum and energy transfer. Since they can be analytically solved only in a limited range of simple cases, they are generally discretized and solved numerically.

Additionally, the code allows to solve other equations in order to describe other processes (i.e. combustion or diffusion of scalar quantities) as well as to use approximating models, such as the ones devoted to describe turbulence phenomena. The general form of the transport equation for an additional scalable variable Φ is:

$$\frac{\partial(\rho\Phi)}{\partial t} + \frac{\partial(\rho u_i\Phi)}{\partial x_i} = \frac{\partial}{\partial x_i}\Gamma\frac{\partial\Phi}{\partial x_i} + S_\Phi \tag{8}$$

where Γ is the diffusivity and S_Φ the variable source.

The transport equations must be coupled with constitutive equations of state for density and for enthalpy, so to form a closed system. State equations are characterised by the general form:

$$\rho = \rho(p, T) \tag{9}$$

with:

$$c_p = c_p(p, T) \tag{10}$$

Naturally, the form of the state equations depends on the fluid type. For example, for incompressible fluids, density is constant and c_p is at most a function of temperature:

$$\rho = \rho_{const} \tag{11}$$

$$c_p = c_p(T) \tag{12}$$

For an ideal gas, c_p is at most a function of temperature and density is calculated from the ideal gas law:

$$\rho = \frac{w\, p_{abs}}{R_0 T} \tag{13}$$

where w is the molecular weight, p_{abs} is the absolute pressure and R_0 is the universal gas constant. Finally, the equation of state for water and steam properties can be provided by the IAPWS-IF97 library, already implemented in the code. Particularly, the IAPWS database considers five distinct thermodynamic regions for water and steam, namely subcooled water (1), supercritical water/steam (2), superheated steam (3), saturation data (4) and high temperature steam (5), shown in Figure 2.1. During the calculation, water properties are transferred into tabular form and they are evaluated as functions of pressure and temperature.

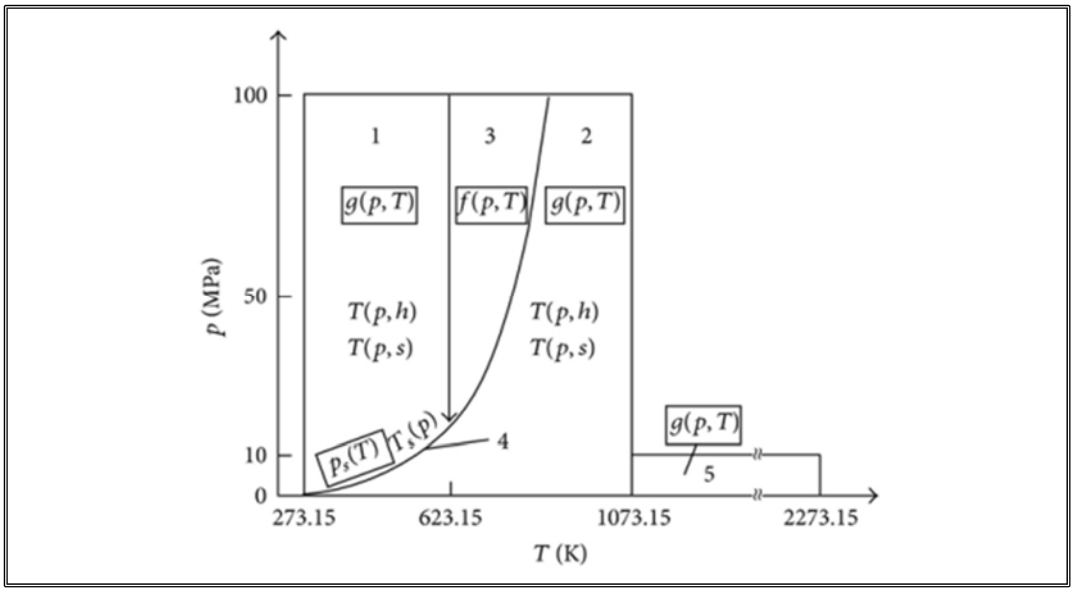

Figure 2.1. Regions and equations of IAPWS IF97 properties.

Turbulent flows behaviour might be directly described by the conservation equations. Nevertheless, since they are characterised by many length and time scales phenomena, prohibitively fine meshes should be set-up in order to describe them effectively. Consequently, statistical turbulence models have been developed and, among them, the k-ε model has been adopted for the following analyses, as explained in [§2.3.1].

As far as statistical turbulence models are concerned, each variable describing a turbulent flow is considered as the sum of a variable, fluctuating component and an average (smoothly varying) component. For example, a velocity component may be decomposed as follows:

$$u_i = \bar{u}_i + u'_i \tag{14}$$

into a time varying component (u'_i) and an average component ($\bar{u}_i$). The latter is obtained as:

$$\bar{u}_i = \frac{1}{\Delta t}\int_t^{t+\Delta t} u_i \, dt \tag{15}$$

where Δt is a time scale that is large if compared to turbulent fluctuations, but small if compared to the analysed transient time scale.

Introducing this division in averaged and fluctuating quantities inside the original Navier-Stokes equations in equation (7) and time averaging these equations, the RANS (Reynolds Averaged Navier-Stokes) equations are obtained ($\bar{p}^*$ has been substituted simply with $\bar{p}$):

$$\frac{\partial\left(\rho\bar{u}_i\right)}{\partial t} + \frac{\partial\left(\rho\bar{u}_i\bar{u}_j\right)}{\partial x_j} = -\frac{\partial\bar{p}}{\partial x_i} + \frac{\partial}{\partial x_j}\left[\mu\left(\frac{\partial\bar{u}_i}{\partial x_j} + \frac{\partial\bar{u}_j}{\partial x_i}\right)\right] - \frac{\partial\left(\rho\overline{u'_i u'_j}\right)}{\partial x_j} + \bar{f}_i''' \tag{16}$$

Once deriving the RANS equations, their system needs to be closed, since Reynolds stresses, defined as $-\rho\overline{u'_i u'_j}$, have introduced new variables.

The closure relations used to evaluate the additional Reynolds stresses define the type of turbulence model. Specifically, RANS turbulence models can be broadly divided into two classes: eddy viscosity models and Reynolds stress models.

The k-ε model belongs to the eddy viscosity turbulence models, which are based on the assumption that in a turbulent flow small eddies are continuously forming and dissipating and that Reynolds stresses can be considered proportional to mean velocity gradients. The following equation illustrates the "eddy viscosity hypothesis", highlighting the relationship between Reynolds stresses and mean velocity gradients as well as μ_t, which represents the turbulent viscosity (also called eddy viscosity):

$$-\rho\overline{u'_i u'_j} = -\frac{2}{3}\rho k\delta_{ij} + \mu_t\left[\left(\frac{\partial\overline{u_i}}{\partial x_j} + \frac{\partial\overline{u_j}}{\partial x_i}\right) - \frac{2}{3}\delta_{ij}\frac{\partial\overline{u_k}}{\partial x_k}\right] \tag{17}$$

where k is the turbulent kinetic energy, defined as:

$$k = \frac{1}{2}\overline{u'^{2}_{i}} \tag{18}$$

Substituting equation (17) into the RANS equations of equation (16), they become:

$$\frac{\partial\left(\rho\overline{u_i}\right)}{\partial t} + \frac{\partial\left(\rho\overline{u}_i\overline{u}_j\right)}{\partial x_j} = -\frac{\partial\tilde{p}}{\partial x_i} + \frac{\partial}{\partial x_j}\left[\left(\mu+\mu_t\right)\left(\frac{\partial\overline{u}_i}{\partial x_j} + \frac{\partial\overline{u}_j}{\partial x_i}\right)\right] + \overline{f}_i''' \tag{19}$$

where:

$$\tilde{p} = \overline{p} + \frac{2}{3}\rho k + \frac{2}{3}\left(\mu+\mu_t\right)\frac{\partial\overline{u_k}}{\partial x_k} \tag{20}$$

Likewise, the Reynolds averaged energy equation and the generic Reynolds averaged transport equation may be expressed respectively as:

$$\frac{\partial\left(\rho\, c_p\,\overline{T}\right)}{\partial t} + \frac{\partial\left(\rho\,\overline{u_i}\, c_p\,\overline{T}\right)}{\partial x_i} = \frac{\partial}{\partial x_i}\left[\left(\lambda + c_p\frac{\mu_t}{\sigma_t}\right)\frac{\partial\overline{T}}{\partial x_i}\right] + \overline{q}''' \tag{21}$$

$$\frac{\partial\left(\rho\overline{\Phi}\right)}{\partial t} + \frac{\partial\left(\rho\overline{u_i}\overline{\Phi}\right)}{\partial x_i} = \frac{\partial}{\partial x_i}\left[\left(\Gamma + \frac{\mu_t}{\sigma_t}\right)\frac{\partial\overline{\Phi}}{\partial x_i}\right] + S_\Phi \tag{22}$$

where σ_t is the Prandtl turbulent number.

Eddy viscosity models are distinguished by the way eddy viscosity (μ_t) is derived. Among them, the two-equation turbulence models are widely used, since they offer a good compromise between numerical effort and computational accuracy.

In particular, the k-ε and the k-ω two-equation models define the turbulent viscosity as the product of a turbulent velocity and turbulent length scale. In two-equation models, the turbulence velocity scale is computed from the turbulent kinetic energy, which is provided from the solution of its transport equation. The turbulent length scale is estimated from two properties of the turbulence field. The k-ε model introduces two new variables into the system of equations. k is the turbulence kinetic energy, it is defined as the variance of the fluctuations in velocity, as shown in equation (18), and it has the dimensions of ($L^2\ T^{-2}$). ε is the rate at which the velocity fluctuations dissipate (the turbulence eddy dissipation) and has dimensions of k per unit time ($L^2\ T^{-3}$).

The k-ε model assumes that μ_t is linked to the turbulence kinetic energy and dissipation via the Prandtl-Kolmogorov relation:

$$\mu_t = C_\mu \rho \frac{k^2}{\varepsilon} \tag{23}$$

where C_μ is a k-ε turbulence model constant (amounting to 0.09).

The values of k and ε are derived from their differential transport equations:

$$\frac{\partial(\rho k)}{\partial t} + \frac{\partial\left(\rho \overline{u_i} k\right)}{\partial x_i} = \frac{\partial}{\partial x_i}\left[\left(\mu + \frac{\mu_t}{\sigma_k}\right)\frac{\partial k}{\partial x_i}\right] + P_k - \rho\varepsilon \tag{24}$$

$$\frac{\partial(\rho \varepsilon)}{\partial t} + \frac{\partial\left(\rho \overline{u_i} \varepsilon\right)}{\partial x_i} = \frac{\partial}{\partial x_i}\left[\left(\mu + \frac{\mu_t}{\sigma_\varepsilon}\right)\frac{\partial \varepsilon}{\partial x_i}\right] + \frac{\varepsilon}{k}\left(C_{\varepsilon 1} P_k - C_{\varepsilon 2}\rho\varepsilon\right) \tag{25}$$

where $C_{\varepsilon 1}$, $C_{\varepsilon 2}$, σ_k and σ_ε are k-ε turbulence model constants (amounting respectively to 1.44, 1.92, 1.0 and 1.3) and P_k is the turbulence production due to viscous forces.

The k-ε model effectively describes the behaviour of a turbulent flow in a wide range of application. Nevertheless, it is not applicable to the fluid in near-wall regions, especially in the viscous laminar sub-layer. This problem could be overcome either adopting the k-ω model or by means of the so-called wall functions. The k-ω model, along with the turbulence kinetic energy k, introduces the transport equation of the turbulent frequency ω, which has the dimensions of (T^{-1}) since it could be assumed proportional to ε/k. k and ω transport equations result:

$$\frac{\partial(\rho k)}{\partial t} + \frac{\partial\left(\rho \overline{u_i} k\right)}{\partial x_i} = \frac{\partial}{\partial x_i}\left[\left(\mu + \frac{\mu_t}{\sigma_k}\right)\frac{\partial k}{\partial x_i}\right] + P_k - \beta'\rho k\omega \tag{26}$$

$$\frac{\partial(\rho \omega)}{\partial t} + \frac{\partial\left(\rho \overline{u_i} \omega\right)}{\partial x_i} = \frac{\partial}{\partial x_i}\left[\left(\mu + \frac{\mu_t}{\sigma_\omega}\right)\frac{\partial \omega}{\partial x_i}\right] + \frac{5}{9}\frac{\omega}{k} P_k - \beta\rho\omega^2 \tag{27}$$

where P_k is still the turbulence production due to viscous forces and β', σ_k, β and σ_ω are k- ω turbulence model constants (amounting respectively to 0.09, 2, 0.075 and 2 in the Wilcox model formulation). Also, the Prandtl-Kolmogorov relation in equation (23) is substituted by:

$$\mu_t = \frac{\rho k}{\omega} \tag{28}$$

On the other hand, wall functions have been devised as analytical expressions which describe the fluid thermal and velocity profile in near-wall regions. One of the major drawbacks of the classical wall-function approach is that the predictions depend on the location of the point nearest to the wall and are sensitive to the near-wall meshing. This problem has been overcome

by ANSYS CFX developing a scalable wall function, which can be applied on arbitrarily fine meshes and allows to perform a consistent mesh refinement independent of the Reynolds number of the application. Since the k-ε model offers a good compromise in terms of accuracy and robustness [6], as far as the calculations described in the following chapters of this thesis are concerned, the k-ε model with scalable wall functions has been adopted.

2.2.2 System Code

RELAP5 is a quasi-2D thermal-hydraulic system code, developed at Idaho National Engineering Laboratory and apt to well describe the thermal-hydraulic behaviour of a single-component, two-phase system, in presence of a non-volatile solute and a non-condensable gas. It is typically employed in the numerical simulation of light water fission reactor thermal-hydraulic transients. Nevertheless, its generic modelling philosophy permits simulating a variety of thermal hydraulic systems and allows it to be used also in fusion relevant applications.

The two-fluid equations of motion that are used as the basis for the RELAP5 hydrodynamic model are formulated in terms of volume and time-averaged parameters of the flow. The system model is solved numerically using a semi-implicit finite-difference technique. Phenomena that depend upon transverse gradients, such as friction and heat transfer, are formulated in terms of the bulk properties using empirical transfer coefficient formulations. In situations where transverse gradients cannot be represented within the framework of empirical transfer coefficients, such as subcooled boiling, additional models specially developed for the particular situation are employed. The RELAP5 thermal-hydraulic model solves eight field equations. The primary dependent variables are pressure, phasic specific internal energies, vapour volume fraction, phasic velocities, non-condensable quality, and boron density. The independent variables are time and distance. The secondary dependent variables used in the equations are phasic densities, phasic temperatures, saturation temperature and non-condensable mass fraction in non-condensable gas phase for the i-th non-condensable species.

Fluid properties are calculated from thermodynamic tables that tabulate saturation properties as a function of temperature, saturation properties as a function of pressure and single-phase properties as a function of pressure and temperature. The properties and derivatives in the tables are saturation pressure, saturation temperature, specific volume, specific internal energy and three derivatives (i.e. the isobaric thermal expansion coefficient, the isothermal compressibility, and the specific heat at constant pressure). The constitutive relations include models for defining flow regimes and flow-regime-related models for interphase drag and shear, the coefficient of virtual mass, wall friction, wall heat transfer, interphase heat and mass transfer and direct (sensible) heat transfer. The constitutive relations, in general, include flow regime effects for which simplified mapping techniques have been developed to control the use of constitutive relation correlations. The detailed description of code equations, models and procedures is out of the scope of this thesis and may be found in its manual [7].

2.3 Operative Procedure

According to the description of the methodology selected to carry out the activity, in order to investigate numerically the nominal steady-state thermal-hydraulic behaviour of the ITER blanket cooling system, a fully 3D steady-state CFD analysis should have been run for each blanket module cooling system. Anyway, the extreme complexity and the wide extension of each blanket module cooling system together with the need to guarantee a minimum mesh spatial density, to be considered mandatory in order to have realistic and reliable numerical solutions, would have implied the development of a very complex finite volume model of each flow domain. This model would have been hard to manage, resulting likely in very long calculation times.

Therefore, a further and more efficient operative procedure has been conceived in order to avoid too lengthy and unmanageable CFD analyses.

The proposed operative procedure is based on the aforementioned observation [§2.1] relevant to the modular structure of a blanket module cooling system. Its particular arrangement indeed suggests the possibility to split the assessment of the thermal-hydraulic performances of a single cooling system into the separate assessment of the performances of its four main hydraulic components in a stand-alone configuration.

This approach results in running a set of 4 separate CFD analyses instead of the single analysis of the whole cooling system. As a consequence, each analysis regards a simpler finite volume model, thus implying the need for sensibly lower calculation time and resources. The target total pressure drop of the single blanket module cooling system at its nominal mass flow rate is finally assessed by simply summing the total pressure drops calculated for its main hydraulic components under the same conditions.

Nevertheless, it has to be underlined that this procedure could imply a slight error in the assessment of the total pressure drop, due to the common assumption of fully developed flow conditions at inlet/outlet sections of each component that results to be un-realistic as they are actually connected to their neighbouring circuital components. Anyway, this error may be considered negligible, in a first-order approximation, if compared to the overall pressure drop to be assessed.

According to the described strategy, the following operative procedure has been settled for each single hydraulic variant of the blanket module cooling system main components (inlet manifold, FW cooling circuit including FPs, SB cooling circuit including coaxial connector cup, outlet manifold):

- identification of all the blanket module cooling systems to which the hydraulic variant belongs;
- determination of the set of N nominal mass flow rates relevant to the aforementioned blanket module cooling systems;

- development of a finite volume model of the hydraulic variant under consideration on the basis of the pertaining CATIA model provided by IO;
- performing of the N steady-state fully 3D CFD analyses of the hydraulic variant at the relevant N different nominal mass flow rates previously selected;
- calculation of the N total pressure drops across the hydraulic variant at the N different nominal mass flow rates previously selected and, consequently, relevant to the N different blanket module cooling systems interested by the hydraulic variant under consideration;
- calculation of the total pressure drops of all the single blanket module cooling systems, by properly combining the previously calculated pressure drops of all the investigated hydraulic variants.

In case of twinned or triplet blanket modules cooling systems, the main hydraulic components of the cooling system are no more connected in series and, as a consequence, this procedure may not be directly applied without a proper modification.

In fact, the parallel connection of twinned or triplet blanket modules cooling circuits implies that the coolant mass flow rate through each of them would be initially unknown, depending on the hydraulic resistance of all the others. In these cases, a purposely-modified procedure has been conceived that relies on the combined use of the ANSYS CFX and the RELAP5 codes.

The proposed modified procedure foresees first the assessment of the hydraulic characteristic function of each single blanket module cooling circuit connected in parallel:

$$\Delta p = \Delta p(G) \tag{29}$$

that gives the functional dependence of the total pressure drop along the module cooling circuit on the corresponding mass flow rate under steady-state conditions. This function is derived by summing the hydraulic characteristic functions of the FW and SB hydraulic variants composing the blanket module cooling circuit, obtained by means of dedicated parametric ANSYS CFX CFD analyses. The characteristic function of the i-th module cooling circuit results, hence, to be given by:

$$\Delta p_i(G) = \Delta p_i^{FW}(G) + \Delta p_i^{SB}(G) \tag{30}$$

Later on, the characteristic functions are used to simulate the whole twinned or triplet blanket modules cooling system with the RELAP5 thermal-hydraulic system code. In particular, they allow to set-up the cooling system 1D finite volume model, where the i-th module cooling circuit is modelled as a concentrated hydraulic resistance whose effective concentrated loss factor, $K_i(G)$, may be derived by imposing that its corresponding concentrated pressure drop, given by:

$$\Delta p_i^{conc}(G) = \frac{K_i(G)}{2\rho A_i^2} G^2 \tag{31}$$

with ρ representing the coolant density and A_i the flow area, might equal that calculated with a CFD approach for the i-th module cooling circuit under the same mass flow rate. It follows that:

$$K_i(G) = 2\rho A_i^2 \frac{\Delta p_i(G)}{G^2} \tag{32}$$

The concentrated hydraulic resistances of both the inlet and outlet multiple-way connections of the considered twinned or triplet blanket modules cooling system depend on mass flow rate branching and, as a first attempt, they are calculated according to the indications given in [8] assuming the reference values of the nominal mass flow rates through each blanket module cooling circuit.

Once set-up the 1D finite volume model, a zero-order analysis is run in order to assess the coolant mass flow rate distribution among the blanket modules cooling circuits. The zero-order mass flow rate branching calculated is therefore compared against the nominal one and, in case the deviations between calculated and nominal mass flow rate would exceed the limit value of 0.1%, next iteration is launched.

The calculated mass flow rates are given in input as either outlet or inlet boundary conditions of CFD analyses dedicated, respectively, to inlet and outlet manifolds, allowing to derive the effective concentrated loss factors relevant to the inlet and outlet multiple-way connections according to the calculated zero-order mass flow rates. These factors are then implemented in the 1D finite volume model and the first-order analysis is run to assess the corresponding coolant mass flow rate distribution among the blanket modules cooling circuits. Whether deviations between previous and updated mass flow rates would exceed the limit value of 0.1%, next iteration is launched, repeating this iterative procedure until the convergence criterion is matched.

Finally, CFD analyses are run for the hydraulic variants composing the twinned or triplet blanket modules cooling circuits at the pertaining calculated mass flow rates in order to assess their actual steady-state total pressure drops when connected in parallel to the twinned or triplet blanket modules cooling system.

2.3.1 CFD Analysis Procedure

The set-up of the finite volume model of each single hydraulic variant and the development of its CFD analysis under nominal steady conditions have been carried out according to the ITER blanket hydraulic calculation guidelines reported in [9], properly integrated with the findings of a series of preliminary sensitivity analyses thoroughly described in the following.

In particular, the finite volume model set-up has been articulated in the following steps:

- flow domain discretization;

- constitutive model definition;
- loads and boundary conditions definition;
- turbulence model definition.

The flow domain discretization has been carried out importing, by means of the ANSYS Design Modeler tool, the CAD file modelling the coolant flow domain of the hydraulic variant to be analysed. Before proceeding to the discretization, as typically recommended, small geometrical structures, which require a very dense mesh to be adequately modelled and whose contribution to the overall thermal-hydraulic behaviour of the circuit may be considered negligible, have been removed in such a way to reduce the geometrical complexity of the domain to be discretized, thus simplifying the meshing process. To this purpose, a significant simplification is produced by the removal of the hypervapotron teeth in the EHF FWs, strongly recommended in order to ease the discretization step against an acceptable deviation in the predicted total pressure drop. Since calculation time strongly depends on the mesh density and topology and, on the other hand, a poor mesh may result in un-realistic predictions, a sensitivity analysis has been carried out to select a mesh fine enough to give stable predictions with a further increase of its density and acceptable calculation times. Typically, a good compromise between results accuracy and calculation time is obtained generating meshes with a node density ranging between 10^7 and 10^8 node/m^3 for FW and SB cooling circuits and between 10^6 and 10^7 for manifolds, with "relevance centre" parameter set to "Medium" or "Fine".

A particular attention has been paid to the discretization of the "near wall" region of the flow domain where, due to the fluid-wall interactions, complex transport processes take place inducing the formation and stabilization of the thermofluid-dynamic boundary layer, which deeply affects the insurgence of distributed pressure drops. In order to realistically simulate these processes and their effects on the flow behaviour, that typically result in very intense velocity gradients in the wall normal direction, inflation layers have been used, since they allow the discretization with elements following the wall shape with a normal thickness ranging from tens of micrometres up to 1 mm. According to the typical dimensions of the hydraulic variants flow domain, a sensitivity analysis [§2.4.1] has highlighted that 10 inflation layers with a normal thickness growing geometrically with ratio 1.41 are enough to obtain a realistic simulation of "near-wall" region processes, at least as far as pressure drop predictions are concerned. Anyway, it has to be underlined that the flow domain geometry deeply affects mesh dimensions, so mesh density has been defined on a case base. The selected modelling strategy allows to complete a single variant cooling circuit CFD analysis in a timeframe that normally ranges from three to five days.

Concerning the constitutive model definition, the water thermofluid-dynamic properties defined in the IAPWS IF97 library, already implemented in the code and previously described in [§2.2.1], have been adopted.

As to the loads and Boundary Conditions (BCs) definition, the presence of the gravity field has not been taken into account. Moreover, at the circuit inlet section the total pressure value has been generally imposed. In particular, ANSYS CFX solves the CFD equations in terms of relative pressure and the absolute pressure is simply calculated as the sum of the relative and the reference pressures. A common practice has been to set the reference pressure to a value close to the average absolute pressure in the whole circuit, in order to reduce round-off errors and pressure wiggles. Furthermore, at the outlet section the target mass flow rate has been typically imposed. The interface between the coolant and the circuit steel walls has been modelled by means of a no-slip condition together with a proper "wall function" algorithm, which allows modelling the fluid-wall interaction effects on the overall total pressure drop. Wall functions simplify the simulation of the complex transport processes that take place in the thermofluid-dynamic boundary layer and, consequently, contribute to save calculation time. In addition, a proper wall roughness value of 15 μm has been agreed with the IO, even though it has been proved that it does not dramatically affects the overall total pressure drop.

Finally, since the increase of coolant temperature envisioned between the inlet and the outlet sections of each cooling circuit is 56°C, isothermal flow conditions have been assumed, setting the coolant temperature to the average value of 98°C. In this way, since pressure drop is not strongly affected by limited temperature variations, energy equation has not been solved thus reducing calculation time without incurring in un-realistic predictions.

Concerning turbulence treatment, the k-ε model has been adopted (as disclosed before in [§2.2.1]) because it offers a good compromise in terms of accuracy and robustness, being recommended for general-purpose simulations [6]. In addition, this model uses the scalable wall-function approach overcoming the drawbacks of the standard wall functions. As to the timescale parameters, the auto timescale option has been selected adopting a maximum value of 10^{-2} s, which may be reduced up to $10^{-3} \div 10^{-5}$ s in order to reach a final converged state.

Once set-up the finite volume model, the analysis settings are properly defined. In particular, steady-state analyses have been carried out adopting the ANSYS CFX "false transient" algorithm to speed-up convergence of numerical simulations.

Initial values can be set automatically if a good initial guess is not known or is not required. Although accurate initial values may not always be available, a good approximation can speed up a steady-state simulation, reducing the chance that its solution fails to converge due to diverging residuals. The more complicated are simulation and models adopted, the more pivotal is to start the solution process with sensible initial values. For this reason, it has been decided to get an initial solution with a less accurate numerical scheme and signally the "upwind" one, properly tuning the maximum time-scale parameter. It has then been implemented as initial condition into a further CFD analysis, to be carried out with the more accurate "high resolution" advection numerical scheme, in order to obtain the more reliable final thermofluid-dynamic solution. As to the calculation time, it depends mainly on the number of nodes and on whether

and how the ANSYS High Performance Computing (HPC) is used. Increasing the number of mesh nodes obviously rises calculation time. On the other hand, ANSYS HPC supports parallel processing, so it has been used to speed-up large numerical analyses.

Finally, once defined analysis settings and convergence controls, the analysis is launched and, once finished, results are easily post-processed with a particular reference to flow velocity field (v), static (p_S) and total pressure (p_T) fields and mass flow rate distribution (G). In particular, the following variables are typically calculated with reference to a generic cross section, A, of the flow domain:

$$u = \frac{1}{A}\iint_A \underline{v}\cdot\underline{n}\,dA \qquad \text{average flow velocity} \qquad (33)$$

$$G = \iint_A \rho\underline{v}\cdot\underline{n}\,dA \qquad \text{mass flow rate} \qquad (34)$$

$$p_T = p_S + \frac{1}{2}\rho\underline{v}\cdot\underline{v} \qquad \text{local total pressure} \qquad (35)$$

$$p = \frac{1}{A}\iint_A p_T\,dA \qquad \text{average total pressure} \qquad (36)$$

where ρ is the coolant density. It hence follows that the total pressure drop of the coolant between the two sections i and j has to be calculated as follows:

$$\Delta p_{ij} = p_i - p_j \qquad \text{total pressure drop} \qquad (37)$$

representing the variation in volumetric density of energy that the coolant experiences flowing between the aforementioned sections due to friction and non-reversible (turbulence) processes, deprived of the gravitational contribution due to the assumption of no gravity loads. In order to take into account the gravitational effect on the total pressure drop between the two sections i and j, the following expression of the overall total pressure drop, (Δp^{grav}) has been calculated by hand in the post-processing phase:

$$\Delta p_{ij}^{grav} = \left(p_i + \rho g z_i\right) - \left(p_j + \rho g z_j\right) \qquad \text{overall total pressure drop} \qquad (38)$$

where z_i and z_j are the vertical coordinates of centroids of sections A_i and A_j, respectively.

A particular attention has been paid in the post-processing phase to the selection of the sections where flow variables had to be averaged. They have been preferably located in correspondence to those flow regions where fully developed flow conditions are nearly attained, so to minimize the dependence of averaged variables on the local distribution of flow velocity field. Moreover, the interface sections of the neighbouring variants have been located exactly in the same positions, avoiding any error due to either missing (pressure drop underestimation) or overlapping (pressure drop overestimation) segments of circuits.

2.4 Preliminary Sensitivity Analyses

The overall dimensions of the blanket module cooling systems, compared to the typical length scale of the hydraulic phenomena that take place within their channels, makes the CFD methodology somewhat borderline applicable. Therefore, sensitivity analyses have been preliminarily carried out aiming to assess the predictive potential of the code in fusion-relevant application. Furthermore, the minimum node density together with the best mesh topology and inflation layers' arrangement (in terms of layers' number, first layer thickness and layers growth rate) have been settled in order to obtain realistic and reliable numerical predictions without incurring in too lengthy calculation time.

Specifically, the most peculiar topological structure of the ITER blanket cooling system have been investigated, i.e. the straight channel and the hypervapotron.

In addition, a single EHF blanket module finger cooling circuit has been studied in order to assess whether hypervapotron channels might be simplified, thus strongly reducing calculation time for EHF blanket FW cooling circuit.

2.4.1 Straight Channel

A sensitivity analysis campaign has been carried out first on a horizontal straight channel (Figure 2.2) whose characteristic dimensions and flow conditions have been drawn from the SB cooling circuit and have been reported for the sake of clarity in Table 2.1.

Numerical results obtained in terms of total pressure drop across the test section length, where fully developed flow conditions are predicted, have been compared with those calculated according to the well-known equation:

$$\Delta p_{Correlation} = \lambda \frac{L_{ts}}{D} \rho \frac{u^2}{2} \tag{39}$$

adopting the Zigrang and Sylvester form of the Colebrook-White equation for the friction factor λ [10].

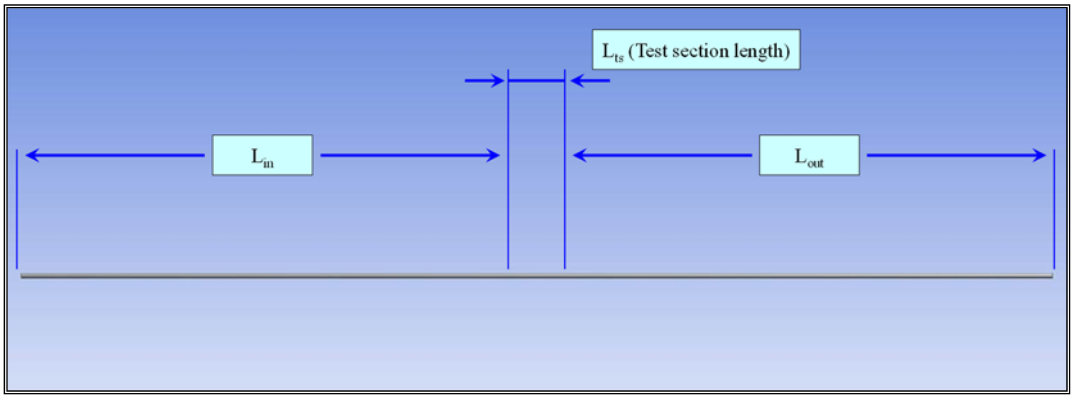

Figure 2.2. Straight channel geometry.

Table 2.1. Straight channel data.

D [m]	0.01
L_{ts} [m]	0.10
L_{in} [m]	1.0
L_{out} [m]	1.0
Mass flow rate [kg/s]	1.0
Velocity [m/s]	12.76
Reynolds number	$1.27 \cdot 10^5$
Wall roughness [μm]	15
$\Delta p_{Correlation}$ [kPa]	19.08

In a first phase, attention has been devoted to the assessment of the best mesh topology to be implemented for the calculation campaign. To this purpose, the following mesh topologies have been considered, assuming in any case no inflation layers:

- hexahedrons sweep;
- multizone;
- tetrahedrons;
- wedges sweep.

For each mesh topology investigated, a parametric analysis has been carried out articulated in six independent CFD analyses characterized by the geometric discretizations shown in figs. from Figure 2.3 to Figure 2.6 and by the increasing node densities reported in Table 2.2.

Table 2.2. Mesh node density [m^{-3}].

Mesh topology	**Model 1**	**Model 2**	**Model 3**	**Model 4**	**Model 5**	**Model 6**
Hexaedrons sweep	$1.46 \cdot 10^7$	$1.93 \cdot 10^8$	$4.95 \cdot 10^8$	$1.95 \cdot 10^9$	$2.32 \cdot 10^9$	$2.02 \cdot 10^{10}$
Multizone	$1.37 \cdot 10^8$	$2.15 \cdot 10^8$	$3.88 \cdot 10^8$	$7.41 \cdot 10^8$	$1.06 \cdot 10^9$	$9.81 \cdot 10^9$
Tetrahedrons	$1.06 \cdot 10^8$	$1.60 \cdot 10^8$	$3.91 \cdot 10^8$	$8.20 \cdot 10^8$	$1.22 \cdot 10^9$	$8.04 \cdot 10^9$
Wedges sweep	-	$1.25 \cdot 10^8$	$2.92 \cdot 10^8$	$6.22 \cdot 10^8$	$1.01 \cdot 10^9$	$9.14 \cdot 10^9$

The numerical results obtained in terms of total pressure drops predicted across the test section length together with the corresponding experimental value, calculated according to equation (39), are reported in figs. from Figure 2.7 to Figure 2.10 versus the node density.

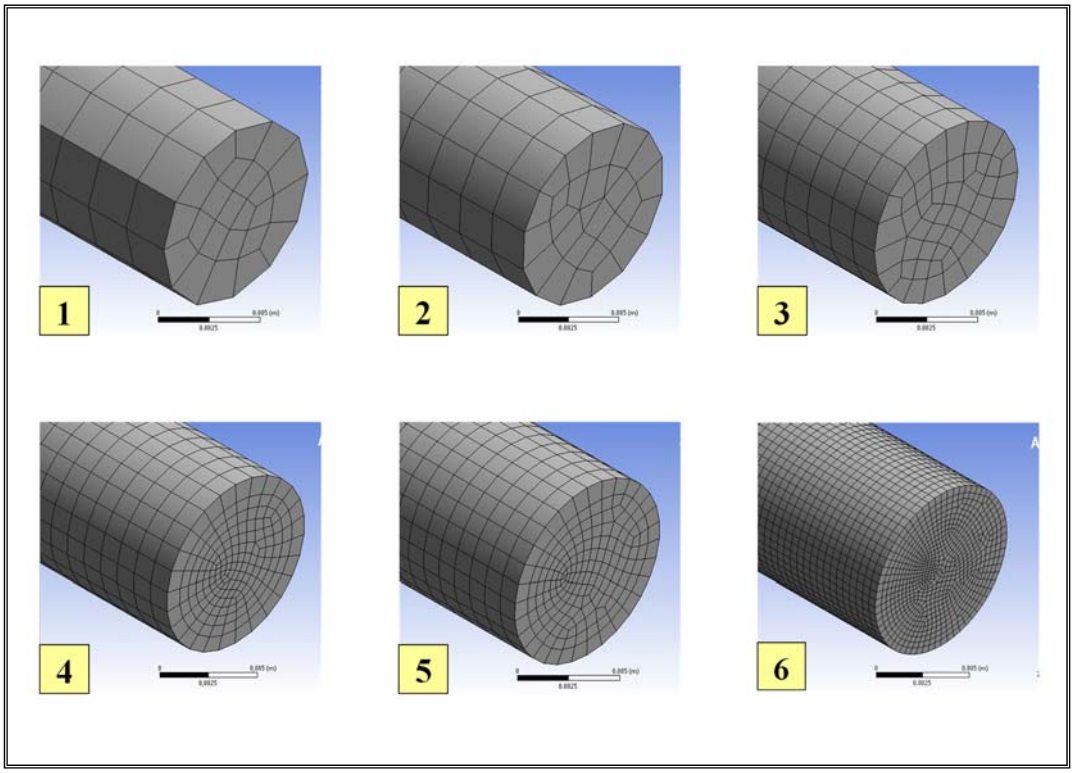

Figure 2.3. Hexahedrons sweep meshes investigated.

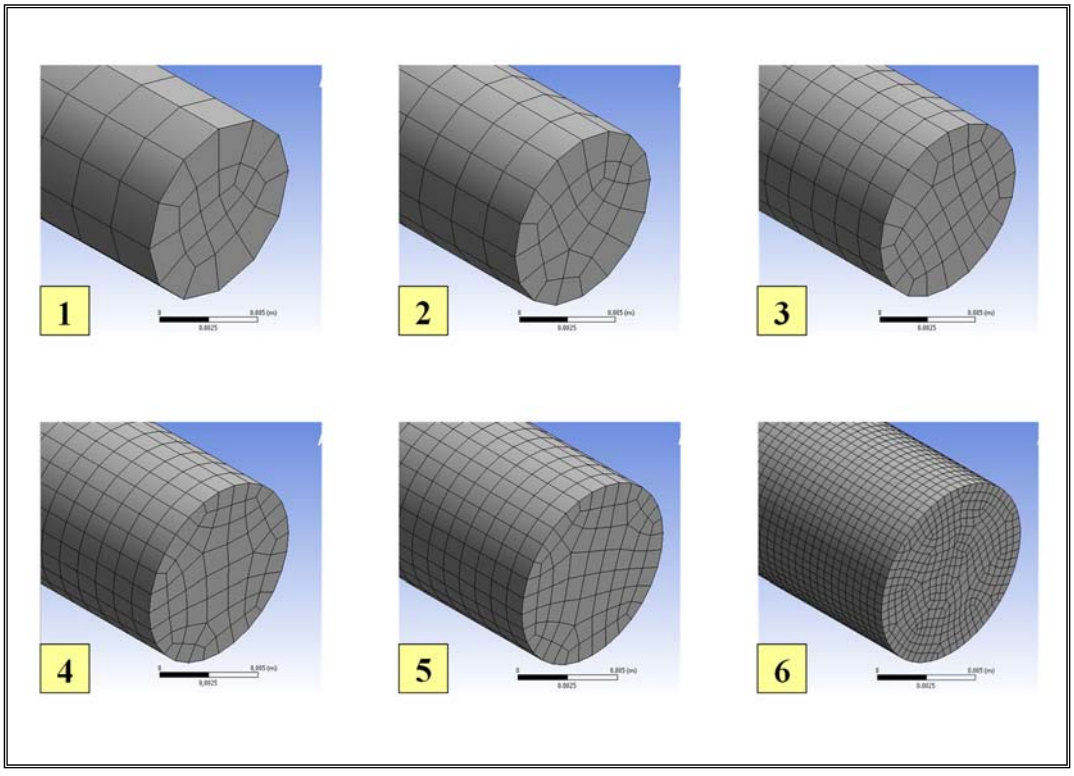

Figure 2.4. Multizone meshes investigated.

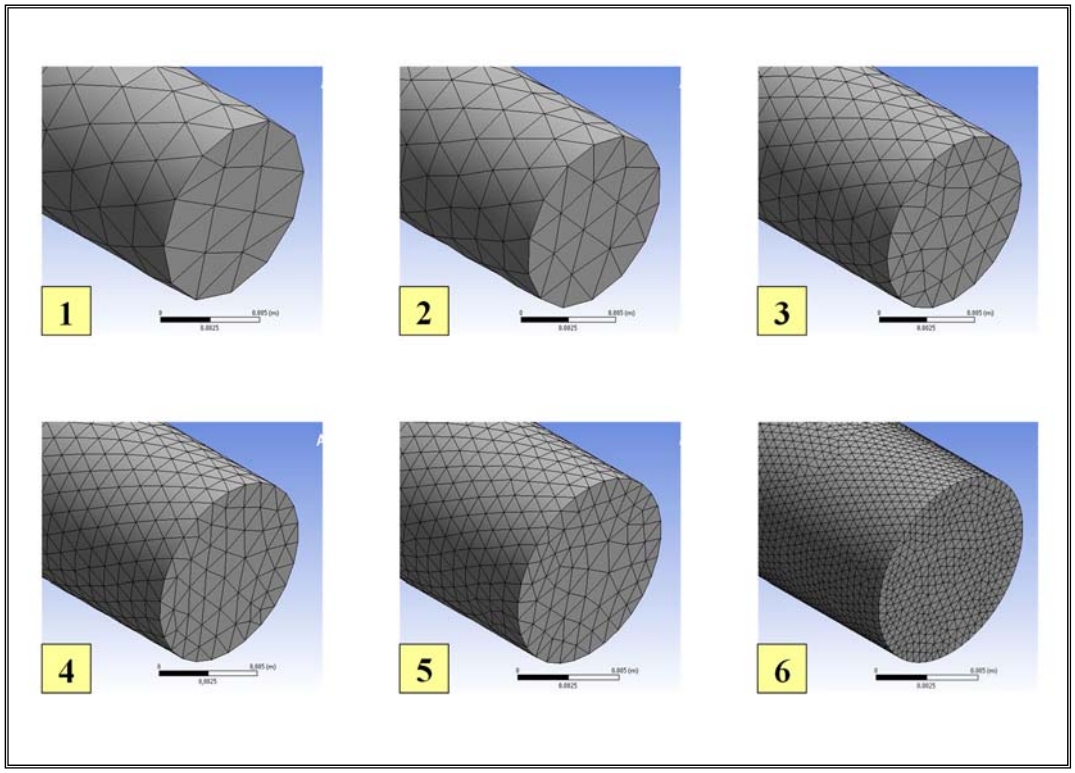

Figure 2.5. Tetrahedrons meshes investigated.

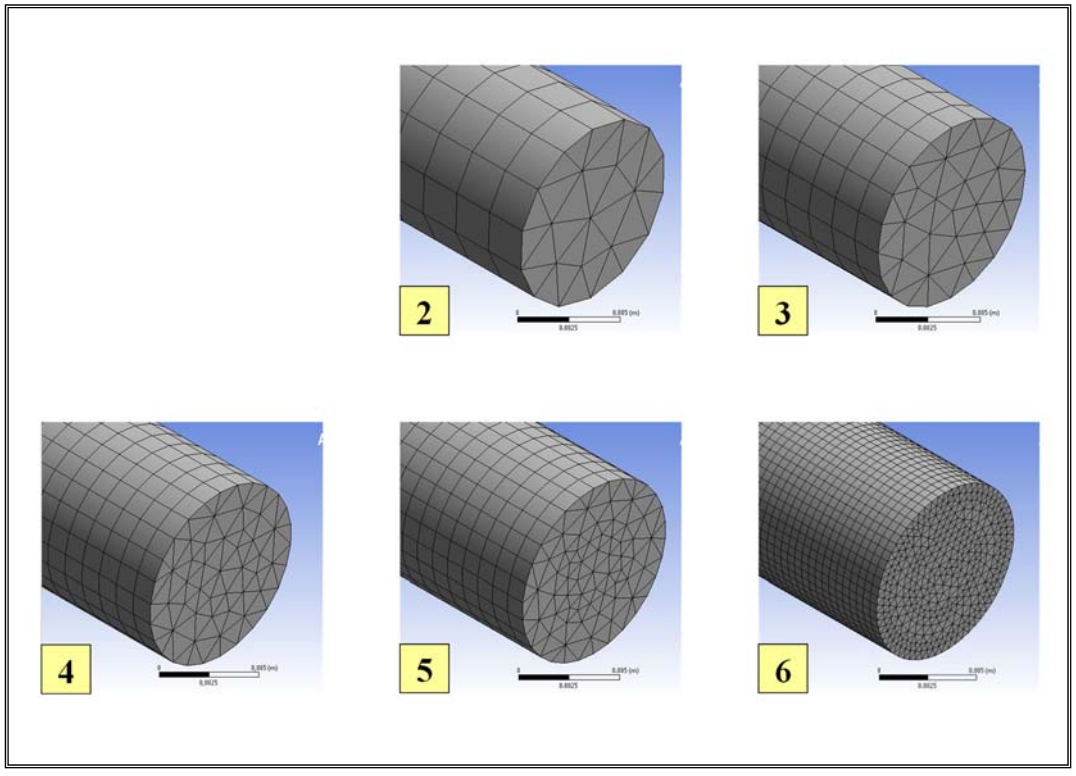

Figure 2.6. Wedges sweep meshes investigated.

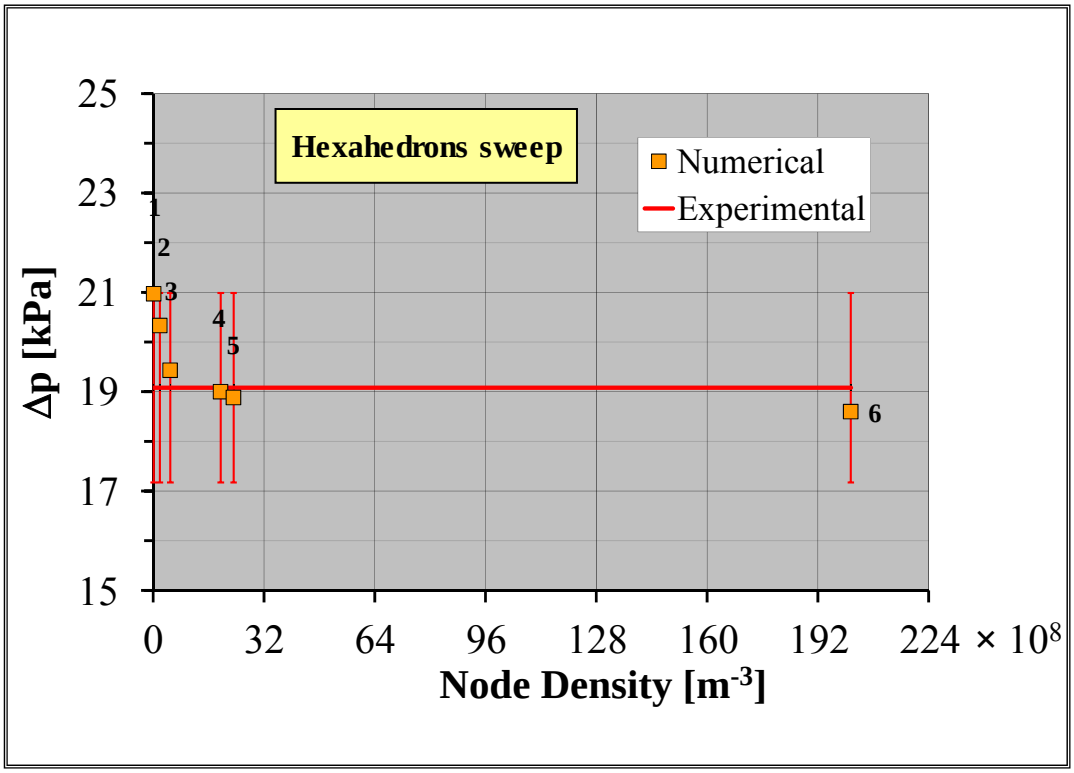

Figure 2.7. Hexahedrons sweep mesh total pressure drop predictions.

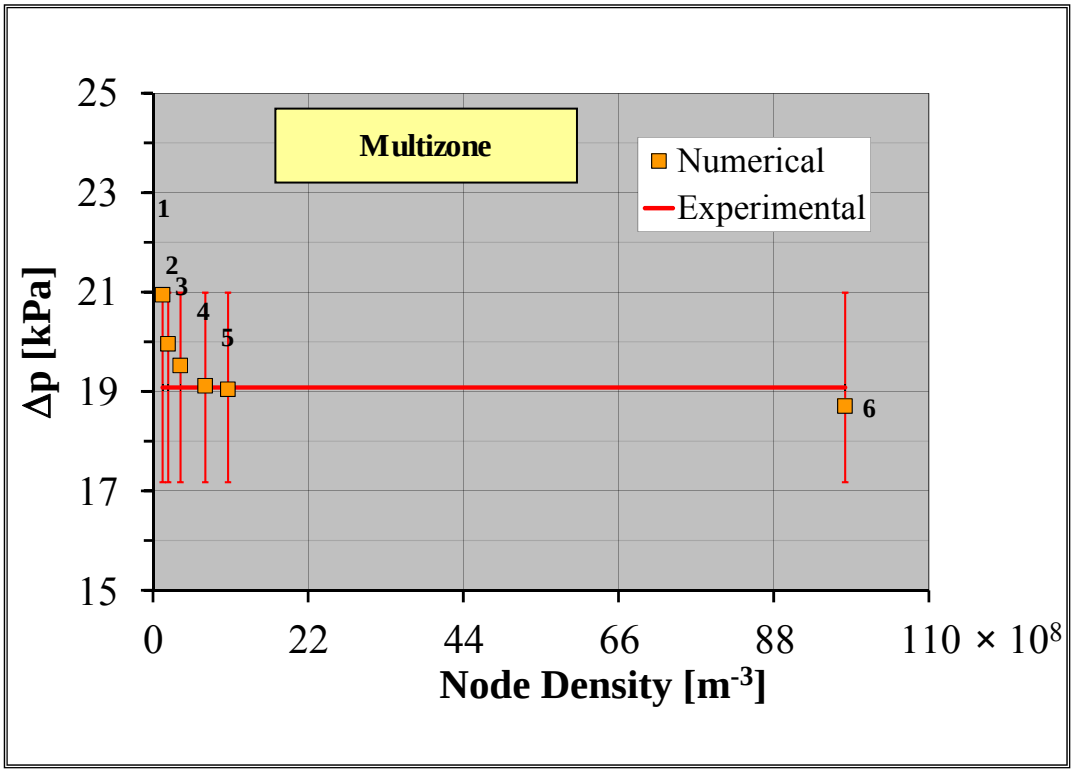

Figure 2.8. Multizone mesh total pressure drop predictions.

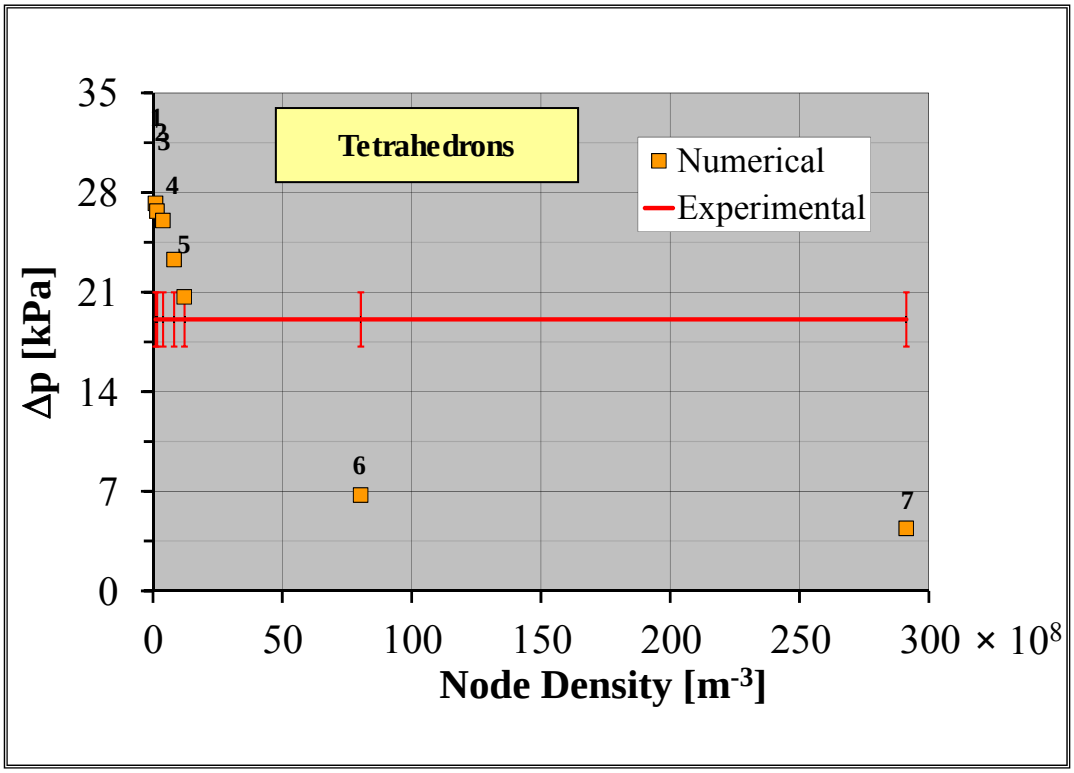

Figure 2.9. Tetrahedrons mesh total pressure drop predictions.

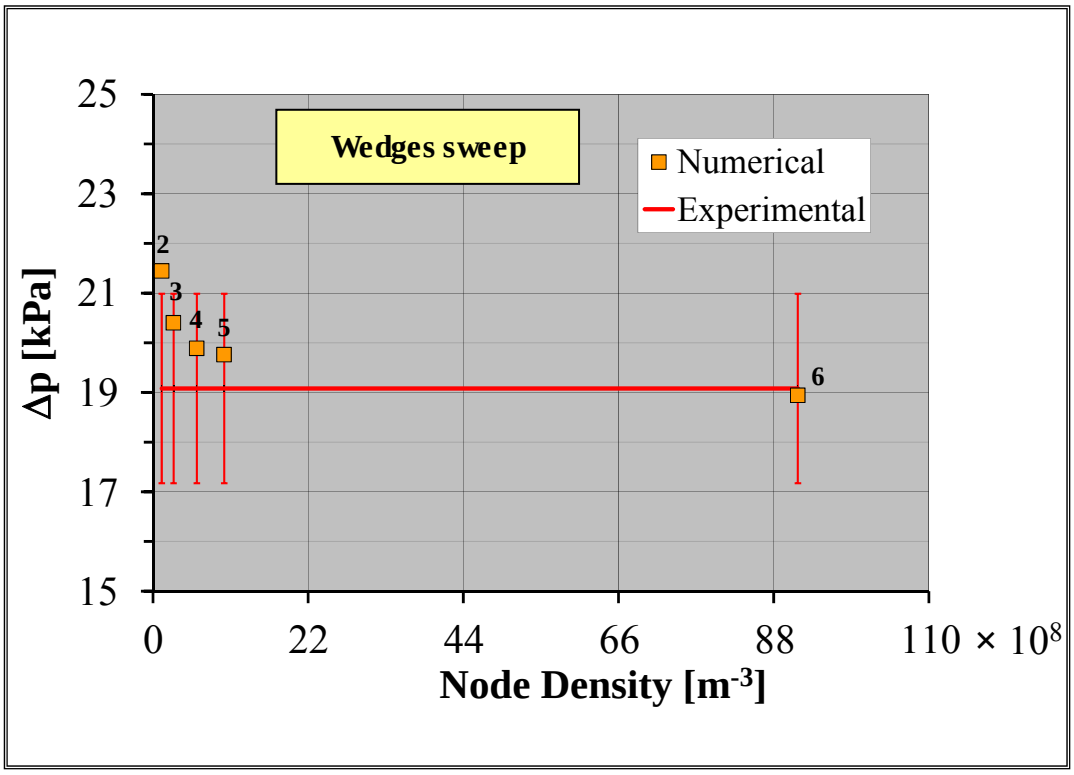

Figure 2.10. Wedges sweep mesh total pressure drop predictions.

The critical comparison of the mesh topologies investigated clearly indicates that structured meshes (i.e. multizone, hexahedron-based or wedge-based meshes) result to be more attractive. In fact, structured meshes allow realistic pressure drop predictions, with deviations of few percent (≈5÷8 %) at acceptable node densities (≈1÷5·10^8 m^{-3}). On the other hand, tetrahedral meshes result severely unfit if not properly equipped with inflation layers, being characterized by "grid independent" deviations higher than 500%.

In a second phase, a parametric analysis has been carried out on the tetrahedral mesh to assess the impact of inflation layers and their arrangement on its total pressure drop predictions, allowing selecting some compromise values suitable to obtain realistic estimates without an unduly high computational effort. Results are reported in Figure 2.11.

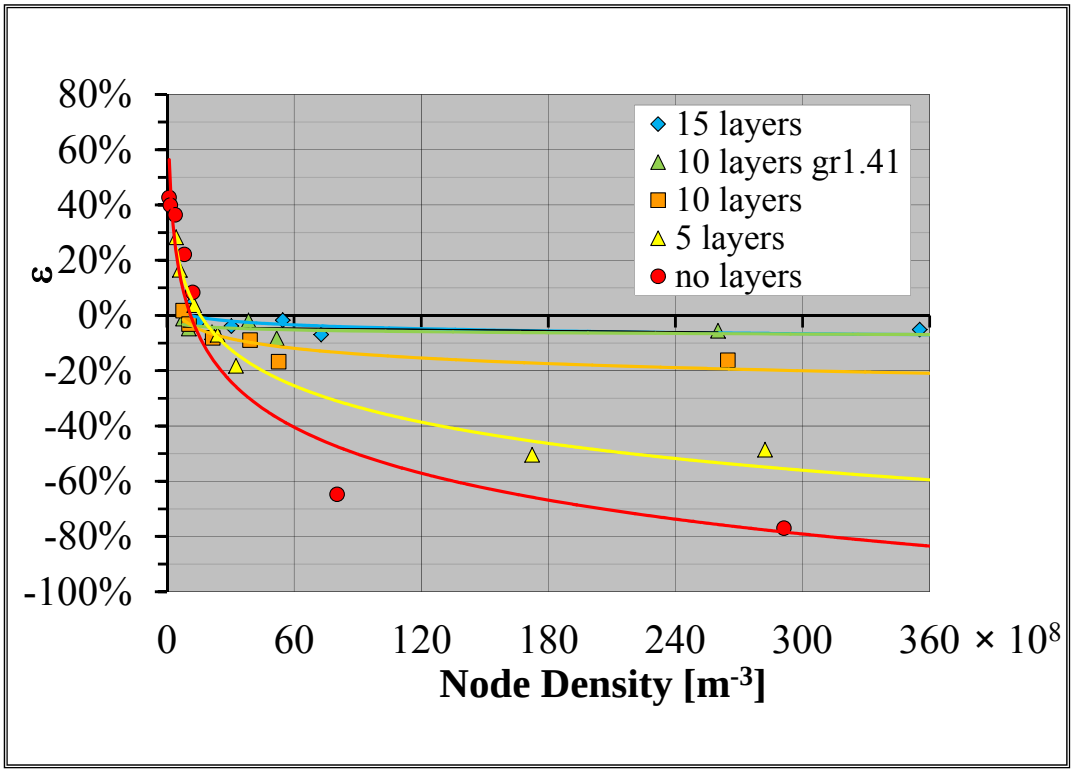

Figure 2.11. Tetrahedrons mesh with inflation layers total pressure drop predictions.

The critical comparison of the results obtained has allowed to conclude that the inflation layers adoption in the discretization of flow domain "near wall" region plays a pivotal role in order to obtain realistic numerical predictions under grid independency conditions. Moreover, it has been possible to conclude that 10 inflation layers with a growth rate of 1.41 and a first layer thickness of 20 μm might be considered as a viable solution to perform the geometric discretization of the complex FW and SB hydraulic variants flow domains. In fact, this selected kind of mesh allows obtaining numerical predictions affected by deviations of few percent with a still manageable node density of ≈1÷5·10^8 m^{-3}.

2.4.2 Hypervapotron

A further parametric study has been carried out on hypervapotron channels (Figure 2.12) whose dimensions and flow conditions are those typical of an EHF FW cooling circuit.

In particular, the hydraulic characteristic functions of two channels with different widths, namely Mock-up 27 and Mock-up 40, have been numerically assessed and then compared with those experimentally evaluated at the Commissariat à l'Energie Atomique (CEA) labs of Cadarache and reported in [11] in terms of total pressure drop for unit length relevant to several values of mass flow rates.

To this purpose, a proper tetrahedral mesh integrated with inflation layers in the "near wall region" of the flow domain has been set-up and its main details are reported in Table 2.3.

Numerical results are reported in Figure 2.13 and Figure 2.14 in comparison with those obtained by CEA either experimentally or analytically by means of their proposed correlation.

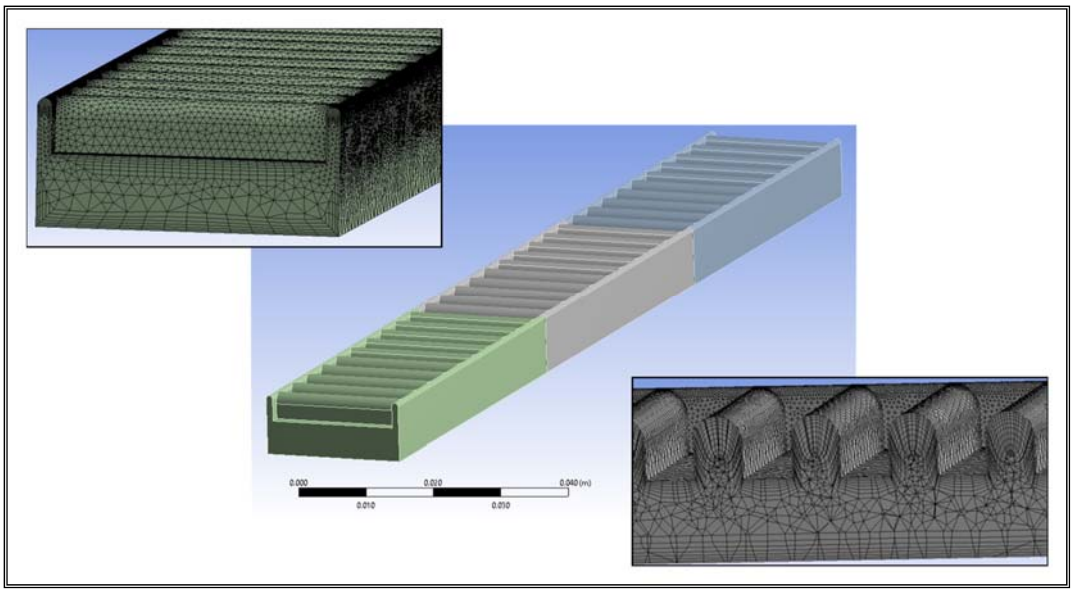

Figure 2.12. Hypervapotron flow domain and mesh (Mock-up 27).

Table 2.3. Hypervapotron mesh details.

	Mock-up 27	**Mock-up 40**
Nodes	464 800	796 650
Elements	1 258 438	2 301 534
First layer height [μm]	20	50
Inflation layers	10	5
Growth rate	1.2	1.2

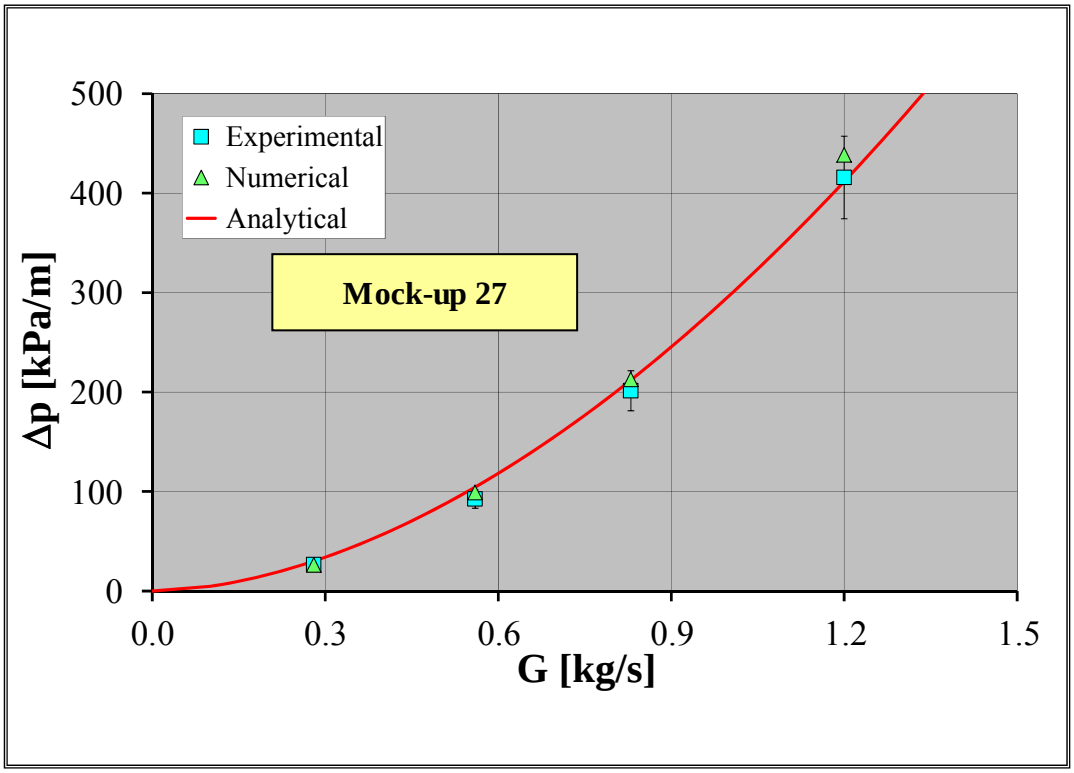

Figure 2.13. Mock-up 27 hydraulic characteristic function.

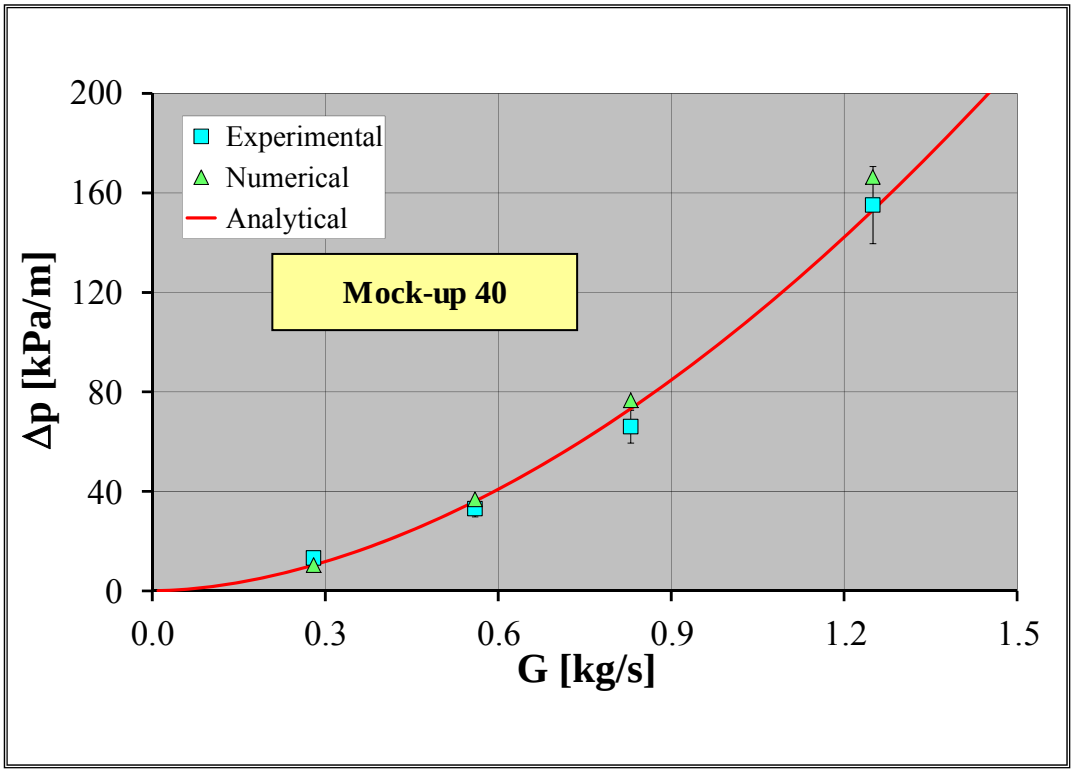

Figure 2.14. Mock-up 40 hydraulic characteristic function.

From the analysis of Figure 2.13 and Figure 2.14, it is possible to conclude that the numerical predictions realistically estimate the experimental values of the total pressure drops at different mass flow rates for both the two hypervapotron geometrical configurations investigated, showing small deviations (< 10%) with respect to either experimental or correlation-calculated values.

Anyway, from the experience of this parametric analysis it may be derived that a mesh composed of $3 \cdot 10^6$ nodes is typically needed to realistically model the fluid-dynamic behaviour of a single finger of EHF FW. Consequently, since this latter is generally composed of twenty fingers, a mesh including at least $6 \cdot 10^7$ nodes, increased up to $7 \cdot 10^7$ nodes to model the remaining part of the FW cooling circuit, should be set-up. Such a huge model would request several weeks to run until residuals have fallen below an acceptable value, resulting absolutely unfit with the tight time-schedule imposed by the research activity.

It has been, therefore, considered a geometrical simplification of the EHF FW fingers flow domain, based on the elimination of the hypervapotron teeth, to ease calculations while obtaining realistic predictions of the total pressure drops. To this purpose, a "filling teeth" procedure (Figure 2.15) has been adopted intended to reduce the variable cross-flow section of the hypervapotron to its throat section that has been uniformly distributed along the whole length of the simplified channel geometry. The coolant has thus been imposed to flow through a reduced cross-flow area, experiencing a higher hydraulic resistance and counterbalancing the pressure drop reduction due to the absence of teeth.

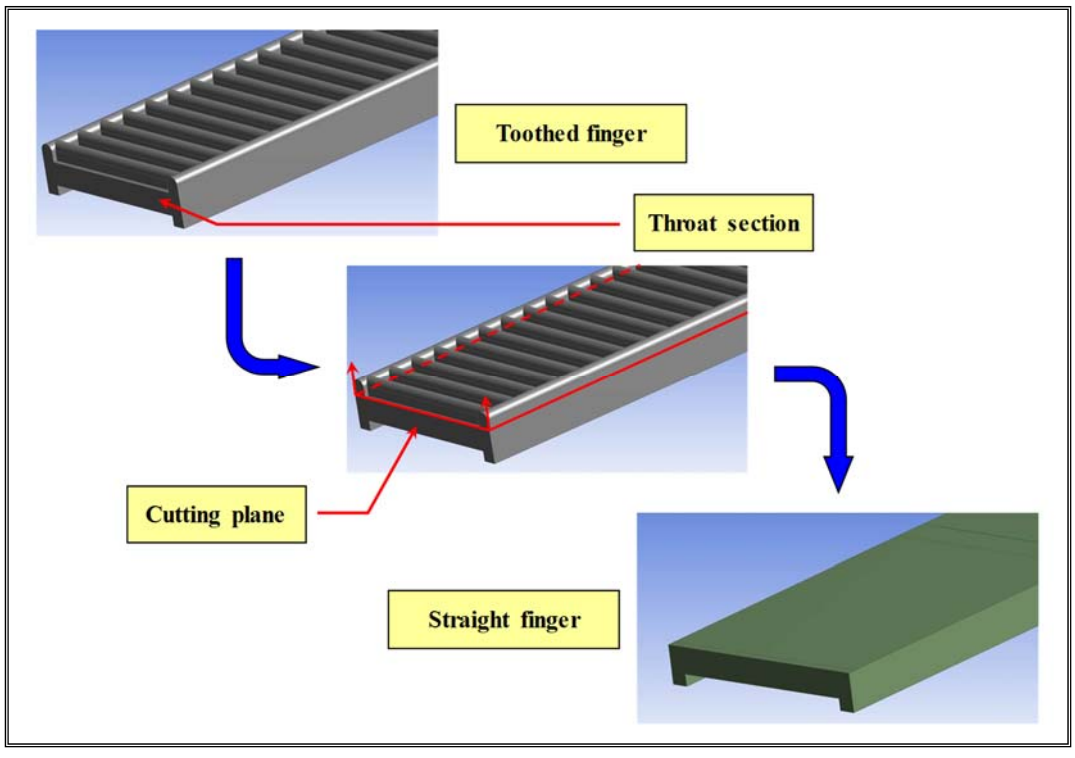

Figure 2.15. Hypervapotron channel "filling teeth" simplification procedure.

In order to justify such a drastic geometrical simplification, the fluid-dynamic behaviour of a single EHF FW finger in a toothed (with hypervapotron teeth) and a straight (without hypervapotron teeth) configuration (Figure 2.16 and Figure 2.17) has been numerically simulated, comparing the total pressure drop (Table 2.4) to check the acceptability of the simplified modelling procedure. To this purpose, a mass flow rate of 0.5 kg/s has been adopted, assuming water coolant to isothermally flow at 98°C and 4.0 MPa.

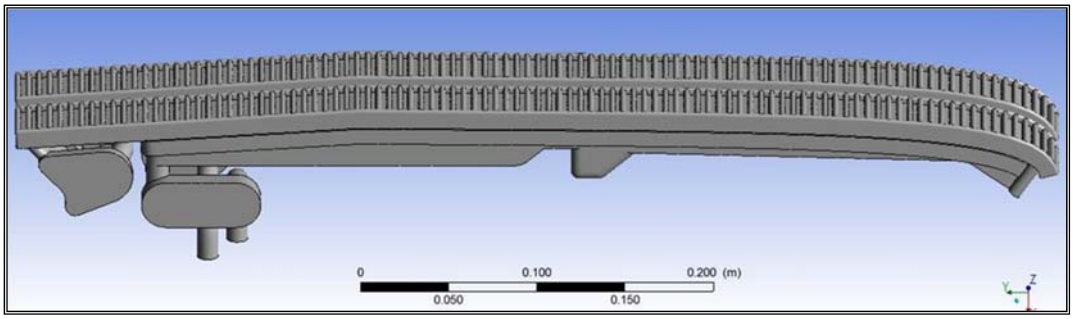

Figure 2.16. Toothed EHF FW finger flow domain.

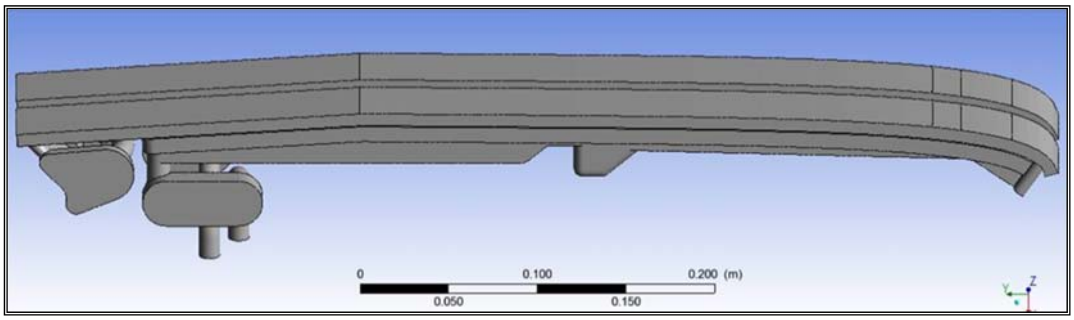

Figure 2.17. Simplified straight EHF FW finger flow domain.

Table 2.4. Total pressure drop predictions.

	Δp [MPa]	**ε [%]**
Toothed finger	0.1118	11.0
Straight finger	0.0995	

The results obtained clearly indicated that the proposed geometric simplification procedure may be adopted for the research campaign, since, adopting a manageable and viable mesh, it allows acceptably underestimating (≈10%) the total pressure drop along a EHF FW finger with respect to that predicted for the actual toothed finger configuration.

Chapter 3

THERMAL-HYDRAULIC RESEARCH CAMPAIGN

3.1 Introduction

The Ph.D. has taken place within the context of the activities carried out at the DEIM in cooperation with the ITER Organisation on the "Hydraulic Analysis of Blanket Cooling System" in a timeframe that goes from the end of 2015 to the end of 2018.

The activity has aimed to investigate numerically the thermal-hydraulic performances of the ITER blanket cooling system under nominal steady-state conditions in view of its final design review, evaluating the total pressure drop occurring in each module cooling system, together with its spatial distribution along the main circuital components. Moreover, attention has been paid also to the assessment of coolant flow velocity spatial distribution in the most critical regions of the investigated flow domains.

In particular, the Ph.D. work has dealt with the investigation and optimisation of the nominal steady-state thermal-hydraulic performances of the following quasi-definitive (or frozen) cooling circuits:

- 23 SB hydraulic variants;
- 15 FW hydraulic variants;
- 31 inlet/outlet manifold hydraulic variants;
- 2 plates;

for an overall of 71 frozen hydraulic variants. Furthermore, the thermal-hydraulic performances of other still-in-work components have been assessed and optimised under nominal steady-state conditions.

The complete description of settings, assumptions and results for each hydraulic variant and blanket module cooling system CFD analysis lies outside of the scope of this thesis, while, for

the sake of clarity, the detailed description of the analyses of cooling system BM14S01 and BM10-11S01 are reported in the following.

Additionally, attention will be focussed also onto the assessment of the steady state fluid-dynamic behaviour of some layout modifications proposed for the FW #14A hydraulic variant, the SB #14A hydraulic variant and their inlet/outlet coaxial connectors, in order to check their effective impact in the improvement and potential optimization of the blanket cooling system thermal-hydraulic performances, mainly in terms of total pressure drop reduction.

3.2 CFD Analysis of Cooling System BM14S01

Cooling system #14S01 is intended to cool blanket module #14S01 that is part of the outboard blanket segment, being located in the middle region of ITER blanket sector 01. The thermal-hydraulic performances of the cooling system of blanket module #14S01 have been investigated under its relevant nominal steady-state conditions (G = 9.12 kg/s) by running separate, steady-state, isothermal CFD analyses of the hydraulic variants relevant to its main components (manifolds #14-S01O02, FW #14A and SB #14A), following the operative procedure previously described in [§2.3].

A summary of the main assumptions, models and boundary conditions adopted is reported in Table 3.1.

Table 3.1. Cooling system BM14S01 CFD analysis: assumptions, models and BCs.

Analysis type	Steady-state
Material library	Water IAPWS IF97
Flow temperature	98 °C
Turbulence model	k-ε
Boundary layer modelling	Wall functions
Absolute wall roughness	15 μm
Loads	No gravity
Inlet boundary condition	Static pressure = 4 MPa
Outlet boundary condition	Mass flow rate = 9.12 kg/s

Figures from Figure 3.1 to Figure 3.4 address cooling system sections where total pressures are calculated and averaged according to equations (35) and (36).

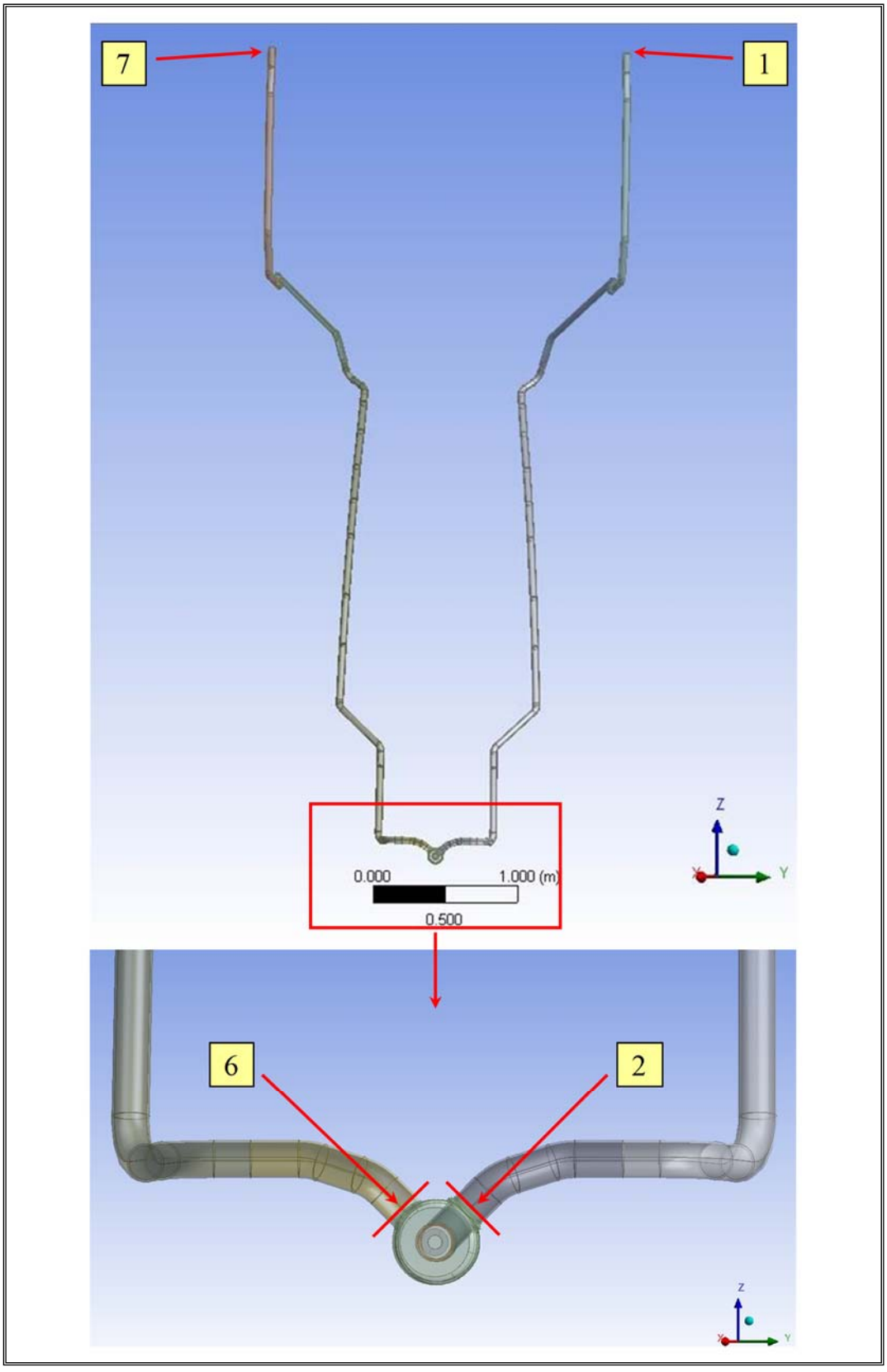

Figure 3.1. Manifolds #14-S01O02 pressure sections.

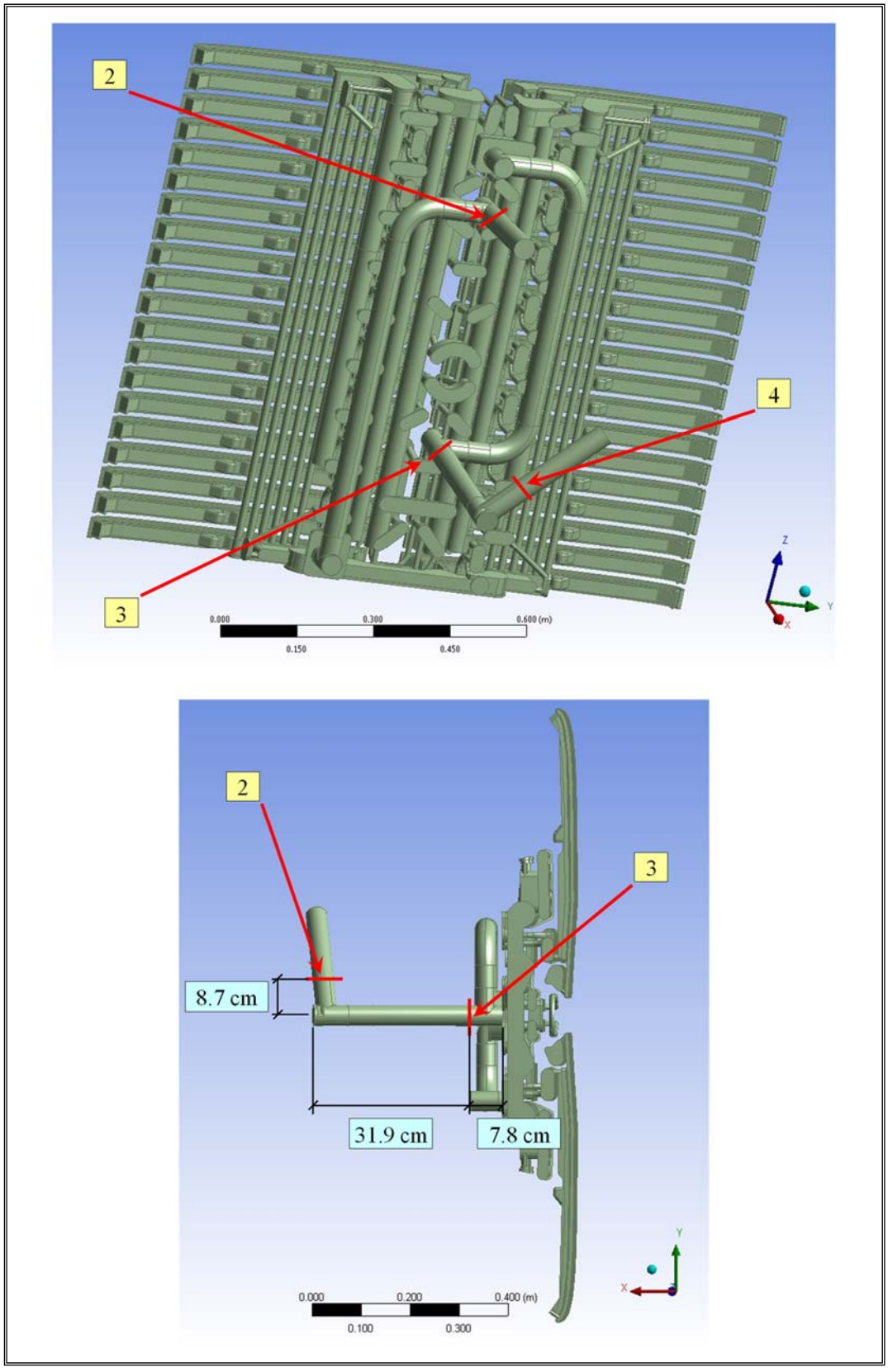

Figure 3.2. FW #14A pressure sections.

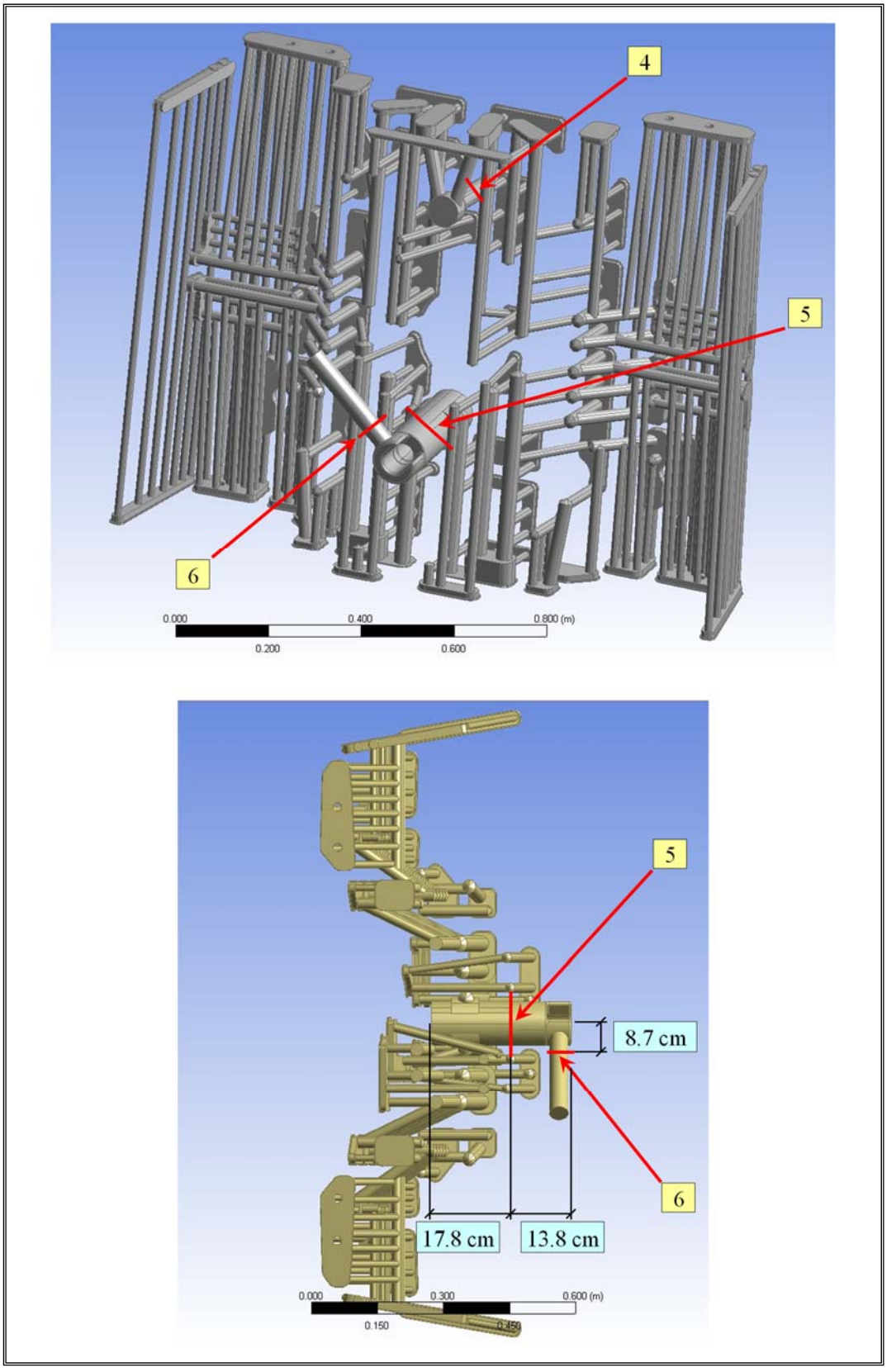

Figure 3.3. SB #14A pressure sections.

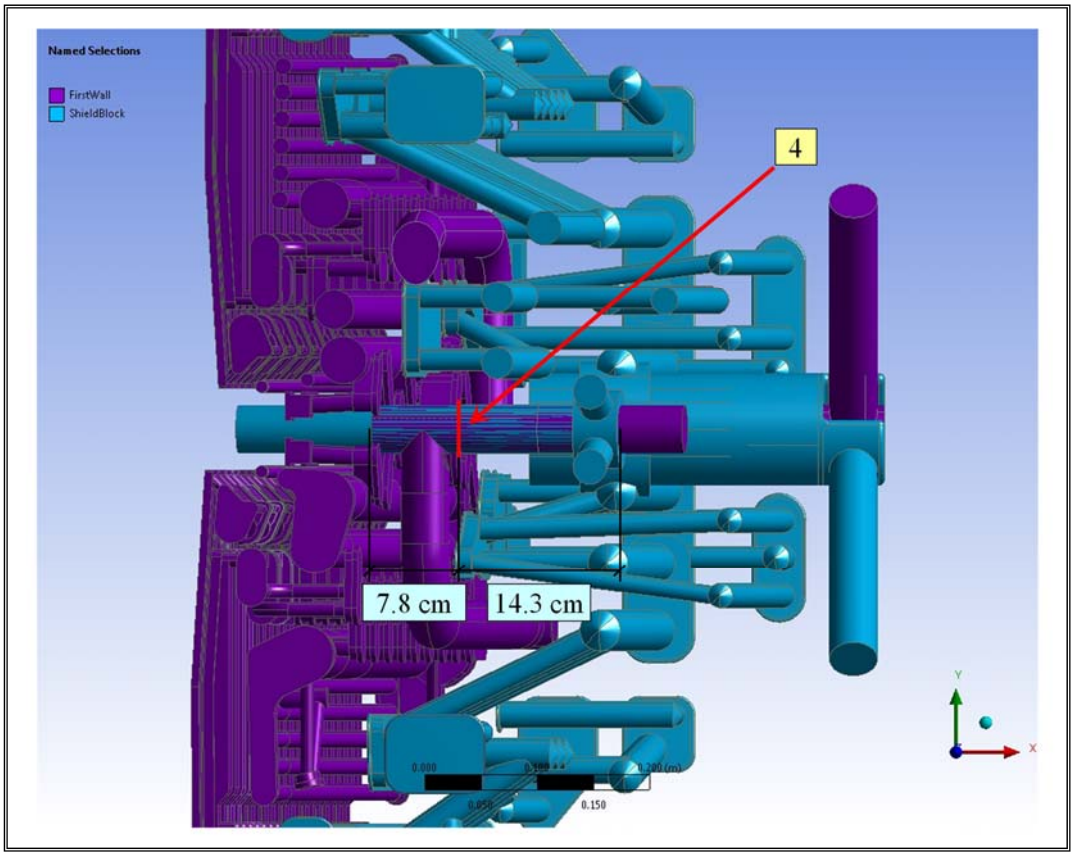

Figure 3.4. FW-SB pressure sections.

Moreover, for the sake of completeness, Table 3.2 reports the elevation change (Δz) of the main hydraulic components of the cooling system, that allows the gravitational contributions to total pressure to be calculated separately.

Table 3.2. Cooling system BM14S01 CFD analysis: main sections and elevation changes.

Component	**Sections**	**$\Delta z = z_{out}-z_{in}$ [m]**
Inlet manifold	1-2	-5.532
ICC + IFS	2-3	-0.061
FW	3-4	+0.485
SB	4-5	-0.485
OCC + OFS	5-6	+0.061
Outlet manifold	6-7	+5.532

To this purpose, it has to be underlined that the total pressure drop of Inlet Coaxial Connector (ICC) and Inner Flow Separator (IFS) are calculated by means of the FW hydraulic variant CFD analysis, their flow domain being integrated with the FW one in the development of the finite volume model, while, similarly, the total pressure drop of Outlet Coaxial Connector (OCC) and Outer Flow Separator (OFS) are calculated by means of the SB hydraulic variant CFD analysis.

3.2.1 Manifolds #14-S01O02 CFD Analysis

Figure 3.5 and Figure 3.6 show inlet/outlet manifolds #14-S01O02 flow domains and details of the relevant discretization adopted for their CFD analyses, while their mesh parameters are reported in Table 3.3.

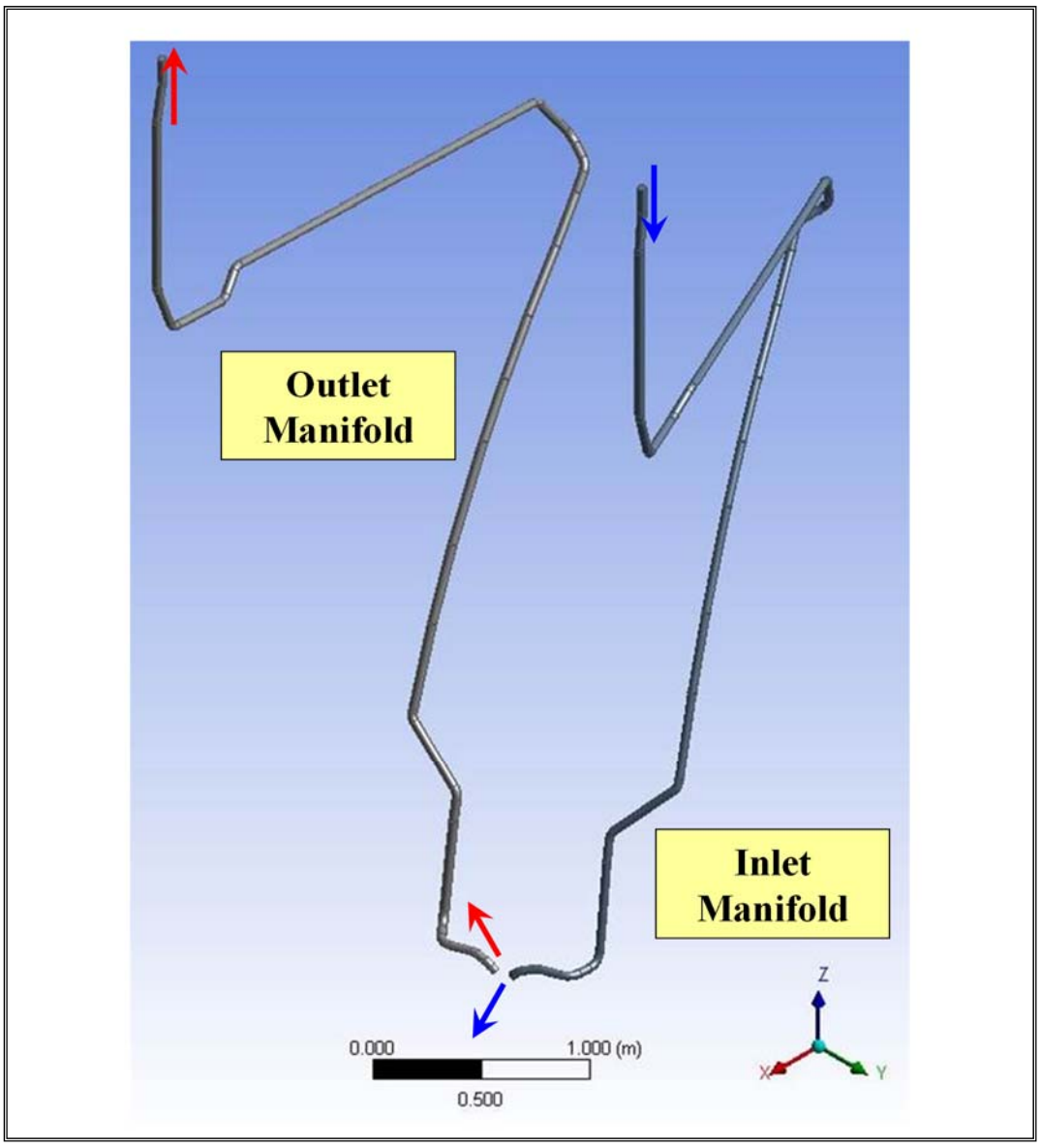

Figure 3.5. Flow domain of manifolds #14-S01O02.

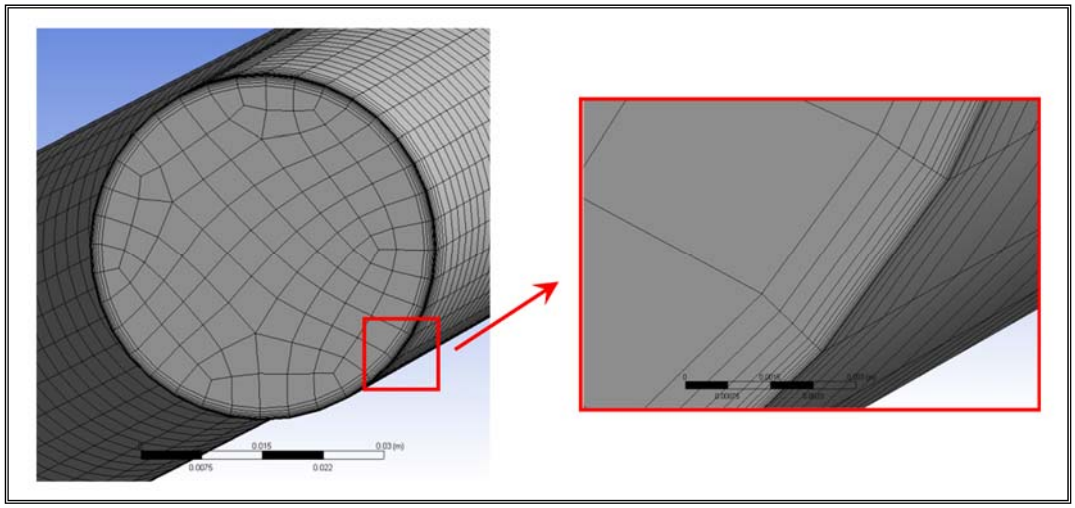

Figure 3.6. Details of manifolds #14-S01O02 discretization.

Table 3.3. Mesh parameters adopted for manifolds #14-S01O02 discretization.

Mesh global parameters	**Inlet manifold**	**Outlet manifold**
Minimum size [m]	$6.5 \cdot 10^{-4}$	$6.6 \cdot 10^{-4}$
Maximum face size [m]	$4.0 \cdot 10^{-3}$	$4.0 \cdot 10^{-3}$
Maximum size [m]	$1.3 \cdot 10^{-1}$	$1.3 \cdot 10^{-1}$
Minimum edge length [m]	$1.9 \cdot 10^{-3}$	$1.9 \cdot 10^{-3}$
Number of nodes	$1.16 \cdot 10^{6}$	$1.19 \cdot 10^{6}$
Number of elements	$1.11 \cdot 10^{6}$	$1.14 \cdot 10^{6}$
Node density [m^{-3}]	$8.58 \cdot 10^{7}$	$8.79 \cdot 10^{7}$
Average length [m]	$4.69 \cdot 10^{-3}$	$4.65 \cdot 10^{-3}$
Inflation layers parameters	**Inlet manifold**	**Outlet manifold**
First layer height [m]	$2.0 \cdot 10^{-5}$	$2.0 \cdot 10^{-5}$
Layers number	10	10
Growth rate	1.41	1.41

The results of the CFD analyses of both inlet and outlet manifolds #14-S01O02 in terms of total pressure drop Δp are reported in Table 3.4, along with the total pressure drop, Δp_{grav}, calculated by hand taking into account the presence of the gravity field.

Table 3.4. Manifolds #14-S01O02 total pressure drops.

Component	G [kg/s]	Δp [MPa]	Δp_{grav} [MPa]
Inlet manifold	9.12	0.0923	0.0401
Outlet manifold	9.12	0.0930	0.1452
TOTAL	9.12	0.1853	0.1853

3.2.2 FW #14A CFD Analysis

FW #14A is endowed with hypervapotrons and its CFD analysis has been performed referring to its "toothless" simplified configuration where hypervapotron teeth have been removed adopting a "filling teeth" procedure.

Figures from Figure 3.7 to Figure 3.9 show FW #14A flow domain and details of the relevant discretization adopted for its CFD analysis, while its mesh parameters are reported in Table 3.5.

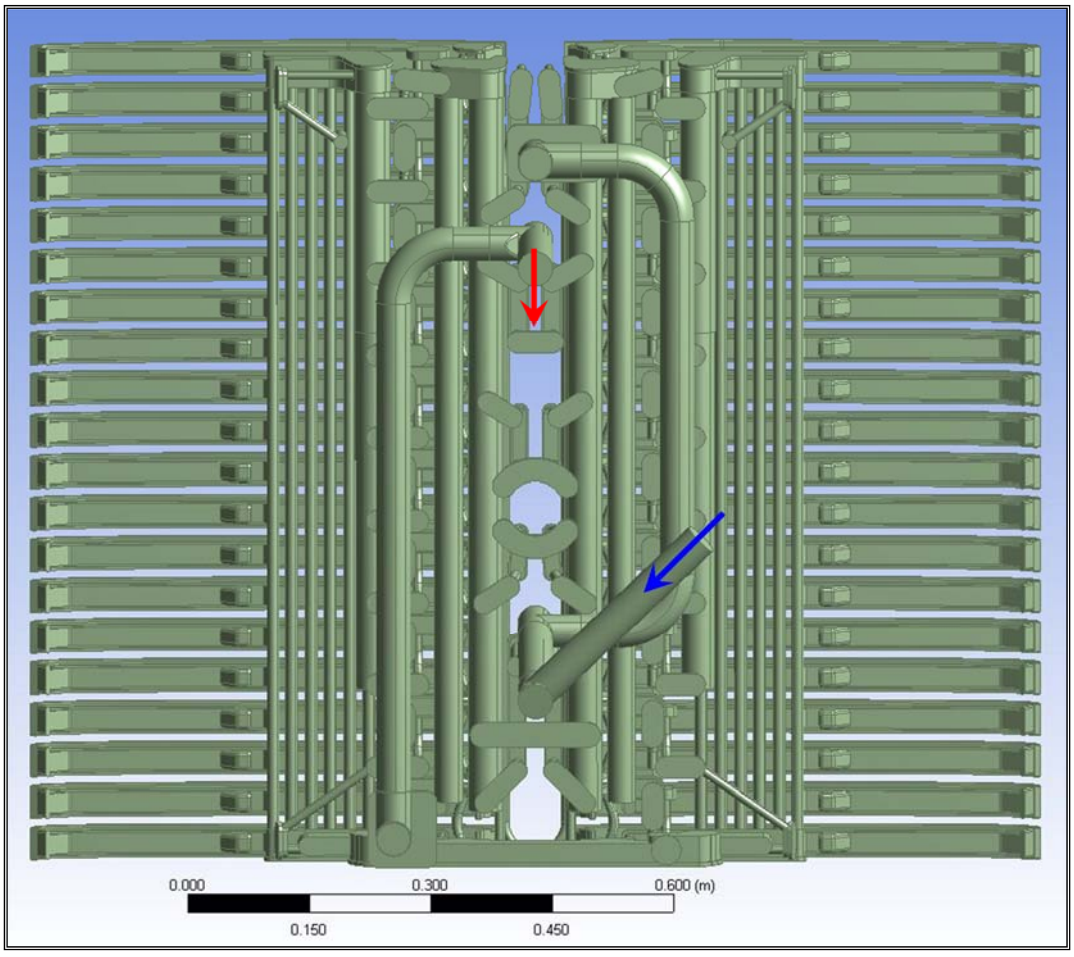

Figure 3.7. Flow domain of FW #14A.

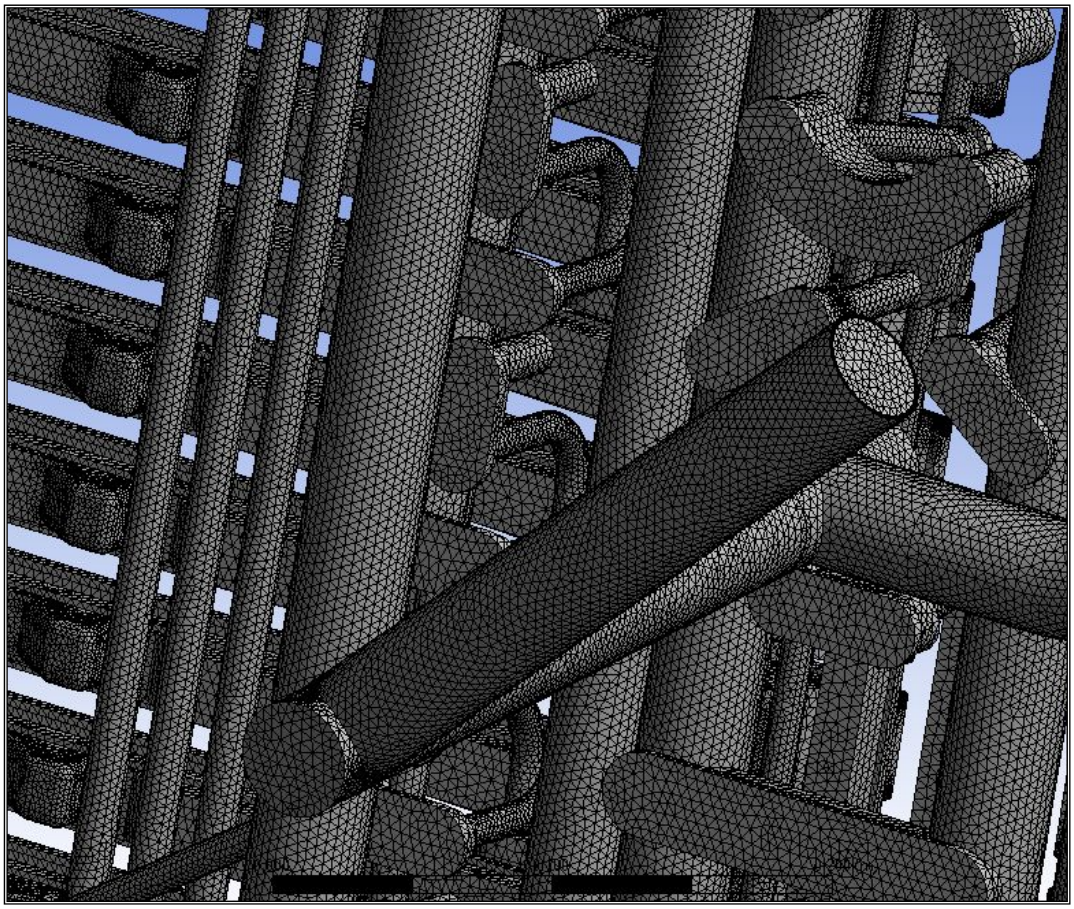

Figure 3.8. Details of FW #14A discretization.

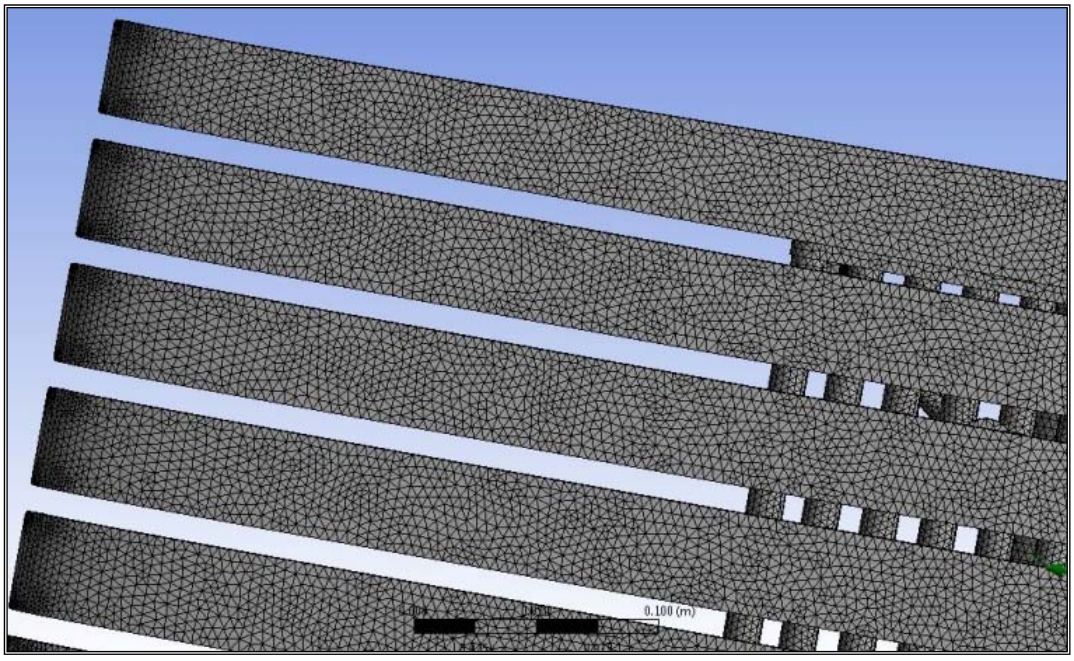

Figure 3.9. Details of FW #14A discretization.

Table 3.5. Mesh parameters adopted for FW #14A discretization.

Mesh global parameters	
Minimum size [m]	$7.0 \cdot 10^{-4}$
Maximum face size [m]	$4.0 \cdot 10^{-3}$
Maximum size [m]	$1.4 \cdot 10^{-1}$
Minimum edge length [m]	$3.6 \cdot 10^{-6}$
Number of nodes	$9.24 \cdot 10^{6}$
Number of elements	$2.09 \cdot 10^{7}$
Node density [m^{-3}]	$3.05 \cdot 10^{8}$
Average length [m]	$2.31 \cdot 10^{-3}$
Inflation layers parameters	
First layer height [m]	$2.0 \cdot 10^{-5}$
Layers number	10
Growth rate	1.41

The results of the FW #14A CFD analysis in terms of total pressure drop Δp are reported in Table 3.6, along with the total pressure drop, Δp_{grav}, calculated by hand taking into account the presence of the gravity field.

Table 3.6. FW #14A total pressure drops.

Component	**G [kg/s]**	**Δp [MPa]**	**Δp_{grav} [MPa]**
ICC + IFS	9.12	0.0257	0.0252
FW	9.12	0.3848	0.3894
TOTAL	9.12	0.4105	0.4146

3.2.3 SB #14A CFD Analysis

Figure 3.10 and Figure 3.11 show SB #14A flow domain and details of the relevant discretization adopted for its CFD analysis, while its mesh parameters are reported in Table 3.7.

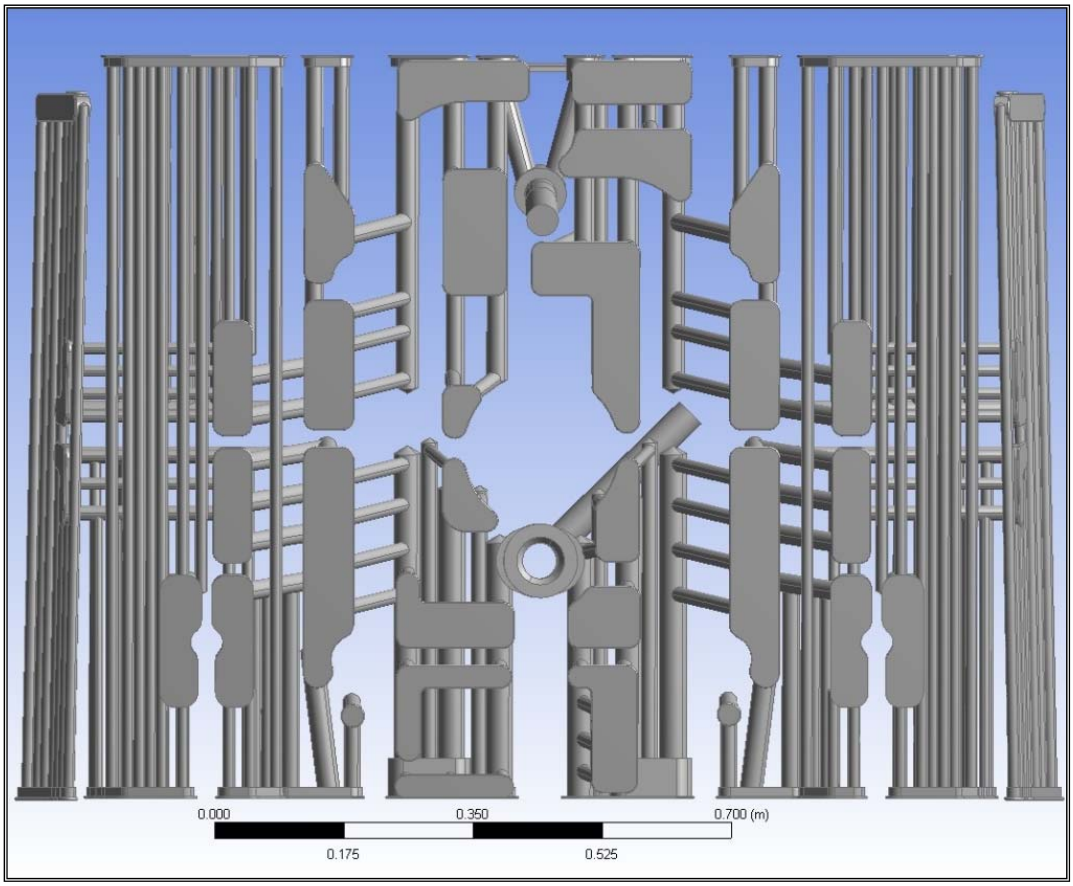

Figure 3.10. Flow domain of SB #14A.

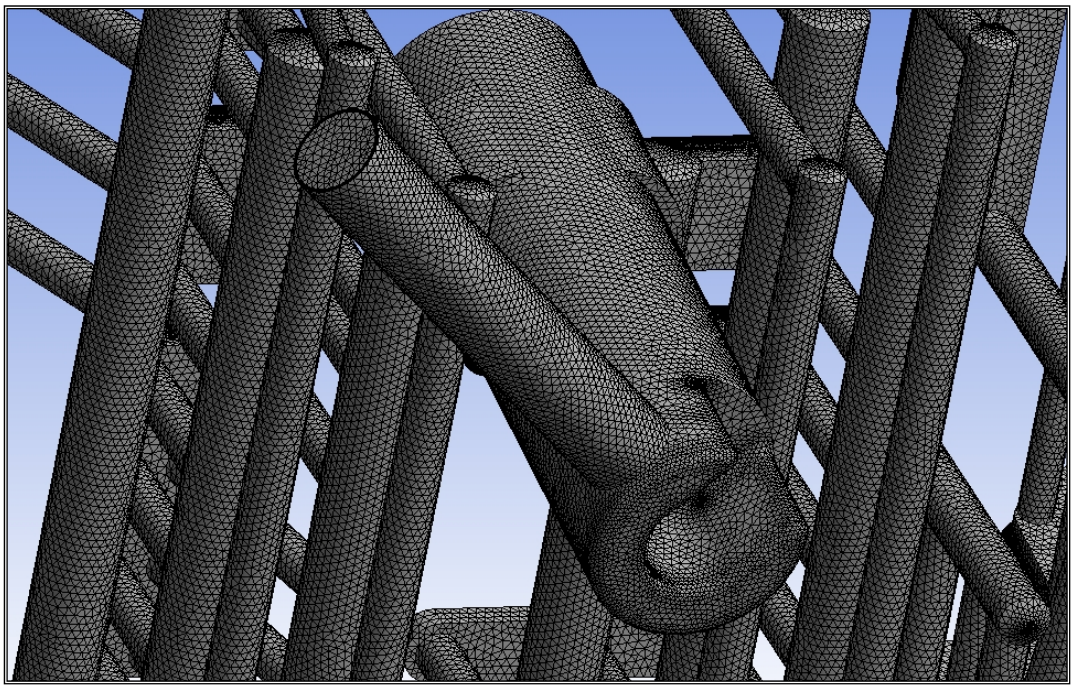

Figure 3.11. Details of SB #14A discretization.

Table 3.7. Mesh parameters adopted for SB #14A discretization.

Mesh global parameters	
Minimum size [m]	$7.4 \cdot 10^{-4}$
Maximum face size [m]	$4.0 \cdot 10^{-3}$
Maximum size [m]	$1.5 \cdot 10^{-1}$
Minimum edge length [m]	$3.0 \cdot 10^{-5}$
Number of nodes	$1.11 \cdot 10^{7}$
Number of elements	$2.64 \cdot 10^{7}$
Node density [m^{-3}]	$3.22 \cdot 10^{8}$
Average length [m]	$2.23 \cdot 10^{-3}$
Inflation layers parameters	
First layer height [m]	$2.0 \cdot 10^{-5}$
Layers number	10
Growth rate	1.41

The results of the SB #14A CFD analysis in terms of total pressure drop Δp are reported in Table 3.8, along with the total pressure drop, Δp_{grav}, calculated by hand taking into account the presence of the gravity field.

Table 3.8. SB #14A total pressure drops.

Component	**G [kg/s]**	**Δp [MPa]**	**Δp_{grav} [MPa]**
SB	9.12	0.2373	0.2327
OCC + OFS	9.12	0.0222	0.0228
TOTAL	9.12	0.2595	0.2555

3.2.4 Summary of Cooling System BM14S01 CFD Analysis

Table 3.9 reports the main results of cooling system BM14S01 CFD analysis, showing that its total pressure drop at the nominal mass flow rate of 9.12 kg/s amounts to 0.8553 MPa.

Table 3.9. Cooling system BM14S01 total pressure drops at 9.12 kg/s.

Component	Δp [MPa]
Inlet manifold	0.0923
FW (Total)	0.4105
SB (Total)	0.2595
Outlet manifold	0.0930
TOTAL	0.8553

3.3 CFD-RELAP5 Analysis of Cooling System BM10-11S01

Cooling system #10-11S01 is intended to cool blanket modules #10 and #11 that are part of the upper-outboard blanket segments, being located in the top region of ITER blanket sector 01.

The thermal-hydraulic performances of the cooling system of twinned blanket modules #10-11S01 have been investigated under the relevant nominal steady-state conditions (G = 12.10 kg/s) by running separate, steady-state, isothermal CFD analyses of its main components hydraulic variants, following the operative procedure previously described in [§2.3] and based on the combined use of the ANSYS CFX and the RELAP5 codes.

In a first phase, parametric CFD analyses have been performed for all the FWs and SBs hydraulic variants composing the blanket module cooling circuits #10 and #11 in order to separately assess their hydraulic characteristic functions that give the functional dependence of the total pressure drop along the considered cooling circuit on the corresponding mass flow rate under steady-state conditions:

$$\Delta p_i^k = \Delta p_i^k (G) \tag{40}$$

where the index i identifies the module cooling circuit (#10 or #11) and the index k represents its main components (FW or SB).

These functions have been derived in the following power-law analytical form:

$$\Delta p_i^k (G) = \alpha_i^k G^{\beta_i^k} \tag{41}$$

where coefficients α_i^k and β_i^k depend on the module cooling circuit (#10 or #11) as well as on its main components (FW or SB). According to the operative procedure adopted, the hydraulic characteristic function of each i-th module cooling circuit has been obtained by means of equation (30) and, taking into account that calculations have suggested that:

$\beta_i^k \square 2 \quad \forall\, i = 10,\ 11$ and $\forall$ k=FW, SB (42)

the following analytical expression has been derived:

$$\Delta p_i(G) = \alpha_i G^2 \tag{43}$$

where:

$$\alpha_i = \alpha_i^{FW} + \alpha_i^{SB} \tag{44}$$

The assessed values of the α_i coefficients are reported in Table 3.10.

Table 3.10. Hydraulic characteristic functions coefficients.

Blanket module cooling circuit	α^{FW} [MPa]	α^{SB} [MPa]	α [MPa]
#10	0.003284	0.001892	0.005176
#11	0.002960	0.002246	0.005206

In a second phase, in order to simulate the whole cooling system BM10-11S01, the RELAP5 1D finite volume model shown in Figure 3.12 has been set up, where each i-th module cooling circuit has been modelled as a concentrated hydraulic resistance.

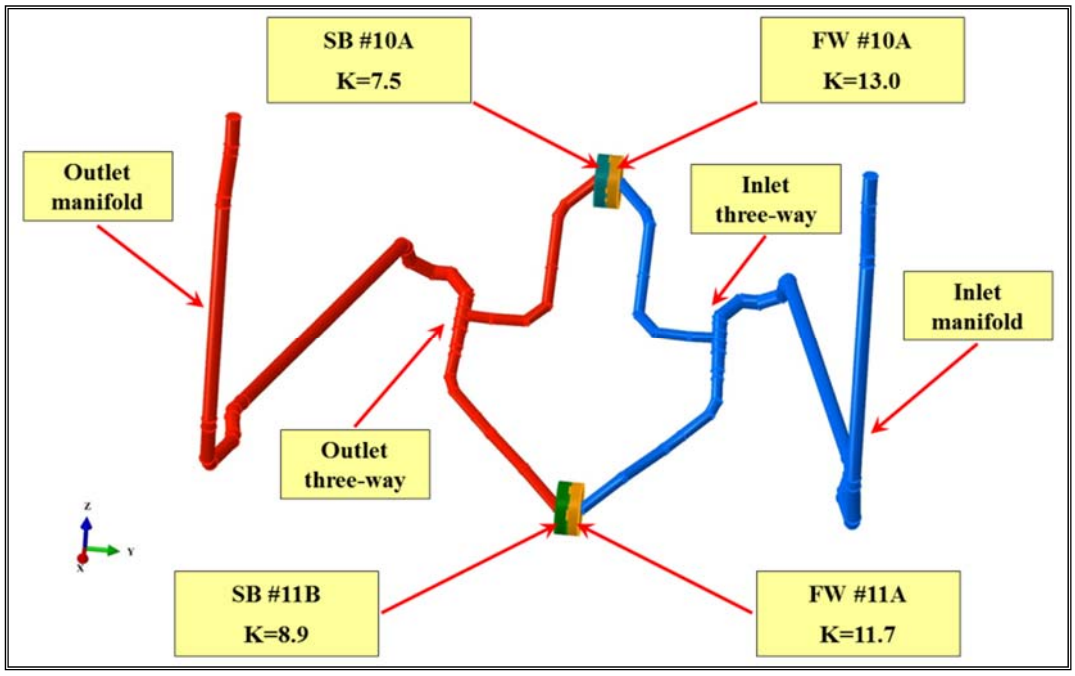

Figure 3.12. 1D finite volume model of the cooling system BM10-11S01.

Effective concentrated loss factor for each i-th module cooling circuit, $K_i(G)$, has been calculated according to equation (32). In particular, due to equations (42) and (43), mass flow rate-independent concentrated loss factors have been derived, whose values, calculated assuming $\rho = 961.59$ kg/m^3 and $A_i = 0.001436036$ m^2, have been reported in Table 3.11.

Table 3.11. Effective concentrated loss factor.

Blanket module cooling circuit	$\mathbf{K^{FW}}$	$\mathbf{K^{SB}}$	**K**
#10	13.0	7.5	20.5
#11	11.7	8.9	20.6

Moreover, as to concentrated hydraulic resistances of inlet/outlet three-way connections of the cooling system BM10-11S01, since they depend on mass flow rate branching, as a first attempt, their effective values have been calculated according to [7], assuming the reference values of the nominal mass flow rates through each blanket module cooling circuit. The numerical values obtained have been reported in Figure 3.12.

Once set-up the 1D finite volume model and fixed the RELAP5 analysis settings (Table 3.12), the combined CFD-RELAP5 iterative analysis procedure described in [§2.3] has been performed to assess the actual coolant mass flow rate distribution between the blanket modules cooling circuits of cooling system BM10-11S01.

Table 3.12. Cooling system BM10-11S01 RELAP analysis: assumptions, models and BCs.

Analysis type	Steady-state
Material library	Water (RELAP5)
Flow temperature	98 °C
Absolute wall roughness	15 μm
Loads	Gravity
Inlet boundary condition	Static pressure = 4 MPa
Outlet boundary condition	Mass flow rate = 12.10 kg/s

The calculated values, G_{calc}, of the actual coolant mass flow rates flowing through the blanket modules cooling circuits when they are connected in parallel into the cooling system BM10-11S01 are reported in Table 3.13, together with the corresponding deviations, ε, from their reference nominal values, G_{nom}.

Table 3.13. Cooling system BM10-11S01 mass flow rate breakdown.

	G_{nom} [kg/s]	G_{calc} [kg/s]	ε [%]
BM #10	6.55	5.94	-9.3
BM #11	5.55	6.16	11.0
Cooling system BM10-11S01	12.10	12.10	0.0

As it may be deduced from the critical analysis of the results obtained, once the twinned blanket modules cooling circuits #10 and #11 are connected in parallel into the cooling system BM10-11S01, a not negligible deviation (≈ 10%) of their coolant mass flow rates is predicted to occur from their nominal values. This unbalanced distribution favours the cooling circuit of blanket module #11 in spite of that relevant to blanket module #10, mainly originating from the highest hydraulic resistance of the latter circuit due to the several bends it houses along its branch pipes. To this purpose, it has to be underlined that, since the acceptability of the calculated mass flow rate distribution mainly depends on the effective CHF margin guaranteed to the less cooled blanket module, it could be considered acceptable, as both blanket modules #10 and #11, being endowed with NHF FW, are expected to undergo relatively low heat fluxes.

In a third phase, CFD analyses have been run for the hydraulic variants composing the twinned blanket modules cooling circuits at the pertaining calculated mass flow rates in order to assess their actual steady-state total pressure drops. The results obtained are reported in Table 3.14 in comparison with that pertaining to the nominal mass flow rates.

Table 3.14. Cooling system BM10-11S01 main components total pressure drops.

Component	G [kg/s]	Δp [MPa]
ICC + IFS + FW #10A	5.94	0.1156
SB + OCC + OFS #10A	5.94	0.0673
ICC + IFS + FW #11A	6.16	0.1137
SB + OCC + OFS #11B	6.16	0.0855
ICC + IFS + FW #10A	6.55	0.1409
SB + OCC + OFS #10A	6.55	0.0811
ICC + IFS + FW #11A	5.55	0.0911
SB + OCC + OFS #11B	5.55	0.0692

3.3.1 Summary of Cooling System BM10-11S01 CFD-RELAP5 Analysis

Table 3.15 reports the main results of cooling system BM10-11S01 combined CFD-RELAP5 analysis, showing that its total pressure drop at the nominal mass flow rate of 12.10 kg/s amounts to 0.2696 MPa. It has to be observed that the total pressure drops reported in Table 3.15 as to cooling circuits 10S and 11S include the contribution due to the branch pipes joining the three-way connections to the inlet/outlet coaxial connectors.

Table 3.15. Cooling system BM10-11S01 total pressure drops at 12.10 kg/s.

<table>
<tr><th>Component</th><th>Hydraulic variant</th><th colspan="2">Δp [MPa]</th></tr>
<tr><td>Inlet manifold</td><td>Manifolds #10-11-S02I01</td><td colspan="2">0.0258</td></tr>
<tr><td>Inlet 3-way 10S</td><td>-</td><td>0.0153</td><td rowspan="3">0.2177
@ 5.94 kg/s</td></tr>
<tr><td>Cooling Circuit 10S</td><td>FW #10A - SB #10A</td><td>0.1913</td></tr>
<tr><td>Outlet 3-way 10S</td><td>-</td><td>0.0111</td></tr>
<tr><td>Inlet 3-way 11S</td><td>-</td><td>0.0027</td><td rowspan="3">0.2177
@ 6.16 kg/s</td></tr>
<tr><td>Cooling Circuit 11S</td><td>FW #11A - SB #11B</td><td>0.2053</td></tr>
<tr><td>Outlet 3-way 11S</td><td>-</td><td>0.0097</td></tr>
<tr><td>Outlet manifold</td><td>Manifolds #10-11-S02I01</td><td colspan="2">0.0261</td></tr>
<tr><td colspan="2">TOTAL</td><td colspan="2">0.2696</td></tr>
</table>

3.4 CFD Analysis of Modified Hydraulic Variants

Within the framework of the research activity carried out during the Ph.D. course, according to its main aims and purposes, attention has been focussed also on the assessment of the steady-state fluid-dynamic behaviour of some layout modifications conceived so to optimise the blanket cooling system thermal-hydraulic performances, mainly in terms of total pressure drop reduction for those blanket module cooling systems with the highest pressure drop in order to ease their integration when connected to the URM. Among the considered ones, a selection will be thoroughly showed in this paragraph and, in particular, those proposed for the following hydraulic variants under investigation:

- inlet/outlet coaxial connectors;
- FW #14A;
- SB #14A.

The effective impact of the selected layout modification on the improvement and potential optimization of the blanket cooling system thermal-hydraulic performances has been investigated. CFD analyses have been purposely run according to the methodology and the operative procedure previously described in [§2.2] and [§2.3].

3.4.1 Inlet/Outlet Coaxial Connectors

As to the inlet coaxial connector, the potential effects of the layout modifications reported in Figure 3.13 and mainly consisting in the elimination of the bend recess have been investigated by running a dedicated CFD analysis on the models represented in Figure 3.14.

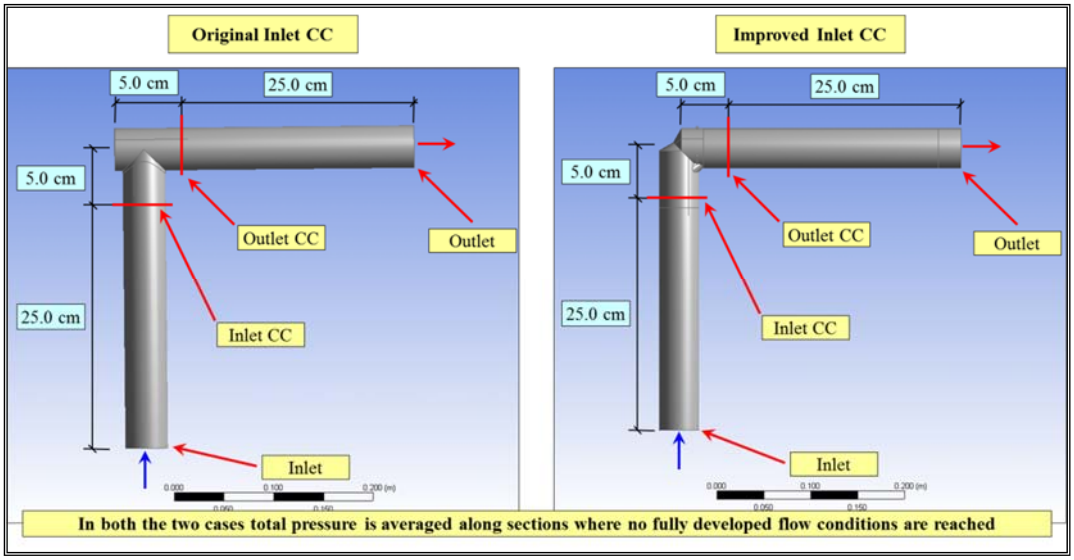

Figure 3.13. Inlet coaxial connector layout modification.

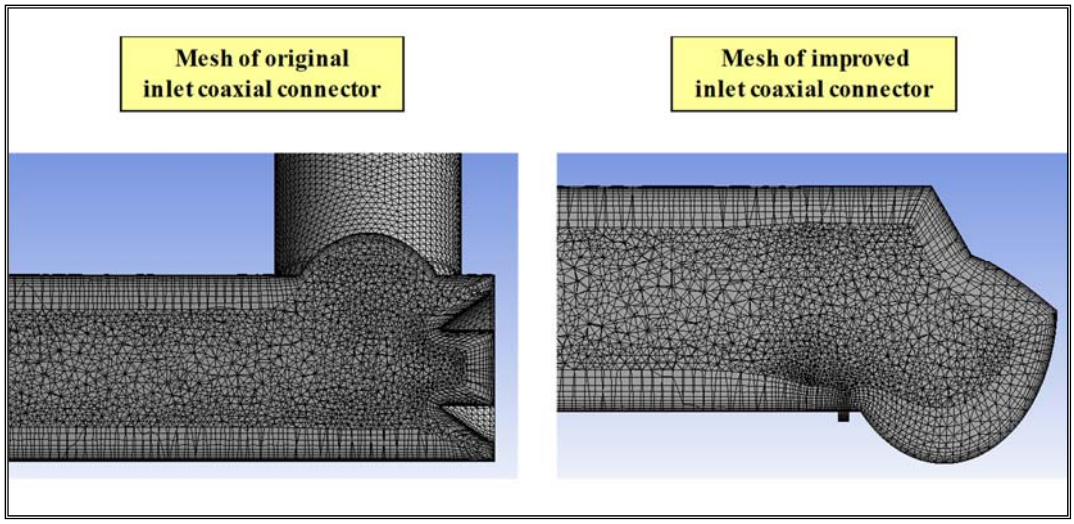

Figure 3.14. Meshes adopted for inlet coaxial connectors CFD calculations.

The results obtained for both original and improved inlet coaxial connectors configurations (Table 3.16) clearly indicate that the modified configuration allows a significant reduction of local pressure drop, its implementation resulting to be, hence, greatly encouraged.

Table 3.16. Inlet coaxial connectors calculations results.

Component	G [kg/s]	Δp [MPa]	ε [%]
Original ICC	9.125	0.0325	-51.4
Improved ICC	9.125	0.0158	

As to the outlet coaxial connector, the potential effects of the layout modifications reported in Figure 3.15 have been investigated by running dedicate CFD analyses on models meshed similarly to those reported in Figure 3.14. Results are reported in Figure 3.16 and Figure 3.17.

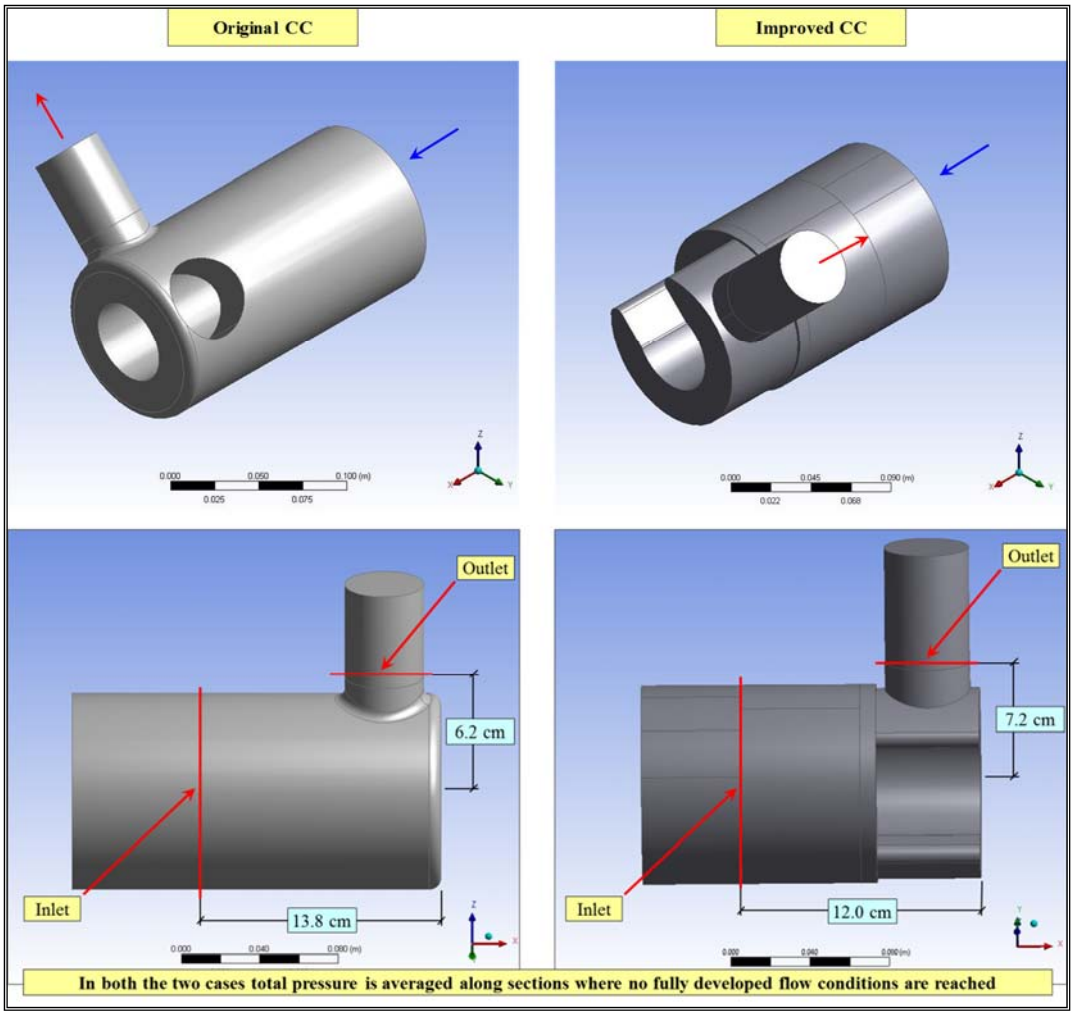

Figure 3.15. Outlet coaxial connector layout modification.

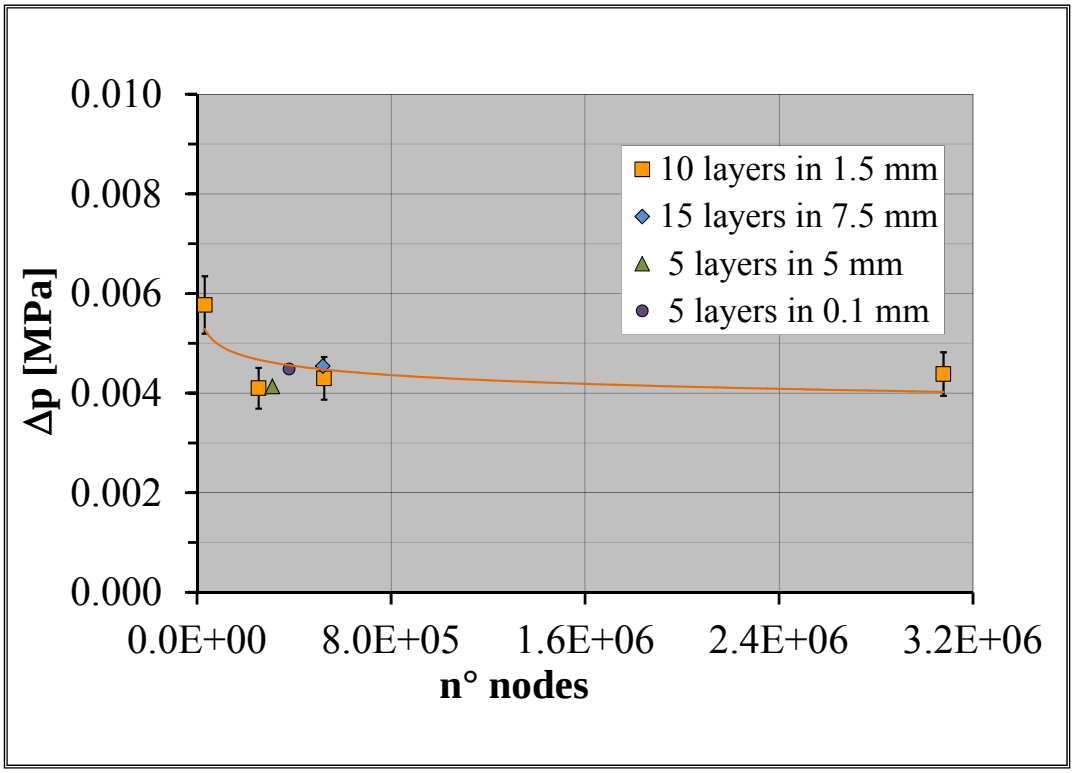

Figure 3.16. Results of original outlet coaxial connectors CFD calculations.

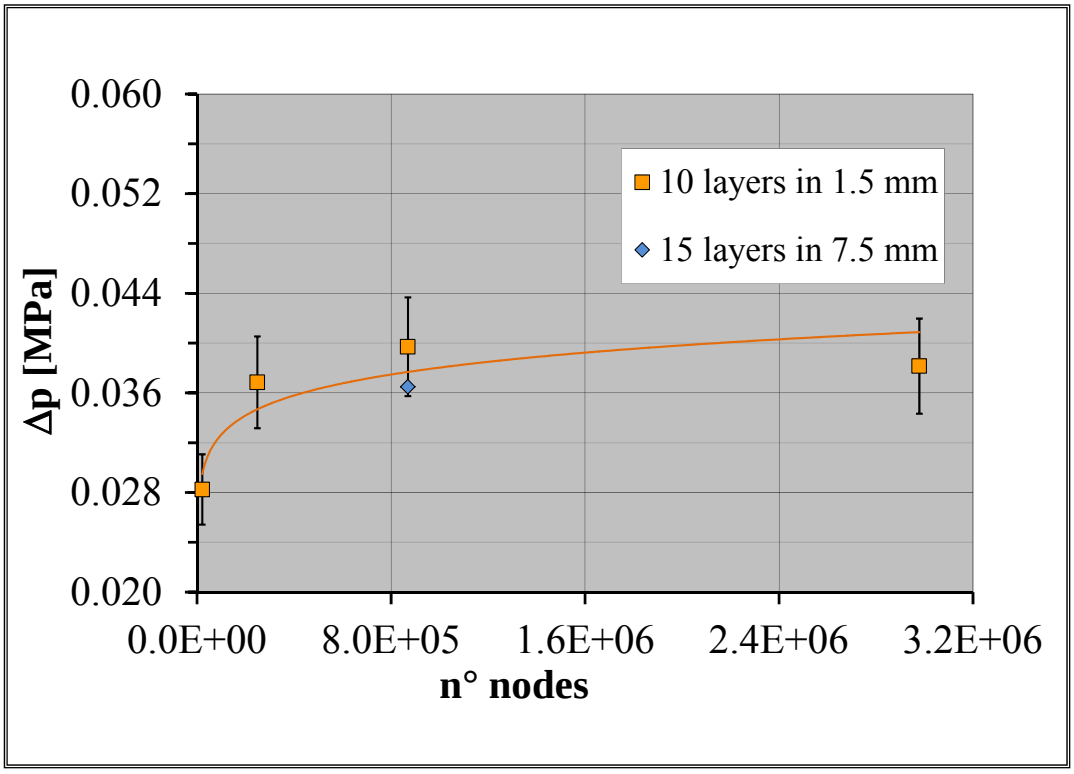

Figure 3.17. Results of improved outlet coaxial connectors CFD calculations.

Original outlet coaxial connector CFD analyses, performed adopting meshes differing as to inflation layers and node density, have indicated that the total pressure drop amounts to 4.1 ÷ 4.5 kPa at the mass flow rate of 9.125 kg/s, while modified outlet coaxial connector CFD analyses, performed similarly, have indicated that the total pressure drop ranges between 36.5 and 39.7 kPa.

It has been concluded, therefore, that the modified configuration implementation has to be discouraged, since it induces a higher total pressure drop with respect to the original one, which seems to be so small (≈ 4 kPa) to make almost useless any optimization.

3.4.2 FW #14A

The modified configuration of FW #14A is endowed with hypervapotrons and its CFD analysis has been performed referring to its "toothless" simplified configuration, where hypervapotron teeth have been removed adopting the already mentioned "filling teeth" procedure.

Figures from Figure 3.18 to Figure 3.22 show its flow domain with the details of locations where main modifications have been made.

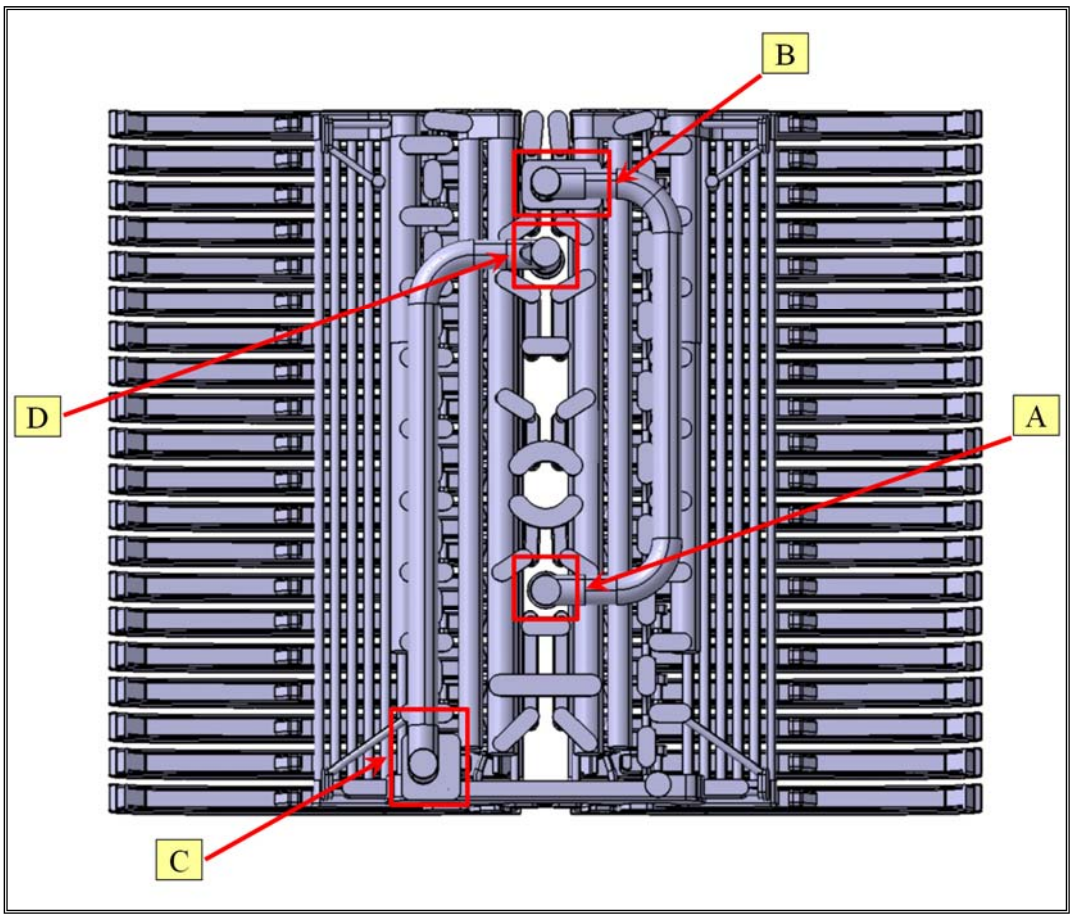

Figure 3.18. FW #14A modifications locations.

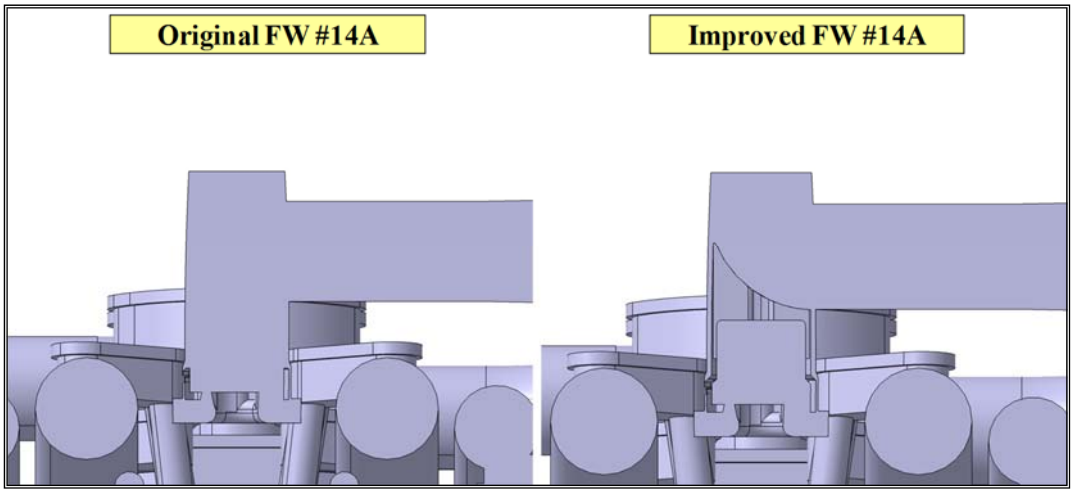

Figure 3.19. Detail of FW #14A modification at location A.

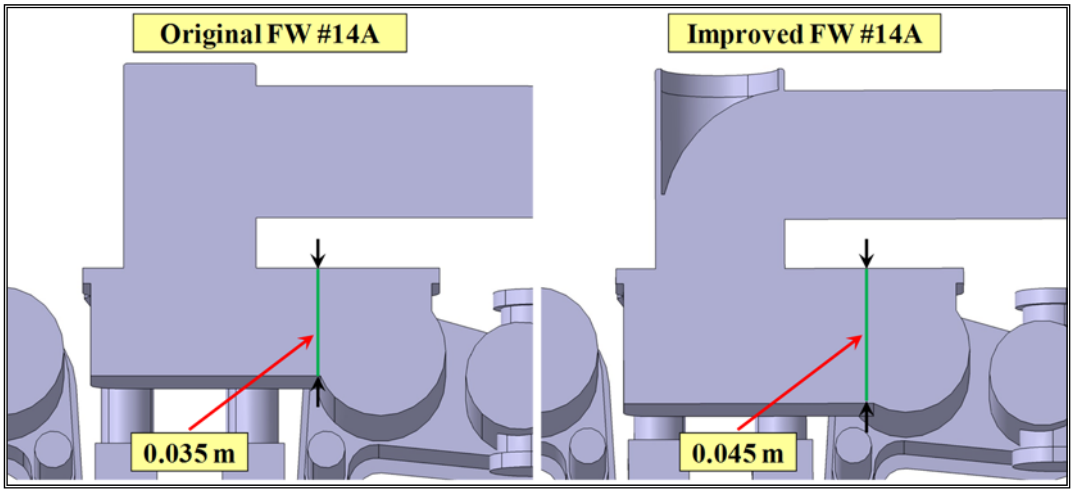

Figure 3.20. Detail of FW #14A modification at location B.

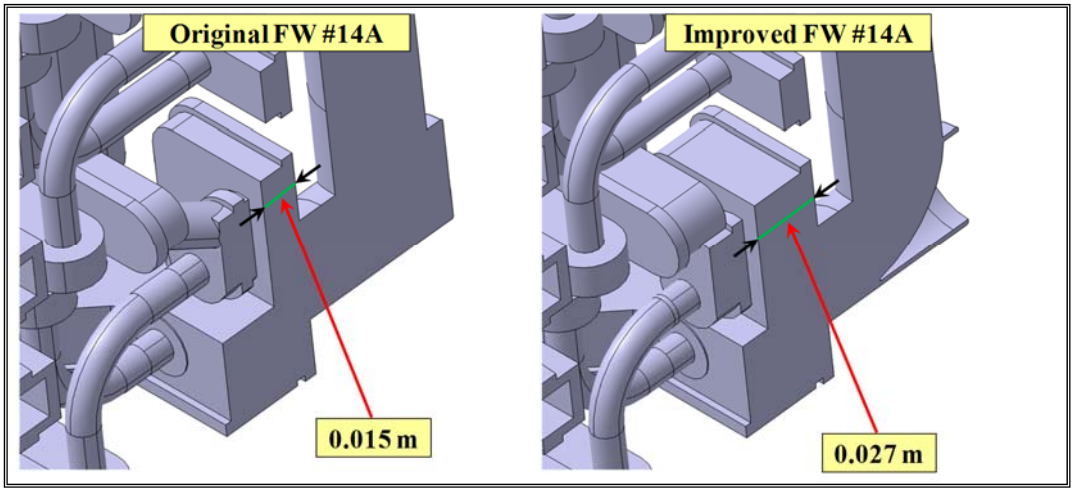

Figure 3.21. Detail of FW #14A modification at location C.

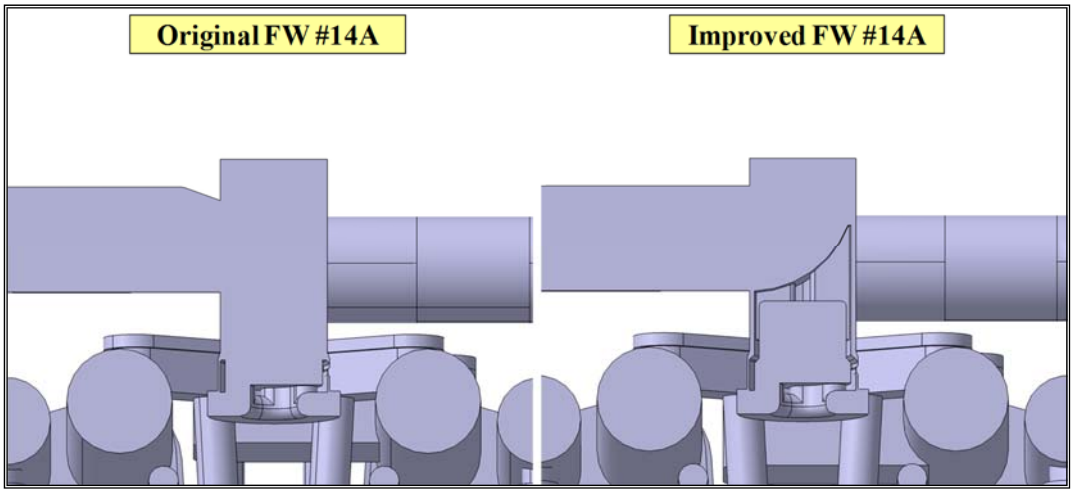

Figure 3.22. Detail of FW #14A modification at location D.

CFD analyses have been run for both the original and modified FW #14A configurations at the reference mass flow rate of 9.125 kg/s. The pertaining results in terms of total pressure drop, Δp_{orig} and Δp_{mod}, calculated between the sections shown in Figure 3.23 are reported in Table 3.17, while the total pressure drops estimated for both the original and the modified configurations of the FW #14A are reported in Table 3.18.

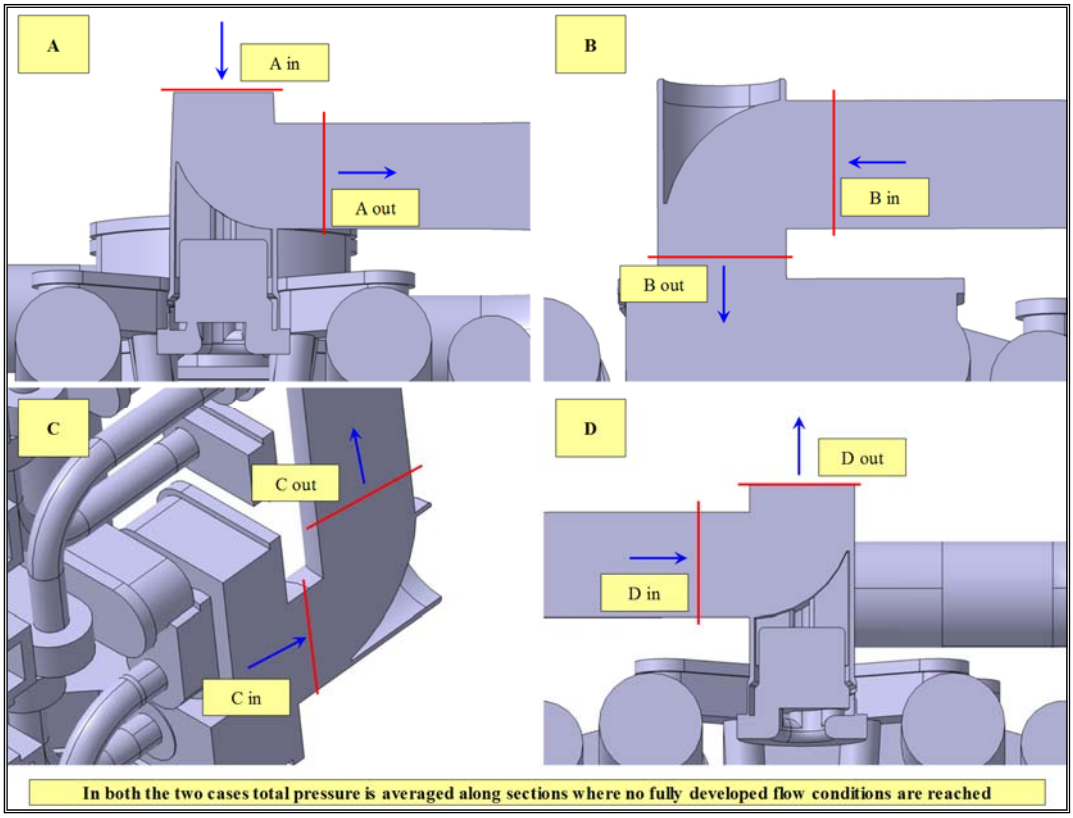

Figure 3.23. Details of FW #14A pressure probing sections.

Table 3.17. FW #14A calculations results.

Component	Δp_{orig} [MPa]	Δp_{mod} [MPa]	ε [%]
A	0.0271	0.0201	-25.8
B	0.0284	0.0189	-33.5
C	0.0370	0.0287	-22.4
D	0.0366	0.0175	-52.2

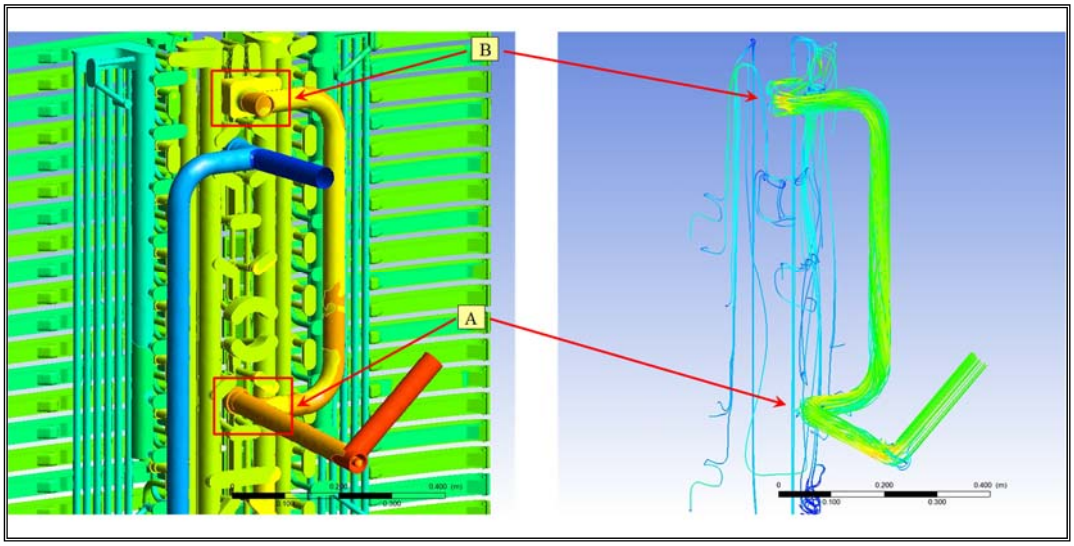

Figure 3.24. Details of FW #14A streamlines at locations A and B.

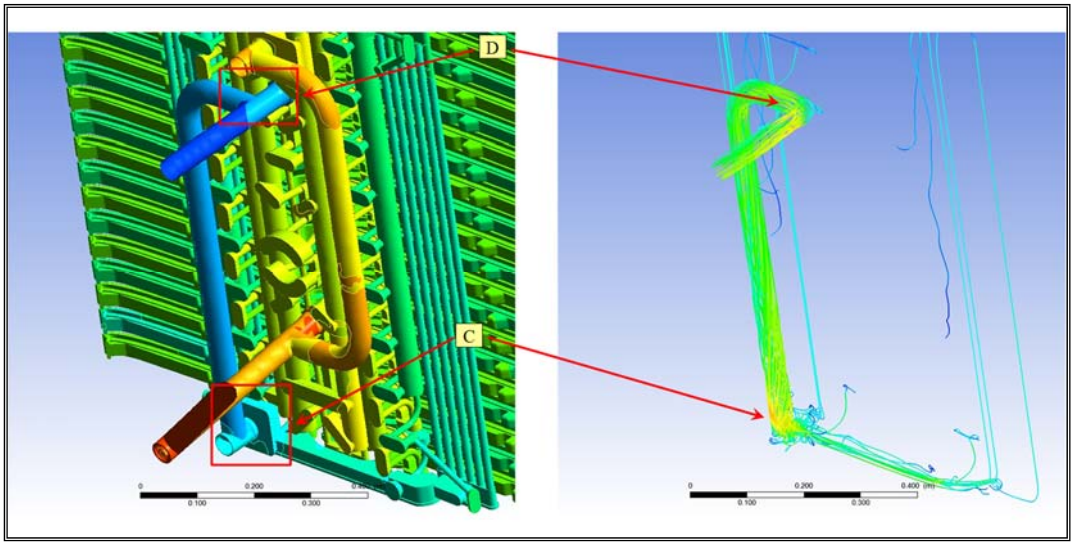

Figure 3.25. Details of FW #14A streamlines at locations C and D.

Table 3.18. FW #14A total pressure drops.

Component	G [kg/s]	Δp [MPa]	ε [%]
Original FW #14A	9.125	0.4149	-19.2
Modified FW #14A	9.125	0.3353	

Results obtained clearly indicate that the FW #14A layout modifications significantly contribute to the reduction of its local concentrated hydraulic resistances and, therefore, to their pertaining total pressure drops, allowing the modified configuration to reduce its total pressure drop to ≈ 80% of the original one and highly encouraging its implementation.

As confirmed by fluid streamlines reported in Figure 3.24 and Figure 3.25 for the considered layout modifications, pressure drop reduction is obtained by easing the coolant flow through the flexible pipes elbows, where a contribution equal to the 31% (0.1291 MPa) of the overall total pressure drop was predicted for the original FW #14A, being reduced up to the 25% (0.0852 MPa) for the modified FW #14A.

3.4.3 SB #14A

The modified configuration of SB #14A is characterized, similarly to FW #14A, by the increase of the thickness of some plate-like headers and by the filleting of some sharp junctions between channels and headers. Figure 3.26 and Figure 3.27 show its flow domain with the details of locations where main modifications have been made.

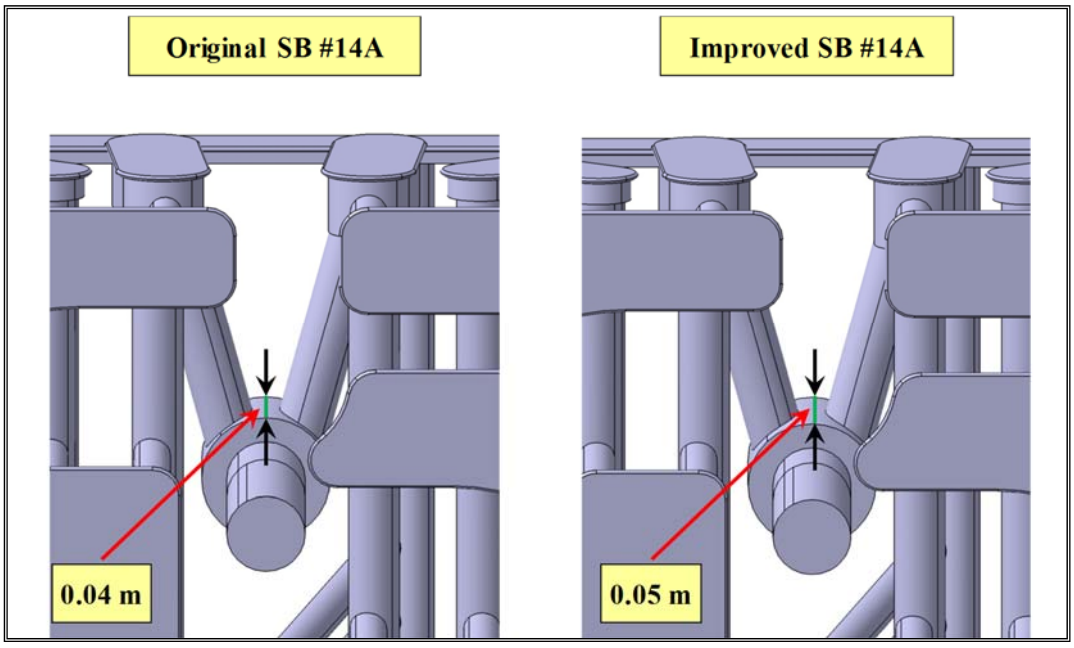

Figure 3.26. Detail of SB #14A modifications.

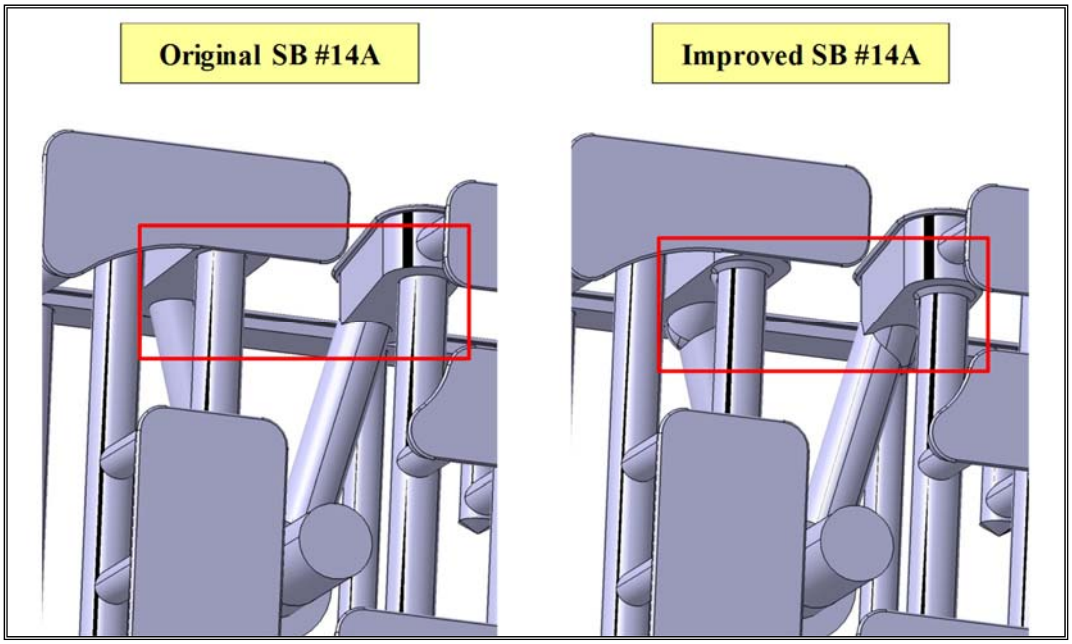

Figure 3.27. Detail of SB #14A modifications.

CFD analyses have been run for both the original and modified SB #14A configurations at the reference mass flow rate of 9.125 kg/s. The pertaining results in terms of total pressure drop for both the original and the modified configurations are reported in Table 3.19.

Table 3.19. SB #14A total pressure drops.

Component	G [kg/s]	Δp [MPa]	ε [%]
Original SB #14A	9.125	0.2519	-7.7
Modified SB #14A	9.125	0.2324	

Results obtained suggest that the SB #14A layout modifications contribute to the reduction of its total pressure drop to ≈ 92% of the original one and, therefore, encourage their implementation.

Conclusions

This thesis has covered the main research activities carried out during the candidate Ph.D. course of the XXXI Cycle on “Energia e Tecnologie dell’Informazione - curriculum Fisica Tecnica e Ingegneria Nucleare” (Energy and Information Technologies - Applied Physics and Nuclear Engineering curriculum), held at the University of Palermo, in the time frame that goes from the end of 2015 to the end of 2018.

In particular, it focusses on the activities carried out at the DEIM in cooperation with the ITER Organisation on the “Hydraulic Analysis of Blanket Cooling System” and it has aimed to investigate the thermal-hydraulic behaviour of the ITER blanket cooling system under nominal steady-state conditions, paying a particular attention to the assessment of the total pressure drop occurring in each module cooling system, together with its spatial distribution along the main circuital components. In addition, the research activity has been intended to fruitfully contribute to:

- the assessment of the blanket cooling system effectiveness in terms of mass flow rate distribution as well as of total pressure drop acceptability;
- the improvement and potential optimization of the blanket cooling system thermal-hydraulic performances by the assessment of the impact of proposed layout modifications on the investigated cooling circuits steady-state thermal-hydraulic behaviour;
- the identification of the potential need for flow regulators within the blanket module cooling systems in order to balance their coolant mass flow rate distribution.

The blanket system represents one of the pivotal components of the ITER reactor, because it provides a physical boundary for the plasma transients and contributes to the thermal and nuclear shielding of the vacuum vessel, the superconducting magnets and the external ITER components. Because of its position and functions, the blanket system is foreseen to undergo a significant heat load under nominal conditions. Therefore, the blanket cooling system design results to be particularly demanding since it has to ensure that an adequate cooling is provided to each module and any risk of CHF insurgence is prevented, optimizing mass flow rate distribution and complying with pressure drop limits.

Due to the extreme complexity of the flow domain of the blanket module cooling systems to be investigated, the research activity has been carried out following a theoretical-computational approach based on the finite volume method and adopting a suitable release of the ANSYS CFX CFD code, integrated, whenever needed, by the RELAP5 Mod3.3 thermal-hydraulic system code.

A proper operative procedure has been outlined to timely and effectively carry out the activity, based on the idea of reducing the assessment of a blanket module cooling system total pressure drop to the proper recombination of those separately calculated for the hydraulic variants of its main components (FW, SB and manifold).

The activity has started in 2015 and, according to CAD availability, it was originally conceived to last for 48 months, being articulated in five subsequent phases. In particular, each phase concerns the investigation and optimisation of the nominal steady-state thermal-hydraulic performances of the following quasi-definitive (or frozen) cooling circuits:

- 24 SB hydraulic variants;
- 10 FW hydraulic variants;
- 16 inlet/outlet manifold hydraulic variants;

for an overall of 50 frozen hydraulic variants per phase and other still-in-work components.

The Ph.D. work has been developed within the context of the first two phases of the activity. Specifically, it has dealt with the investigation and optimisation of the nominal steady-state thermal-hydraulic performances of the following quasi-definitive (or frozen) cooling circuits:

- 23 SB hydraulic variants;
- 15 FW hydraulic variants;
- 31 inlet/outlet manifold hydraulic variants;
- 2 plates;

for an overall of 71 frozen hydraulic variants. Furthermore, the thermal-hydraulic performances of other still-in-work components have been assessed and optimised under nominal steady-state conditions.

Moreover, attention has been focussed also onto the assessment of the steady state fluid-dynamic behaviour of some layout modifications, in order to check their effective impact in the improvement and potential optimization of the blanket cooling system thermal-hydraulic performances, mainly in terms of total pressure drop reduction.

As to the results shown in this thesis, they indicate that the total pressure drop of the investigated blanket module cooling systems widely ranges from 0.2696 MPa for the cooling system of BM10-11S01 to a maximum of 0.8553 for the cooling system of BM14S01, as a consequence of the different mass flow rates and layouts characterizing the cooling systems.

Concerning the assessment of the steady state fluid-dynamic behaviour of the layout modifications proposed for the FW #14A hydraulic variant, the SB #14A hydraulic variant and their inlet/outlet coaxial connectors, the numerical results obtained have indicated the opportunity to implement the lay-out modifications suggested for the FW #14A, the SB #14A and the inlet coaxial connector, while discouraging the implementation of those proposed for the outlet coaxial connector.

Acknowledgements

The work leading to this Thesis has been partially funded by the ITER Organisation under the contract CT-43-1195.

The author would like to offer special thanks to Dr.s Mario Merola, Renè Raffray, Raphael Mitteau and Barbara Calcagno for the expertise and competence with which they have kindly supported and cooperated to the realization of this work.

References

[1] A. R. Raffray et al., *The ITER blanket system design challenge*, Nuclear Fusion 54 (2014) 033004, DOI: 10.1088/0029-5515/54/3/033004.

[2] P. Edwards et al., *ITER blanket manifold final design and validation*, Fusion Engineering and Design 124 (2017) 328-332, DOI: 10.1016/j.fusengdes.2017.03.110.

[3] S. Garitta, R. Mitteau, *Introduction to hydraulic pressure drop analysis of Blanket Cooling System*, Ref. ITER_D_RB48SJ v1.0, ITER internal report.

[4] B. Remi, R. Mitteau, *Mass flow rate distribution in individual BMs*, Ref. ITER_D_33ADNL v3.0, ITER internal report.

[5] ANSYS CFX - Solver Theory Guide.

[6] ANSYS CFX - Solver Modeling Guide.

[7] RELAP5 Mod3.3 code - Theory Manual, INEL Nuclear Safety Analysis Division.

[8] I. E. Idelchik, *Handbook of Hydraulic Resistance*, 1986.

[9] E. Vallone, R. Mitteau, *Hydraulic codes benchmarking for mass flow balancing among BMs*, Ref. ITER_D_QE8W2K v1.0, ITER internal report.

[10] D. J. Zigrang, N. D. Sylvester, *Explicit approximations to the solution of Colebrook's friction factor equation*, AIChE Journal 28 (1982) 514-515.

[11] F. Cismondi, F.Escourbiac, *Critical heat flux testing on hypervapotron. Intermediate report 1*, CFP/NTT-2002.036, DIR/SIPP, CEA-Cadarache internal report.